2008

Comparison of Silica Polyamine Composites and Crosslinked Polystyrene Resins

Jessica Lee Wood
The University of Montana

Comparisons of Silica Polyamine Composites and Crosslinked Polystyrenes Resins

By

Jessica Wood

B.S. Chemistry, The University of Montana, Missoula, MT 2006
B.A. German, The University of Montana, Missoula, MT 2006

Thesis

Presented in partial fulfillment of the requirements

for the Degree of

Master of Science

The University of Montana

June 2008

Approved by
Dr. David A. Strobel, Dean
Graduate School

Dr. Edward Rosenberg, Committee Chairperson
Department of Chemistry

Dr. Mark Cracolice, Committee Member
Department of Chemistry

Dr. Holly Thompson, Committee Member
Department of Chemistry

Dr. James Gannon, Committee Member
Department of Biological Sciences

Wood, Jessica L., June, 2008
Chemistry

Comparison of Silica Polyamine Composites and Crosslinked Polystyrene

Chairperson: Edward Rosenberg, Department of Chemistry

Abstract:

The development of silica polyamine composites (SPC) was inspired by the need for more environmentally benign ways of extracting and recovering technologically important and environmentally dangerous metals from waste streams. These solid phase adsorbents are designed to endure the extreme conditions associated with environmental remediation and the metal processing industry. In order for the silica polyamine composites to be viable in industry, their performance must meet or exceed the current methods of metal extraction from aqueous media. A study was undertaken to compare three silica polyamine composites: WP-2, BPAP, and CuWRAM, with their closest crosslinked polystyrene resin analogs. The studies undertaken consisted of tests of industrial relevance: metal ion capacity, pH dependence of capacity, mass transfer kinetics, metal ion selectivity, and the efficiency of recovering the metal from the adsorbent. To further compare these ion exchange matrices, some new synthetic procedures for making analogs of existing polystyrene resins on the silica polyamine matrix were explored.

These in-depth studies have demonstrated that while crosslinked polystyrene chelator resins sometimes exhibit higher equilibrium batch capacities, SPCs exhibit faster mass transfer kinetics and equivalent flow capacities, with higher or similar purity. Explorations into developing direct analogs of polystyrenes chelator resins led to a new reaction pathway for a currently commercially produced SPC that is simpler and more cost effective.

A study aimed at understanding the nature of the polymer-surface interface in SPCs was undertaken. This study explored the influence of changing the structure of the silane linker between the silica surface and the polyamine on metal ion selectivity. It was found that substituting the more rigid and bulkier chlormethylphenyltrichlorosilane linker for the chloropropyltrichlorosilane resulted in a marked increase in the selectivity of Fe^{3+} over Cu^{2+}, but only in the case of the linear polymer polyallylamine (PAA). In the case of the branched polymer polyethyleneimine (PEI), no such change in selectivity was observed. While these results are not well understood at this time, this allows the Rosenberg group and Purity Systems Inc. another way of fine tuning the metal selectivities of silica polyamine composites.

Acknowledgements

My time in the Rosenberg group here at the University of Montana has been very educational and fulfilling. I would like to sincerely thank the entire Rosenberg group for their support and guidance over the past two years. I would like to especially thank Dr. Mark Hughes for his mentorship when I first began working on my project. I would also like to thank Brianne Cross and Chauncey Means for the time and research that they donated to the completion of my project. I owe much gratitude to the entire Chemistry department for helping me choose this particular path in life; the members of this department not only inspire but also provide the direction needed to succeed. Most particularly I would like to express my gratitude to Dr. Edward Rosenberg; he has been an inspiration to all of us that have worked for him. He has provided me with limitless guidance, support and knowledge throughout my research process. His confidence in me and my abilities have guided me through the last two years. Finally I must thank my friends and family who have supported me not only over the past two years in this endeavor to obtain my master's but throughout my entire life and in every endeavor I undertake.

Table of Contents

LIST OF FIGURES

LIST OF TABLES

Chapter 1: Background

1.1 Introduction

In recent years the price of metals has risen significantly. Much of this is due to the high demand for many metals for technological applications. Figure 1.1 shows the trend in rising metal prices from January of 1990 to April of 2008[1]. In all metals pictured (Cu, Au, Pb, Ag, Ni and Sn), the significant rise in metal prices began around January 2004 and has not significantly decreased since. Due to this extreme rise in metal prices it has become profitable to explore new methods of metal extraction on lower grade mineral ores. In some cases it may now be possible to recover metals from abandoned mine sites while remediating the environmental hazards that the sites present.

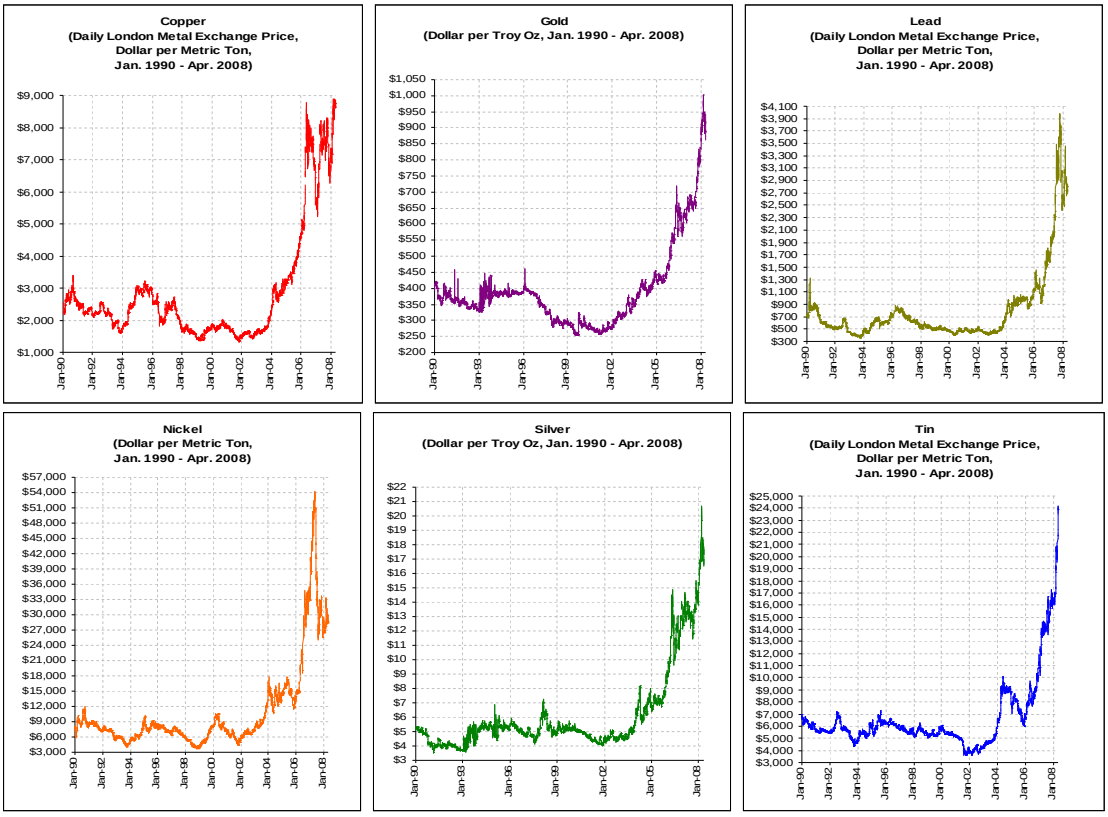

Figure 1.1: Trend of 6 metal prices from January 1990 to April 2008.[1]

Considering these recent developments it is important to summarize methods of metal recovery. Metals are extracted from the earth's surface in the form of ores by two methods: surface mining and subsurface mining. Surface mining is used when there is a thin layer of soil and rock overlaying the mineral deposits, while with subsurface mining, the mineral deposits lie deeper in the earth's crust and are removed via tunnels or shafts made in the overlaying rock. Once these ores are obtained, the metals must be extracted from the ore. Pyrometallurgy and hydrometallurgy are the two processes used to extract the metals from the ore. Pyrometallurgy uses high temperature to convert the ore into pure metals, usually by reduction with carbon.[2] Hydrometallurgy is a process where aqueous chemistry is employed to convert the ore into the raw metals.[3] The composition and the presence of contaminates often determines which process is used. In most cases the presence of oxides dictates the use of hydrometallurgy, while the sulfide ores are usually processed via pyrometallurgy.

Pyrometallurgy denotes a class of high-temperature industrial processes by which metals are extracted from ore and refined to market specifications.[2] Pyrometallurgical processes include drying, calcining, roasting, and smelting. Drying is the thermal removal of non-chemically bound liquid moisture from a metal ore.[2] This is accomplished by contacting the moisture-latent ore with hot combustion gases generated by burning fossil fuels. This process is conducted in industrial dryers such as rotary dryers, fluidized bed dryers, and flash dryers. Calcining consists of the thermal decomposition of a material.[2] Common calcining processes include the conversion of ferric hydroxide to ferric oxide and water vapor, and calcium carbonate to calcium oxide and carbon dioxide.[2] The calcining process is conducted in furnaces such as shaft

furnaces, rotary kilns, and fluidized bed reactors. Roasting consists of thermal gas-solid reactions, which include oxidation, reduction, chlorination, sulfation, and pyrohydrolysis.[2] The most common roasting process is the oxidation of metal sulfide ores, such as roasting of copper sulfide.

$$Cu_2S + 3/2\ O_2 \rightarrow Cu_2O + SO_2 \qquad \text{(Eq. 1)}$$

Smelting involves thermal reactions in which at least one product is in a molten phase.[2] Metal oxides can be smelted by heating with coke or charcoal, a reducing agent that liberates the oxygen as carbon dioxide, leaving a partially refined metal.[2] Carbonate ores can also be smelted but often required being calcined first.

Hydrometallurgy involves the dissolution of oxide ores in mineral acid, usually in H_2SO_4, followed by extraction of the desired metal into an organic phase containing a metal selective chelating ligand. The organic phase containing the complexed metal is then contacted with an aqueous acidic phase into which the desired metal is extracted. The metal is then recovered by electrolytic deposition. This overall process is called solvent extraction.[3]

Pyrometallurgy and hydrometallurgy processes require large amounts of resources such as energy in order to provide high grade metals. These processes also produce large amounts of pollutants which are harmful to the environment. Pyrometallurgy produces toxic gases such as SO_2 and mercury vapor and CO as well as the greenhouse gas CO_2. Solvent extraction in particular suffers from several disadvantages including the use of toxic, flammable solvents, an inability to extract metals to very low levels, and slow kinetics. Ion exchange offers a more efficient and environmentally benign alternative to

such processes. Ion exchange is capable of removing metals to very low levels at high purities.

While metals are important to society, mining and the extraction processes involved in mining lead to some negative societal impacts. First, there is the aesthetic aspect of mining. Surface mining often leaves a large hole where the ore and materials were removed to be processed. This can easily be seen in Butte, Montana with the presence of the Berkeley Pit, a large surface mine that has now filled up with toxic water. Subsurface mining is more aesthetically pleasing, yet still causes environmental damage. Both types of mines lead to acid mine drainage.

Acid mine drainage is outflow of acidic water from abandoned metal mines.[4,5] This occurs when air and water come in contact with metal sulfides, causing the oxidation of these sulfides. The oxidation of sulfides produces sulfate ions, metal ions, and often hydrogen ions that are released into the water (Equations 1.2 and 1.3)

$$FeS_2 + 3.5\ O_2 + H_2O \rightarrow Fe^{2+} + 2\ SO_4^{2-} + 2\ H^+ \qquad \text{(Eq. 1.2)}$$

$$2\ Fe^{2+} + 0.5\ O_2 + 5\ H_2O \rightarrow \text{“}Fe(OH)_3\text{”} + 4\ H^+ \qquad \text{(Eq. 1.3)}$$

These released protons then further dissolve metal containing compounds. Furthermore, the pH drop promotes growth of *Thiobacillus, Ferroplasma* and *Acidithiobacillus* bacteria[6,7], which convert insoluble metal sulfides into soluble ions, producing even more acid. This process results in release of toxic metals such as Cu, Zn, Mn, Cd, and As.

Efficient recovery of dissolved metals has two advantages: decreased accumulation of toxic metals in the environment, and the recovery of valuable metals. Processes for recovery of valuable metals from aqueous media are solvent extraction, ion exchange, and polymer filtration.[8-16] The negatives associated with solvent extraction

include evaporation of volatile, flammable, and often-toxic organics, a finite solubility of extractants and modifiers in the aqueous layer, and build-up of solid crud at the solid-liquid interface.[12] It is also difficult to recover the extracted ion from the organic solvent and reduce metal ion concentrations in the aqueous phase to negligible levels.[8] Problems that arise from polymer filtration consist of sensitivity to colloidal particles, causing the polymer to act as a flocculent with solvent extraction.[14] Soluble polymers of high molecular weight are often degraded by hydrolysis and mechanical shearing in polymer filtration while sorption of the polymer into the membrane also occurs, causing a negative effect on the permeate flux.[17] Ion exchange offers the most environmentally benign approach, and for this reason the research focused only on ion exchange extraction systems, in particular two types of ion exchange materials, divinylbenzene crosslinked polystyrene and amorphous silica gel polyamine composites (SPCs).

1.2 Divinylbenzene crosslinked Polystyrene

Polystyrene ion exchange resins are produced by reacting polystyrene with divinylbenzene (DVB).[18] Equation 1.4 depicts the formation of crosslinked polystyrene. The polystyrene can be reacted with H_2SO_4 to form an ion exchanger, as seen in Equation 1.5. The metal ion capturing functional groups are introduced by chlormethylating the phenyl rings followed by nucleophilic substitution or by direct reaction with the chelating ligands.[19] Equation 1.6 demonstrates one such reaction with iminodiacetic acid (IDA).

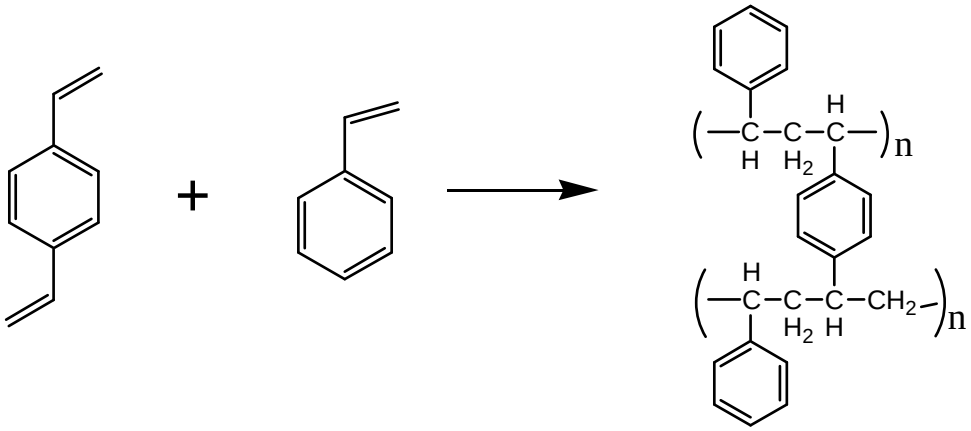

(Eq. 1.4)

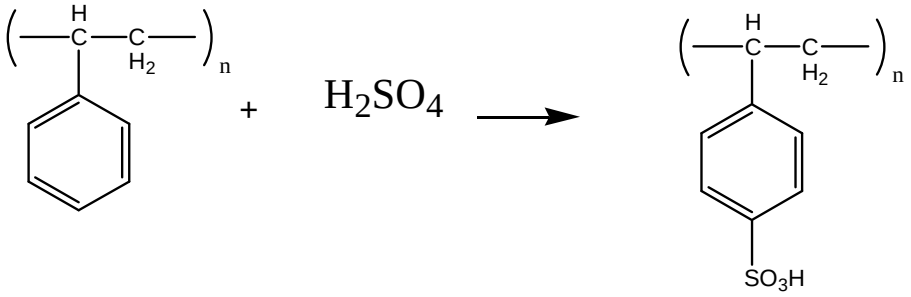

(Eq. 1.5)

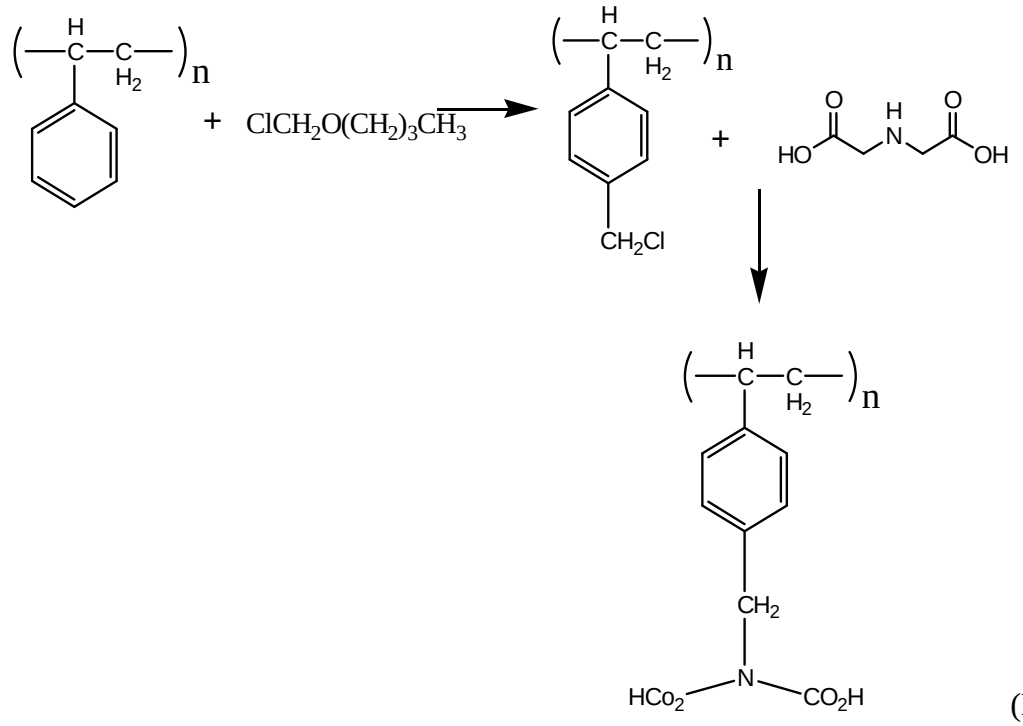

(Eq 1.6)

DVB is the most conventional cross-linking agent used for preparing ion exchange resins. Cross-linking is employed to give the polymer matrix more rigidity and

better thermal properties. While cross-linking makes polystyrene more suitable for the use as ion exchangers, these resins swell significantly, allowing the migration of water molecules and ions within the swollen polymeric structure.

Styrene-DVB is the most commonly employed matrix for cross-linking agents due to its ability to bear a wide diversity of functional groups and its proven chemical and mechanical stability. The degree of crosslinking is the density of the cross-links within the polymeric chains. The degree of crosslinking is shown to affect the structure, elasticity, swelling ability, and diffusion characteristics of the resins. Lower crosslinking allows for improved mass transfer kinetics, while higher crosslinking increases the mechanical stability of the resins. The characteristic range of crosslinking is 1 to 8% in commercial ion exchangers. The most typical percentage of DVB crosslinking matrixes is 6%, allowing for the greatest stability, while maintaining reasonable mass transfer kinetics.[18]

Disadvantages of crosslinked polystyrene include instability at elevated temperatures, shrink-swell tendencies[20], and poor mass transfer kinetics. Crosslinked polystyrene resins can begin losing its stability at temperatures between 60 and 80˚C. The shrink-swell tendencies of the crosslinked polystyrene imposes limitations on processes conducted in fixed bed (column reactors), due to the fact that the resin is subject to large volume variations. Crosslinked polystyrene has been shown to exhibit poor mass transfer kinetics due to hydrophobic interactions between the matrix and aqueous solutions. Degree of crosslinking, particle size, and concentration of the functional groups can also have negative influences on the mass transfer kinetics of the resin.[21,22]

1.3 Silica Polyamine Composites (SPCs)

SPCs are a new class of inorganic-organic hybrid chelating ion exchange materials developed by the Rosenberg Research Group at The University of Montana.[14,17,21-33] The Rosenberg Group obtained patents on the developed materials in cooperation with Purity Systems, Inc. (PSI).[23-26] SPCs were developed in the hope of overcoming some of the major flaws in other extraction systems, such as solvent extraction, polymer filtration, and polymeric ion exchangers such as the DVB crosslinked polystyrene resins.

SPCs consist of amorphous silica gel functionalized with a silane layer to which a polyamine is then attached. Figures 1.2 and 1.3 depict the synthetic pathway for the production of SPCs. The polyamine can then be further functionalized with a variety of metal selective ligands, yielding various novel inorganic/organic hybrid chelating ion exchange materials.

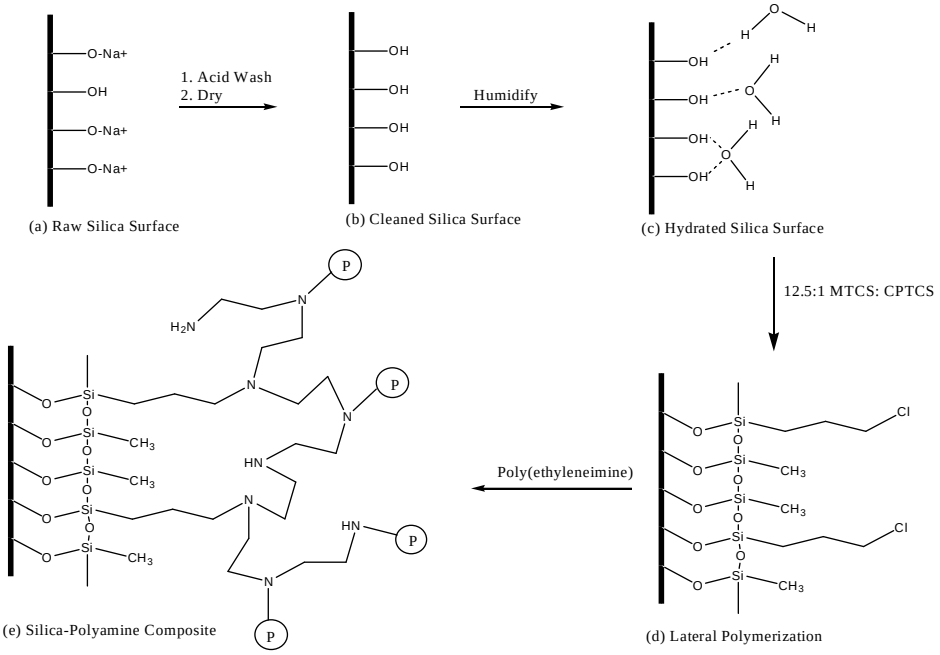

Figure 1.2: Step by step production scheme of the patented SPCs using PEI as the polymer.

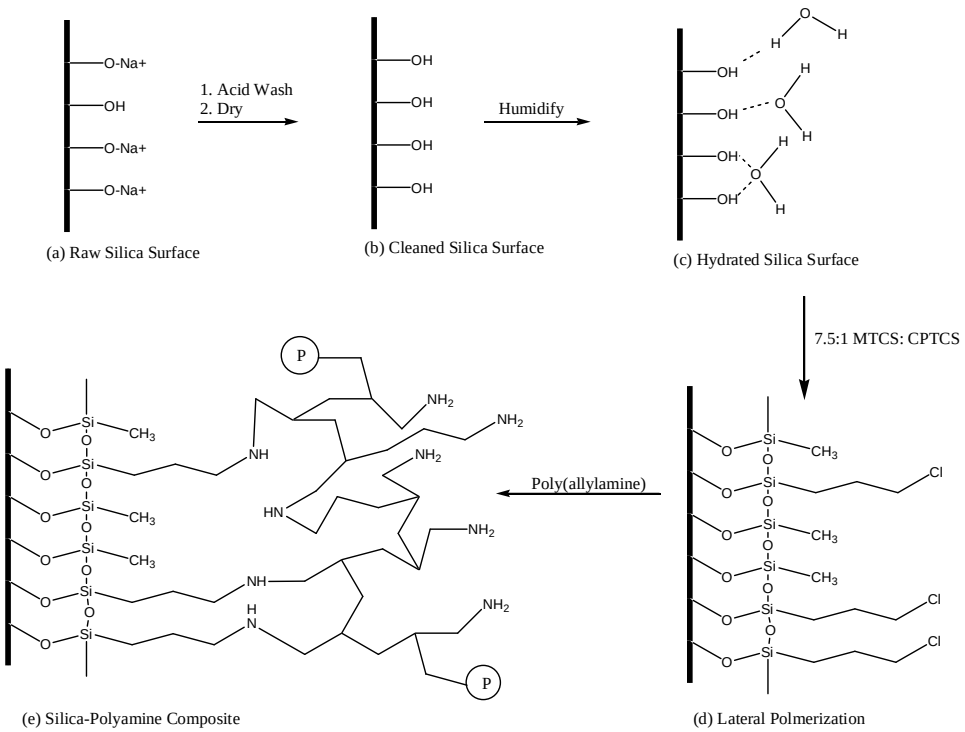

Figure 1.3: Step by Step production scheme of patented SPCs using PAA as the polymer.

This thesis provides a detailed comparison of the metal recovery capabilities of polystyrene based chelator resins and SPCs. In addition, the impact of altering the silane anchor on SPCs properties is explored.

1.4 Factors Controlling Metal Coordination and Geometry

The three factors that govern the coordination number of a metal complex are the size of the central atom or ion, the steric interactions between the ligands and the electronic interactions between the central atom or ion and the ligands. Metals with large radii, located lower down on the periodic table favor higher coordination numbers, while bulky ligands often result in low coordination numbers for steric reasons.

Common coordination numbers for metal complexes are four and six. The majority of complexes are six-coordinate complexes, which have octahedral geometry. Typically four coordinate complexes are favored over higher coordinate complexes if the

central atom is small or the ligands are large; these complexes are tetrahedral in geometry. Another four coordinate complex is observed for metals with d^8 configurations and these complexes have square planar geometry.

The electronic structure of these complexes can be determined though two different widely used models; crystal-field theory and ligand-field theory. Crystal-field theory is where a lone pair is modeled as a point negative charge that repels electrons in the d orbitals of the metal ion. It focuses on the resulting splitting of the d orbitals into groups with different energies and uses that splitting to rationalize and correlate the optical spectra, thermodynamic stability and magnetic properties of the complexes. Ligand-field theory simply expands upon crystal-field theory by using molecular orbital theory and accounts for a wider range of properties.

As discussed above there are typically 3 common metal structures; octrahedral, square planar and tetrahedral. Below are the splitting patterns for each type of complex based on crystal and ligand field theory.

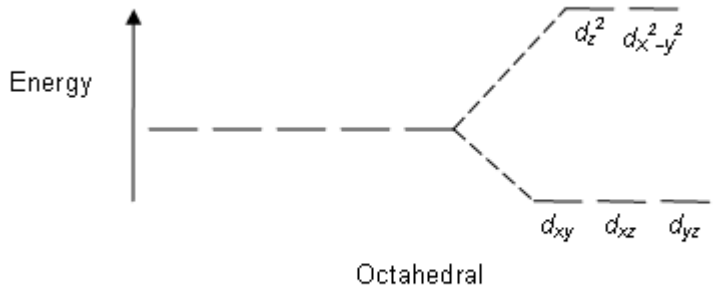

Figure 1.4: Octahedral splitting pattern for six coordinate metal complexes.

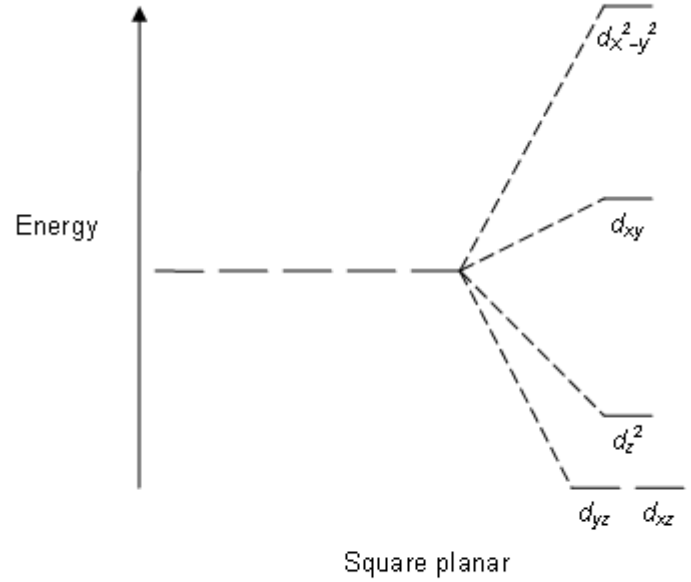

Figure 1.5: Square planar splitting pattern for four coordinate d8 metal complexes.

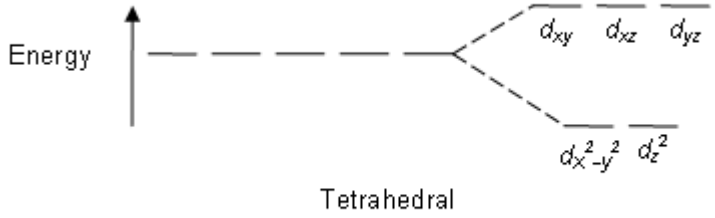

Figure 1.6: Tetrahedral splitting pattern for four coordinate metal complexes.

The separation of the sets of orbitals in the above digrams is the ligand-field splitting parameter Δ. The value of Δ is affected by both the ligands and the metal center. A series of ligands was found to affect the Δ in the same manner regardless of the metal ion. This ligand series is a called the spectrochemical series[34], in which the ligands are arranged in order of increasing energy of transitions that occur when they are present in a complex.

$I^- < Br^- < S^{2-} < \underline{S}CN^- < Cl^- < N\underline{O_2}^- < N_3^- < F^- < OH^- < C_2O_4^{2-} < H_2O < \underline{N}CS^- <$

$CH_3CN < py < NH_3 < en < bipy < \underline{N}O_2^- < PPh_3 < \underline{C}N^- < CO$

Δ increases at the ligands are varied along the series. Ligands such as CO that give rise to a high-energy transition are referred to as strong-field ligands, whereas one such as Br that gives rise to low-energy transitions is a weak-field ligand.

The ligand field strength also depends on the identity of the central metal ion, the order being approximately[34]:

$Mn^{2+}<Ni^{2+}<Co^{2+}<Fe^{2+}<V^{2+}<Fe^{3+}<Co^{3+}<Mo^{3+}<Rh^{3+}<Ru^{3+}<Pd^{4+}<Ir^{3+}<Pt^{4+}$

Δ increases with increasing oxidation number of the central metal ion and also increase down a group.

In ligand-field theory the placement of electrons is determined by the ligand-field stabilization energy LFSE. The LFSE is dependent upon d orbital population. It determines whether it is energetically more favorable for electrons to occupy the higher energy states or pair in the lower energy states. If Δ is small, this is considered a weak-field case and lower energy is obtained by the electrons occupying the upper orbitals. When Δ is large, a strong-field case is established and a lower energy results from the electrons occupying lower orbitals despite the cost of the pairing energy. When either of these cases are possible, the species with the smaller number of parallel electron spins is called a low-spin complex, while the species with the greater number of parallel electrons spins is called a high-spin complex. The pairing of electrons can also determine the magnetic properties of the complex.

Together all of these factors influence the coordination and geometry of a metal complex. The following is a survey of 5 metals that have been used throughout the following thesis research.

Copper

Copper is a ductile metal with excellent electrical conductivity[35]. Unlike many metals that are silver or white in color, copper is pinkish in color. It is often used as a heat conductor, electrical conductor, as a building material, and in jewelry and decoration[28].

It is and essential trace nutrient to plants and animals. Copper is found in blood stream of humans and other animals as a co-factor in various enzymes. However in sufficient amounts is can be poisonous and even fatal to organisms[36].

Common Copper Ores include:

- Chalcopyrite ($CuFeS_2$)
- Bornite (Cu_2FeS)
- Covellite (CuS)
- Chalcocite (Cu_2S)
- Azurite ($Cu_3(CO_3)_2(OH)_2$)
- Malachite ($Cu_2CO_3(OH)_2$)
- Cuprite (Cu_2O)

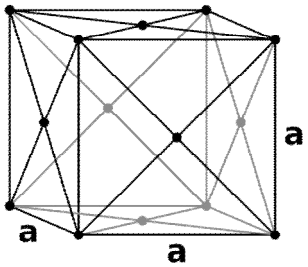

Figure 1.7: The crystal structure of copper: face-centered cubic.

Copper Electron Configuration:
$1s^2\ 2s^2\ 2p^6\ 3s^2\ 3p^6\ 4s^1\ 3d^{10}$

All copper samples used were in the +2 oxidation state.
$Cu^{+2} = 1s^2\ 2s^2\ 2p^6\ 3s^2\ 3p^6\ 4s^0\ 3d^9$

Metal Coordination of Cu^{2+}

Copper(II) consists of a d^9 configuration. In the presence of H_2O and a coordination number of six, copper exists as an octahedral geometry. While with a bulkier ligand such as picolylamine copper only has a coordination number of four and prefers the square planar geometry.

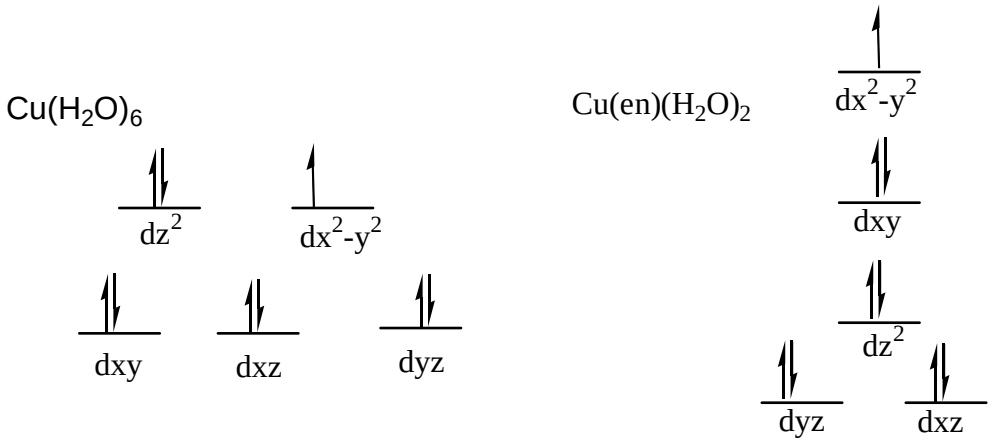

Figure 1.8: The d-orbital splitting patterns for two copper complexes which demonstrate the octahedral and square planar geometries of copper complexes.

Nickel

Nickel is a hard and ductile metal. Its uses include stainless steel, magnets, coinage, plating, tinting glass green, jewelry, decoration and for cathodes in rechargeable batteries[37].

Nickel has numerous roles in microorganisms and plants, which includes NiFe-hydrogenase which catalyzes the oxidation of molecular H_2. Humans should not be exposed to excessive amounts of nickel[38,39]. Nickel Sulfide fume and dust are suspected of being carcinogenic. A number of humans have allergies to nickel that cause skin rashes, typically this allergy is seen with earrings that contain nickel[39].

Common Nickel Ores:

Limonite (Fe, Ni)O(OH)
Garnierite $(Ni, Mg)_3Si_2O_3(OH)$
Pentlandite $(Ni, Fe)_9S_8$

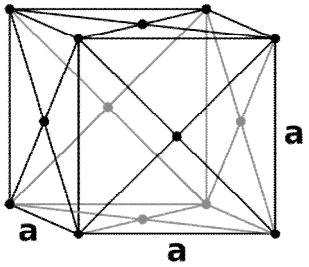

Figure 1.9: the crystal structure of Nickel: face-centered cubic.

Nickel Electron Configuration:
$1s^2\ 2s^2\ 2p^6\ 3s^2\ 3p^6\ 4s^2\ 3d^8$

All nickel samples used were in the +2 oxidation state.
$Ni^{+2} = 1s^2\ 2s^2\ 2p^6\ 3s^2\ 3p^6\ 4s^0\ 3d^8$

Nickel(II) consists of a d^8 configuration. In the presence of H_2O and a coordination number of six, nickel exists as an octahedral geometry. Nickel can exist in both square planar and octahedral geometries depending on the ligands. Thus a d^8 Ni^{2+} in $Ni(CN)_4^{2-}$ is square planar while is the ligands employed in this thesis octahedral geometry maybe preferred.

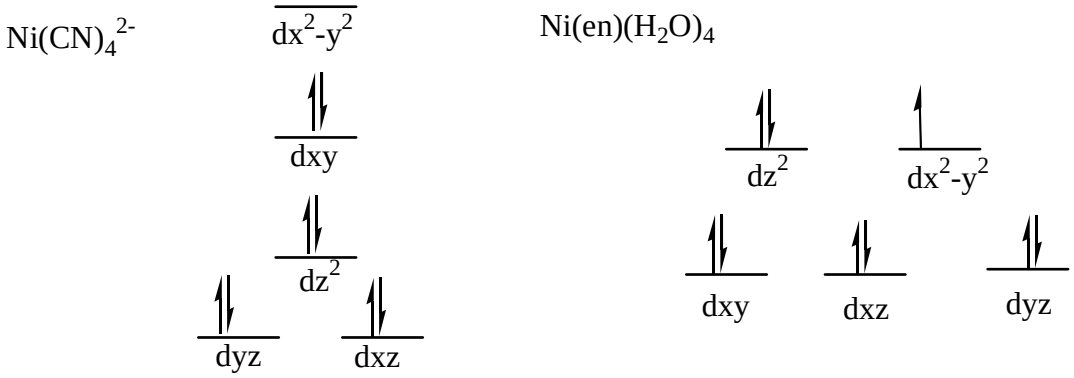

Figure 1.10: The d orbital splitting patterns for two nickel complexes.

Zinc

Zinc is a bluish-gray metal that is moderately active and tarnishes in moist air[40]. It is used to galvanize steel to prevent corrosion, in alloys particularly brass, in American pennies and as anodes in alkaline batteries[40].

Zinc is among the essential elements necessary for sustaining life. It is involved in olfaction, in fact a deficiency causes anosmia or loss of smell[36]. It is an activator of enzymes such as carbonic anhydrase. Excessive absorption of zinc can cause suppression of copper and iron adsorption[36].

Common Zinc Ores:

Sphalerite (ZnS)
Smithsonite ($ZnCO_3$)
Hemimorphite ($Zn_4Si_2O_7(OH)_2 \cdot H_2O$
Franklinite $(Fe, Mn, Zn)(Fe, Mn)_2O_4$
Gahnite ($ZnAl_2O_4$)

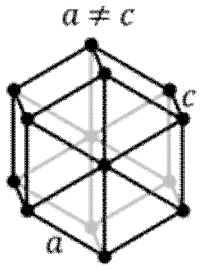

Figure 1.11: The crystal structure of zinc: hexagonal.

Zinc Electron Configuration:
$1s^2\ 2s^2\ 2p^6\ 3s^2\ 3p^6\ 4s^2\ 3d^{10}$

All zinc samples were in the +2 oxidation state.
$Zn^{+2} = 1s^2\ 2s^2\ 2p^6\ 3s^2\ 3p^6\ 4s^0\ 3d^{10}$

Exists in octahedral geometry because there is no LFSE due to the d^{10} configuration where all d orbitals are filled.

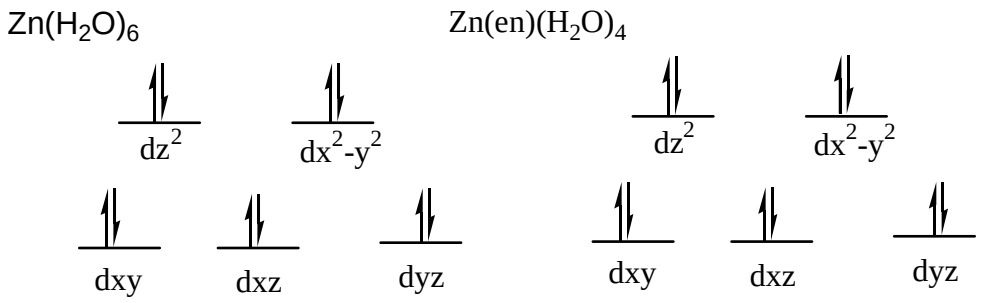

Figure 1.12: The d orbital splitting patterns for two octahedral zinc complexes, showing the filled d orbitals in the complexes.

Cobalt

Cobalt is a lustrous silver-grey metal that is hard. It is used in preparation of magnetic, wear-resistant and high-strength alloys. Cobalt is used in the sterilization of medical supplies and waste, for radiation treatment of foods for sterilization, catalysts, drying agents, color pigments and lithium ion battery electrodes[41].

Cobalt is required in small amounts by mammals in the form of Vitamin B12. Higher levels of exposure have shown signs of mutagenic and carcinogenic effects[42].

Common Cobalt Ores:

Cobaltite (CoAsS)
Erythrite ($Co_3(AsO_4)_2 \cdot H_2O$)
Glaucodot (Co, Fe)AsS
Skutterudite (Co, Ni, Fe)As_3

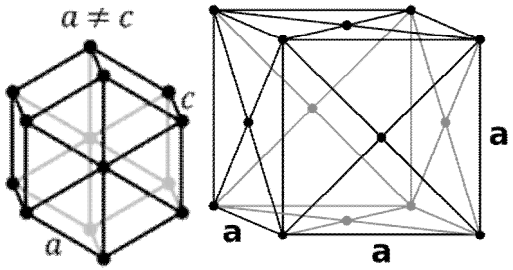

Figure 1.13: Two common crystal structures for cobalt: often found in a combination of hexagonal close packed (left) and face centered cubic (right)

Cobalt Electron Configuration:
$1s^2\ 2s^2\ 2p^6\ 3s^2\ 3p^6\ 4s^2\ 3d^7$

All cobalt samples used were in the +2 oxidation state.
$Co^{+2} = 1s^2\ 2s^2\ 2p^6\ 3s^2\ 3p^6\ 4s^0\ 3d^7$

It is possible to from tetrahedral geometries in a weak field case and octahedral complexes in a strong field case.

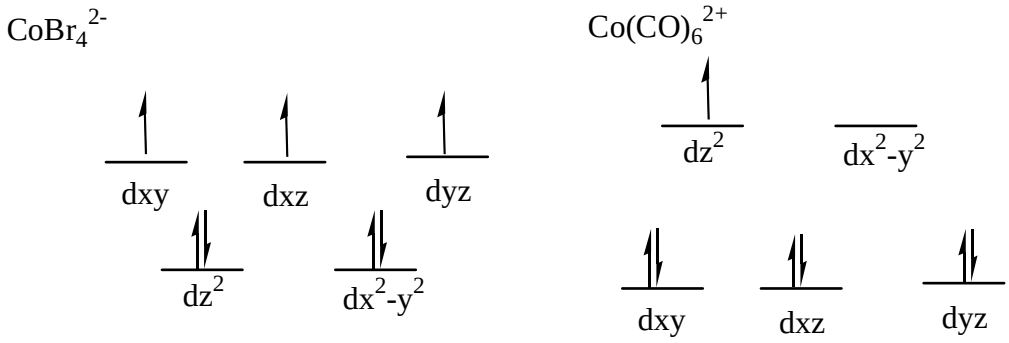

Figure 1.14: The d orbital splitting diagrams for : (left) a tetrahedral weak field cobalt complex and (right) an octahedral strong field cobalt complex.

Iron

Iron is thought to be the sixth most abundant element in the Universe. It is a lustrous, soft silver metal. Due to the low cost and high strength iron is the most widely used of all metals[43]. It is used in the construction of machinery, machine tools, automobiles, hulls of large ships, and structural components for buildings[43]. It is most often used in the form of steel.

Iron is a necessary trace element used by most living organisms[36]. Iron containing enzymes participate in catalysis of oxidation reactions in biology and in the transport of a number of soluble gases such as oxygen. Excess iron can be toxic, it causes the formation of free radicals, which are highly reactive and can damage DNA, proteins and lipids[36].

Common Iron Ores:

- Hematite (Fe_2O_3)
- Magnetite (Fe_3O_4)
- Goethite ($FeO(OH)$)
- Limonite ($FeO(OH)\cdot nH_2O$)
- Siderite ($FeCO_3$)

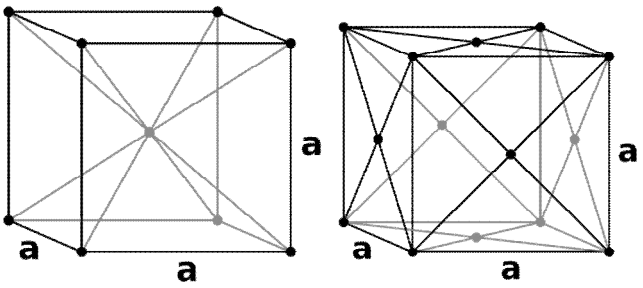

Figure 1.15: Two common crystal structures for Iron: body centered cubic (left) and face centered cubic (right).

Iron Electron Configuration:
$1s^2\ 2s^2\ 2p^6\ 3s^2\ 3p^6\ 4s^2\ 3d^6$

All iron samples used were in the +3 oxidation state.
$Fe^{+3} = 1s^2\ 2s^2\ 2p^6\ 3s^2\ 3p^6\ 4s^0\ 3d^5$

Iron commonly exits in both 2+ and 3+ oxidation states such as with $Fe(CN)_6^{4-/3-}$ complexes which are both low spin complexes with octahedral geometry. Iron complexes exist in both tetrahedral and octahedral geometries. $FeCl_4^{2-}$ is a high spin tetrahedral geometry where $Fe(H_2O)_6^{2+}$ is a high spin octahedral complex. This shows how there is ligand field stabilization energy and sterics influencing the geometry of the iron complexes.

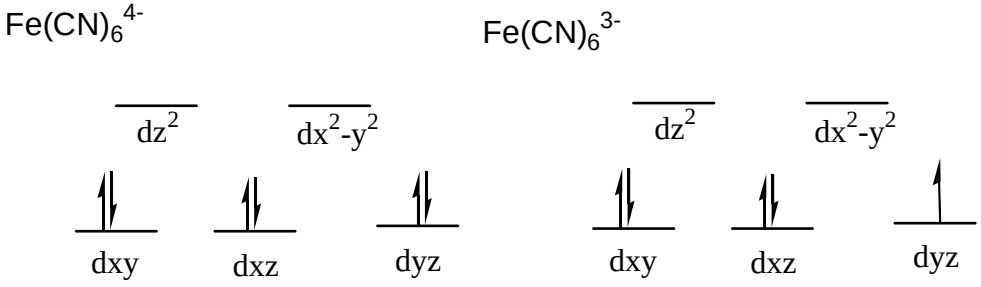

Figure 1.16: The d orbital splitting patterns for two Fe(CN) complexes exhibiting both common iron oxidation states.

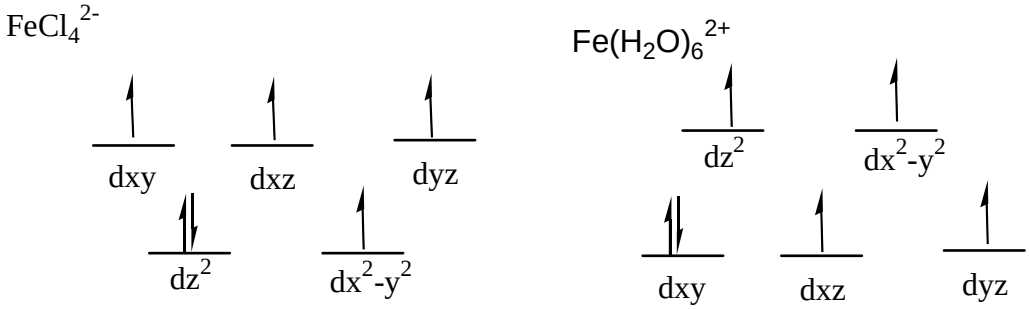

Figure 1.17: The d orbital splitting patterns for two iron complexes demonstrating the tetrahedral and octahedral binding tendencies of iron complexes based on sterics and LFSE.

1.5 Research Goals

1. Develop and implement a comprehensive comparison of crosslinked polystyrene resins and Silica Polyamine Composites, two distinct ion exchange materials. It should provide a clear picture of the advantages and disadvantages of each material. The research procedure must provide as little bias as possible for both materials.
2. Synthesize direct analogs on silica polyamine composite foundations to currently commercially available divinylbenzene crosslinked polystyrene.
3. Explore the influence of silane anchor structure on metal selectivity of silica polyamine composites.

Chapter 2: Comparison Studies

2.1 Development of an experimental procedure for polystyrene and SPC comparisons

In order to produce a format to study these materials, one must first know the requisite criteria for an effective metal ion removal system. First, the system must exhibit a high metal ion sorption capacity. It must also selectively remove one metal ion from a mixture of metal ions at a high purity. It is further required to be operational across a range of pH values. It must reduce the metal ion concentrations in the effluent to very low levels. These materials are required to possess mechanical and chemical integrity for an extended lifetime. The materials must exhibit favorable mass transfer kinetics to allow high throughputs. Finally, the materials must be economically viable. The aforementioned criteria are necessary to establish experiments that will demonstrate the effectiveness of each material as an advanced metal ion removal method. A number of experiments can be used to effectively determine the required information: pH batch profiles, breakthroughs, batch kinetics, and Langmuir isotherms.

The pH batch profiles are accomplished by measuring 0.100 ± .005 gram of the ion exchange material and placing it in a 20 mL scintillation vial. 10.0 mL of a predetermined concentration of metal solution is added. This was allowed to sit for 24 hours in order for the system to equilibrate. This experiment determines the capacity of the materials for each metal over a pH range at chemical equilibrium. It can also provide information on possible selectivities of the ion exchange materials. This is determined by looking at all of the metal capacities for a particular material. Large differences between sorption of two metals at a given pH indicate the likelihood that the material will provide

efficient separation of those particular metals. Breakthrough flow experiments are done to test these predictions obtained from the batch experiments.

Breakthrough flow experiments are performed using a column, slurry-packed with the desired ion exchange resin. These experiments allow determination of capacity, selectivity, and purity of the ion exchange material at a particular pH and flow rate. The overall breakthrough curve can be used to determine the mass transfer kinetics of the ion exchange material. This is most easily determined by the column utilization factor (Equation 2.1)[44]:

$$U = \frac{\text{(BV at Initial Breakthrough)}}{\text{(BV at Full Breakthrough)}} \qquad U = C_o/C_f \qquad \text{(Eq. 2.1)}$$

BV stands for bed volume. The column utilization factor is defined as a ratio of the number of column volumes fed through at initial breakthrough of the metal ion (Co) and the number of column volumes when the flow reaches the concentration of the metal ion in the feed solution (Cf).

Batch kinetics are performed the same way as batch tests. Aliquots were taken at specified time intervals to determine the sorption equilibrium point and to evaluate mass transfer kinetics of the system.

Langmuir isotherms are produced using protocol a similar to the pH batch kinetics. With these isotherms, the metal solutions are added to the ion exchange material at different concentrations of metal ion in solution, ranging from 20 mmol/liter to 2 mmol/liter and are held at a constant pH. The Langmuir sorption model demonstrates the relationship between the concentration of the metal ion adsorbed onto a material and the concentration of a metal ion remaining in a solution at equilibrium. It

assumes sorption occurs as a monolayer on a homogenous surface without interactions between metal ions.[45]

The Langmuir equation relates the adsorption of metal on a solid surface to concentration of metal in solution. The equation is as follows:

$$Q_e = \frac{K_{ads} \cdot C_e}{1 + K_{ads} \cdot C_e} \qquad \text{(Eq. 2.2)}$$

Where Q_e equals the percent coverage of metal ions on the surface, C_e is the concentration of metal in solution and K_{ads} is a constant. K_{ads} which is defined as the Langmuir isotherm constant predicts the driving force for the sorption process. It increases with the strength of adsorption.

The above equation is derived from the equilibrium of empty surface sites (S), metal in solution (M) and filled surface sites (SM):

$$S + M \leftrightarrow SM \qquad \text{(Eq. 2.3)}$$

Therefore the equilibrium constant K of the above equation is:

$$K = \frac{[SM]}{[S][M]} \qquad \text{(Eq. ?)}$$

Since the number of filled surface sites (SM) are directly proportional to Q_e, the number of empty surface sites is proportional to $1-Q_e$, and finally the metal in solution is proportional to the C_e, the equations can be written as:

$$K_{ads} = \frac{Q_e}{(1-Q_e)\, C_e} \qquad \text{(Eq. 2.4)}$$

This equation can be rearranged to yield equation 2.2.

Optimization of the Langmuir equation can be achieved by linear regression in this case particularly using the Langmuir linear regression. A Qmax term maybe added

to equation 2.2 to obtain an estimation of the theoretical quantity of surface sites available for sorption.

$$Q_e = \frac{Q_{max} K_{ads} C_e}{1 + K_{ads} C_e} \qquad \text{(Eq. 2.5)}$$

Therefore the Langmuir linear regression of equation 2.2 yields the following equation:

$$\frac{C_e}{Q_e} = \frac{C_e}{Q_{max}} + \frac{1}{Q_{max} K_{ads}} \qquad \text{(Eq. 2.6)}$$

The concentration of metal ions in solution at equilibrium is represented by Ce (mmol/g), while Qe (mmol/g) corresponds to the concentration of metal ions adsorbed onto the ion exchange resin. The slope of the straight line for the plot Ce/Qe vs. Ce allows for the calculation of Qmax, while the y-intercept equals $1/ Q_{max} K_{ads}$ and allows the determination of $K_{ads.}$ If the line proves to be non-linear, then either the sites are not independent of one another or the metal is occurring as colloids therefore not susceptible to true ion exchange reactions, it is also possible that precipitation of the metal has occurred. A linear relationship between the variables demonstrates non-cooperative binding of the metal at the surfaces sites at equilibrium.

The divinylbenzene crosslinked polystyrenes and SPCs that are to be compared must have similar metal sorption properties. The matrices of these two ion exchange resins are extremely different, and therefore were matched by similar metal chelating ligands. Four polystryrene resins were chosen: M-4195, XFS 43084, IRC-748 and Duolite. These materials have functional groups and metal selectivities similar to the SPCs CuWRAM, WP-2, and BPAP.

2.2 CuWRAM:M4195:XFS43084 Comparison

The first comparison was that of CuWRAM (Figure 2.1), a SPC developed in the Rosenberg group that is currently produced on an industrial scale, with Dowex M-4195 (Figure 2.2) and Dowex XFS-43084 (Figure 2.3). All three of these materials were designed with similar applications in mind, namely Cu^{2+}/Fe^{3+} separations and Ni^{2+}/Co^{2+} separation from acidic solutions (pH 0 to 2). The CuWRAM is a mixed silane linear polyamine platform further modified with 2-picolyl chloride, while the ligand on M-4195 is a divinylbenzene matrix that has been chloromethylated and functionalized with bis-picolylamine, and XFS-43084 has been functionalized with a 2-hydroxypropyl picolyl ligand. M-4195 and XFS-43084 proved to be the most closely related polystyrene analogs to CuWRAM.

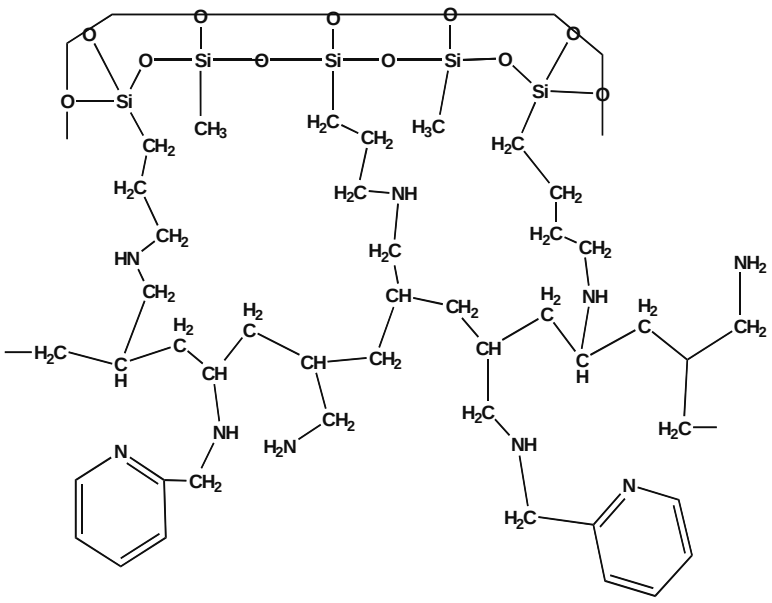

Figure 2.1: A proposed structure of CuWRAM; a picolylamine ligand supported by a silica polyamine matrix.

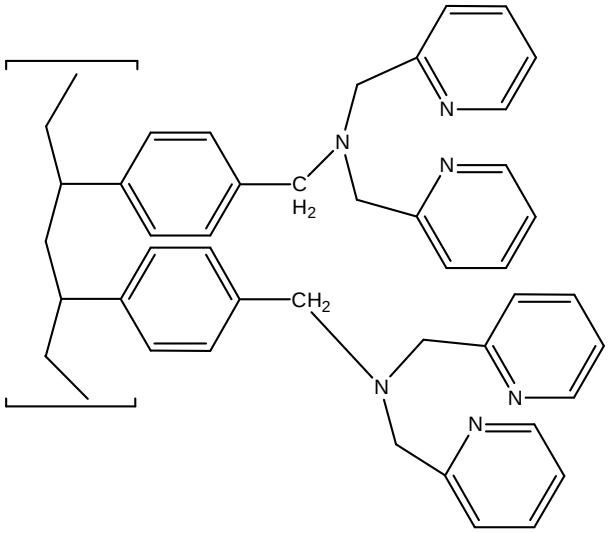

Figure 2.2: The chemical structure of Dowex M-4195.

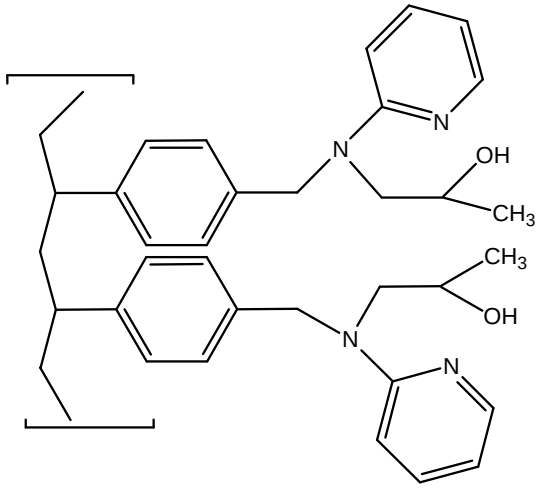

Figure 2.3: The chemical structure of Dowex XFS-43084.

Dowex M-4195 and CuWRAM were compared by performing both a copper-ferric and nickel-cobalt separation. These separations were performed under the recommended procedures for the polystyrene resins, which included a 20% dead space in the column to accommodate the shrink swell tendencies of the polystyrene in the breakthrough flow experiments. The SPCs do not require this dead space, but it was used to make the tests equivalent.

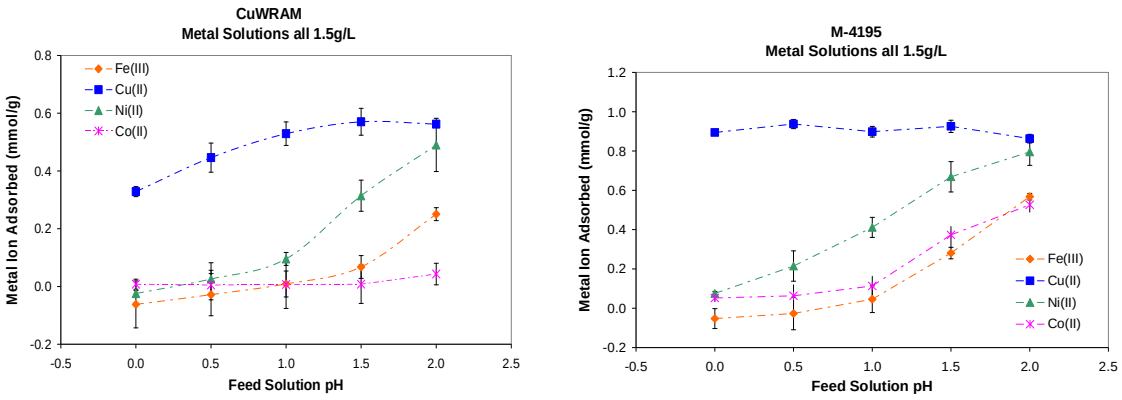

Figure 2.4: Left: Equilibrium pH batch profile for SPC CuWRAM. Right: Equilibrium pH batch profile for crosslinked polystyrene M-4195.

Equilibrium batch studies reveal the capacities of various metals for both CuWRAM and Dowex M-4195 (Figure 2.4). The studies show that Dowex M-4195 has a pH independent capacity of .85 mmol/g for copper, while this was not true for CuWRAM. It shows pH dependent capacities for copper ranging from .35 to .55 mmol/g as the pH increased from pH 0 to pH 2. The sorption capacities for Fe^{3+}, Ni^{2+} and Co^{2+} are very similar over the pH range studied. The pH independent capacity observed for copper with M-4195 suggests that copper will be difficult to strip. This will not be the case for Fe, Ni, Co, and Zn with M-4195 and for all the metals with CuWRAM.

The breakthrough experiments for the copper-ferric separation are performed with a metal solution containing 1 g/L copper and 4 g/L ferric with the pH adjusted to 1 using H_2SO_4. Figures 2.5 and 2.6 are the breakthrough curves for the copper-ferric separations, which were run at a rate of 1 mL per minute or .25 BV/min for both CuWRAM and M-4195.

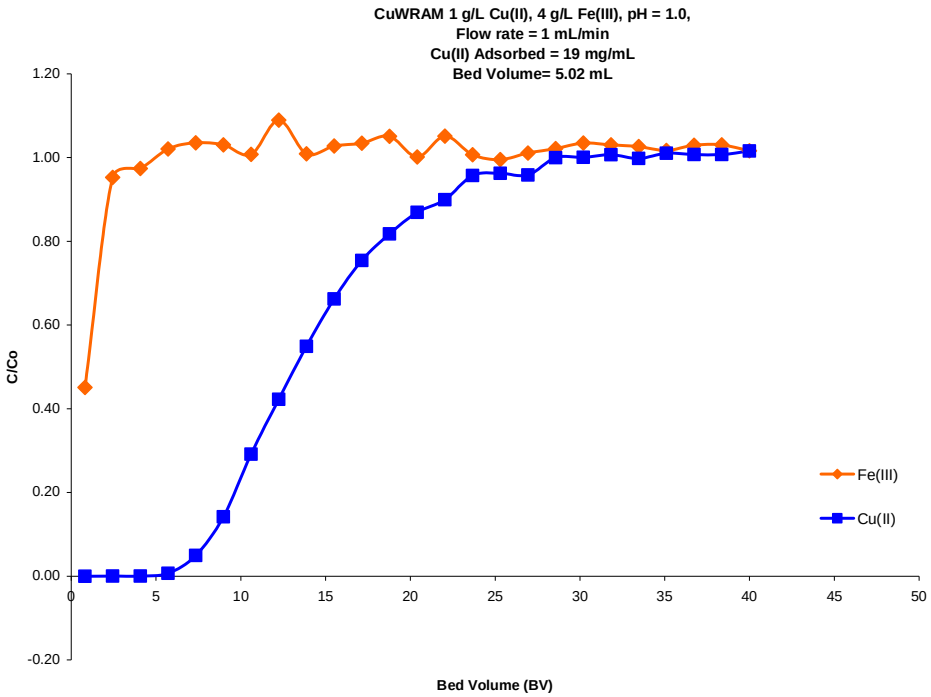

Figure 2.5: Copper-Ferric breakthrough curve for CuWRAM.

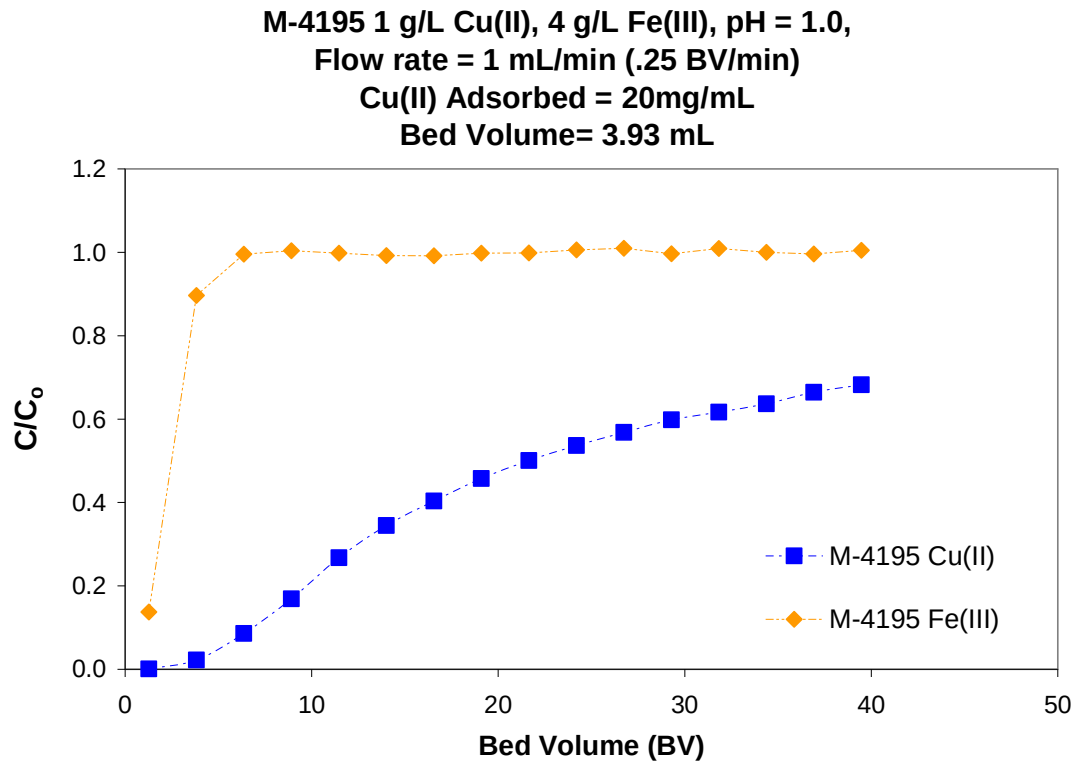

Figure 2.6: Copper-Ferric breakthrough for M-4195.

These breakthroughs demonstrate that both materials show iron rejection. However, it is also clearly apparent that the two materials are breaking at different points. CuWRAM begins to break at 12 bed volumes, while M-4195 breaks after only 4 bed volumes. It is also important to note that CuWRAM reaches full break (the point at with the affluent concentrations match that of the initial feed solution) at approximately 40 bed volumes, while M-4195 only reaches 60% of the original concentrations at 40 bed volumes. The breakthroughs clearly demonstrate the differences in the mass transfer kinetics of the two materials. The number of bed volumes required to reach fullbreak clearly depicts how fast the materials are removing the desired metal from solution at a particular flow rate. It is important to note that kinetics will improve for both materials if the flow rate is decreased. The slope of the breakthrough curve also demonstrates the superior mass transfer kinetics of CuWRAM over M-4195. The column utilization factor (Eq. 2.1) for each breakthrough displays the efficiency of the column.

CuWRAM U(for Figure 2.5) = 12/40= .30 (Eq. 2.3)

M-4195 U(for Figure 2.6) = 4/40+ < .10 (Eq. 2.4)

This shows that CuWRAM preformed greater than 3 times more efficiently than M-4195 in this copper iron separation. The curve is steeper in the CuWRAM breakthrough then the M-4195 breakthrough, meaning that the copper is loading on the column at a faster rate. The steeper slope also testifies to a cleaner separation of the two metal ions.

Separation of the two metals can be seen in the strip profiles (Figure 2.7).

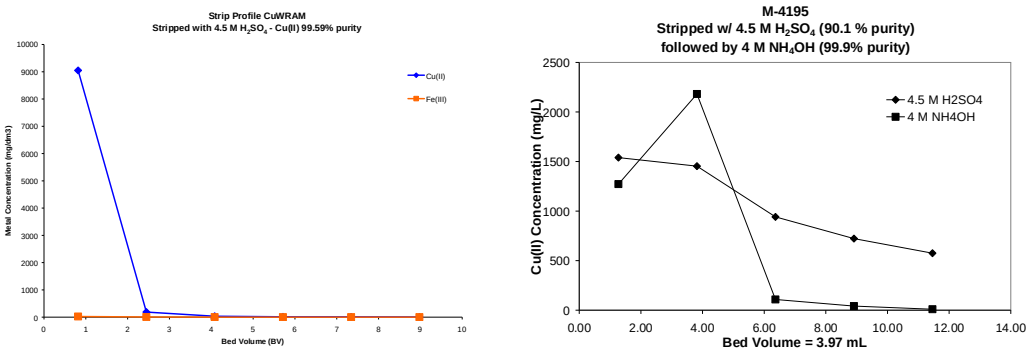

Figure 2.7: Strip Profiles for copper-ferric separations; left CuWRAM, right M-4195.

One can clearly see that Dowex M-4195 does not strip copper efficiently with only acid. It requires ammonium hydroxide to remove the remaining copper. It can also be noted that the purity of the acid strip was only 90.1%, which demonstrates that there is a 9.9% contamination of ferric. Yet when CuWRAM was used, the copper was completely striped with 4.5 M H_2SO_4 within 6 bed volumes, with a purity of 99.3%. The capacity for both materials proved to be 21 mg/ml after 40 bed volumes of copper-ferric solution was passed through the columns. These results suggest that if taken to full breakthrough, M-4195 would have a higher capacity but at the expense of very slow kinetics.

Since M-4195 has been shown to be effective in the separation of nickel from cobalt, it was deemed worthwhile to perform a nickel-cobalt separation using CuWRAM. The breakthrough curves for this separation of nickel at 1.5 g/L from cobalt at 1.5 g/L with pH 2 are shown in Figures 2.8 and 2.9. The strip profiles are shown in Figure 2.10.

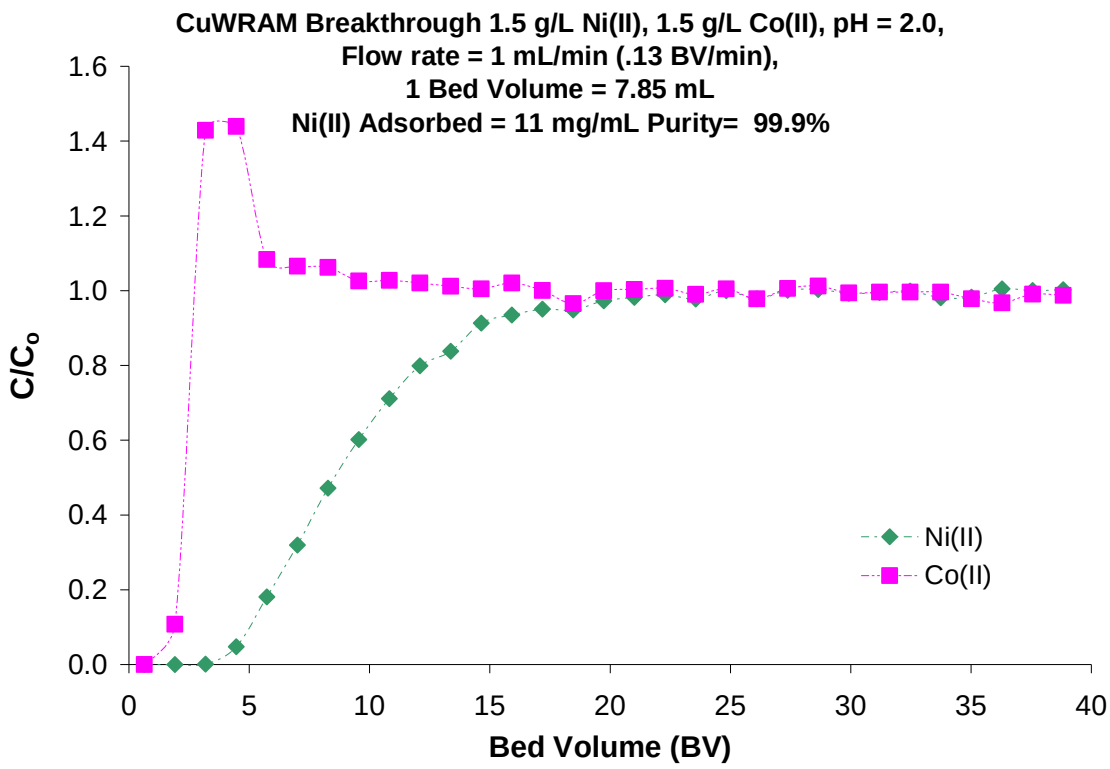

Figure 2.8: Nickel-Cobalt column separation using CuWRAM.

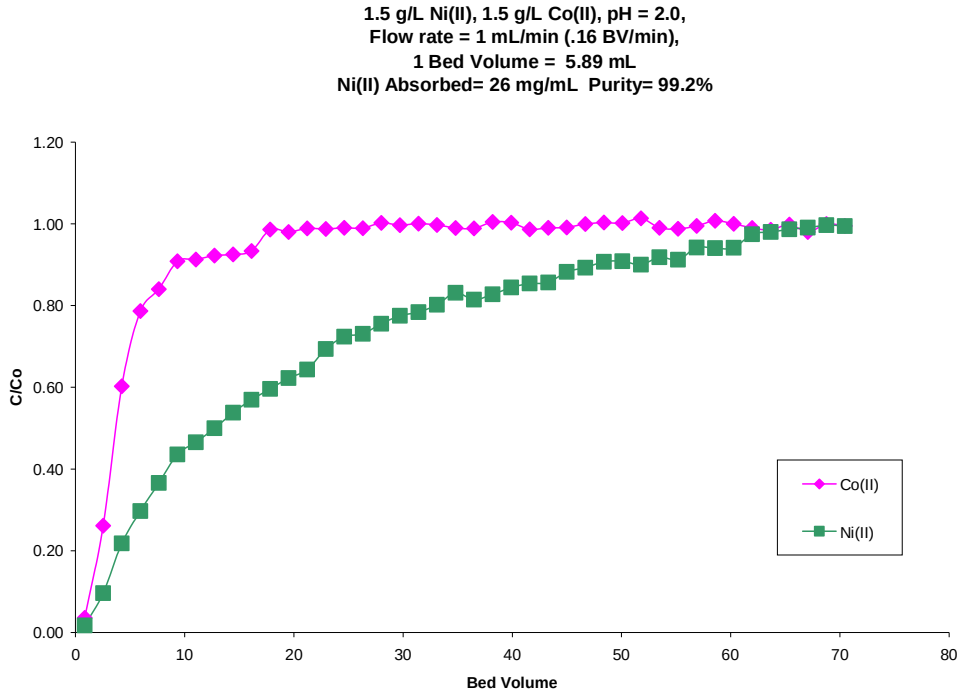

Figure 2.9: Nickel-Cobalt column separation using M-4195

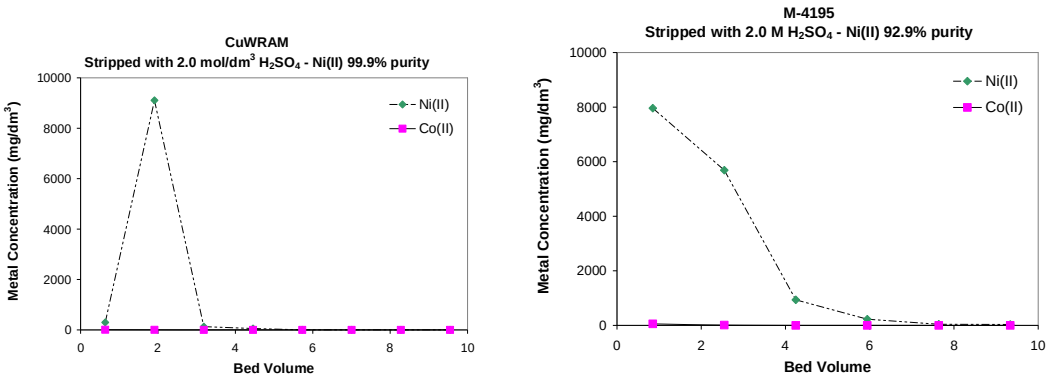

Figure 2.10: Strip Profiles for the Nickel-Cobalt separation, left: CuWRAM, right: M-4195.

Figures 2.8 and 2.9 show that at relatively high concentrations both materials break early, M-4195 almost immediately and CuWRAM after only 4 bed volumes. The strip profiles show similar purities for both CuWRAM and M-4195, but CuWRAM has a slightly higher purity of 99.9% than M-4195's 92.9%. The major difference is that while CuWRAM reached full break before 40 bed volumes, it took nearly 70 bed volumes for M-4195 to reach fullbreak. The purity of a strip for M-4195 after 40 bed volumes is only 92.3%, which means that purity improves significantly upon reaching full break. M-4195 has a capacity 2.5 times that of CuWRAM. This is due to the greater number of active sites per mL material for M-4195. Nickel requires an octahedral configuration, which is a coordination of 6. M-4195 has a tridentate ligand while CuWRAM has only a bidentate ligand explaining the large capacity of M-4195 to CuWRAM. This increased denticity and the greater number of active sites explain the difference in capacities. This difference is not seen with the copper separations because copper has a coordination number of 4 rather than 6, which is square planar. The copper does not require the tridentate ligand to efficiently bind. With the tridentate ligand in M-4195 the copper is binding too well and is not easily released.

The breakthroughs show that with both materials, cobalt is co-loaded and pushed off as more nickel is introduced to the column. This trend is more apparent with CuWRAM, where the cobalt spikes at 2 column volumes, whereas with M-4195, the cobalt is only slightly elevated in concentration later in the breakthrough and remains so until full break is reached. [21] Again this reflects the faster capture kinetics of CuWRAM.

Figure 2.11 depicts the batch kinetics for CuWRAM and M-4195. The graph on the left shows the adsorption of Cu^{2+} by each resin over a 24 hour period, while the graph on the right shows only the initial 250 minutes, in order to better view the sorption patterns of the two materials. M-4195 proves to have a higher capacity for copper than CuWRAM, but CuWRAM is achieving equilibrium at a faster rate. CuWRAM reached equilibrium around 50 minutes while it takes close to 400 minutes for M-4195 to reach equilibrium. This is due to the slower mass transfer kinetics of the polystyrene.

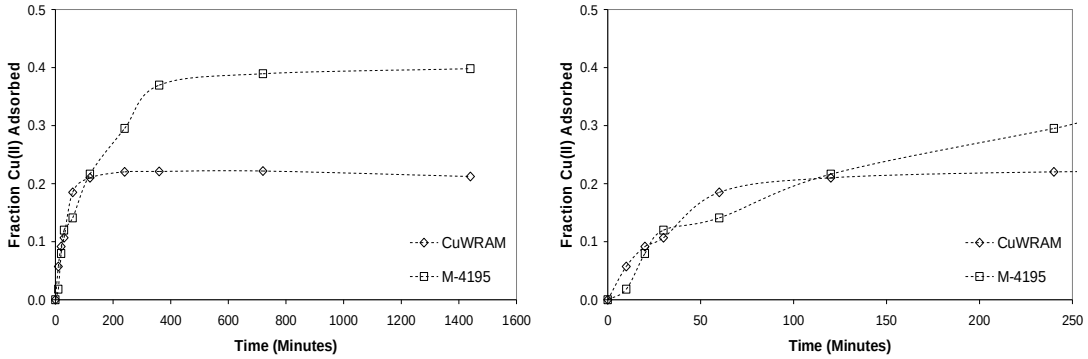

Figure 2.11: Batch Kinetics for CuWRAM and M-4195: Right 24 hours; Left first 250 minutes.

Due to the inability of M-4195 to strip copper, Dow developed a new resin Dowex XFS-43084, which contains a 2-hydroxypropyl picolyl ligand. Figure 2.12 is the pH batch profiles for XFS-43084, which can be compared to both M-4195 and

CuWRAM. The most apparent difference is that XFS-43084 does not have the pH independence that M-4195 did when loading copper. This is important for the stripping ability of the material. It can also be noted that XFS-43084 has little to no capacity for nickel, cobalt, and iron at pHs below 2, while at pH 2 the capacities increase significantly. The means that there may be better separations of copper from the other metals at pHs below 2 than with other materials. There is hardly any loading at pHs 0-.5 for copper, so there would not be efficient separations at the very low pHs ranges due to poor copper capacities.

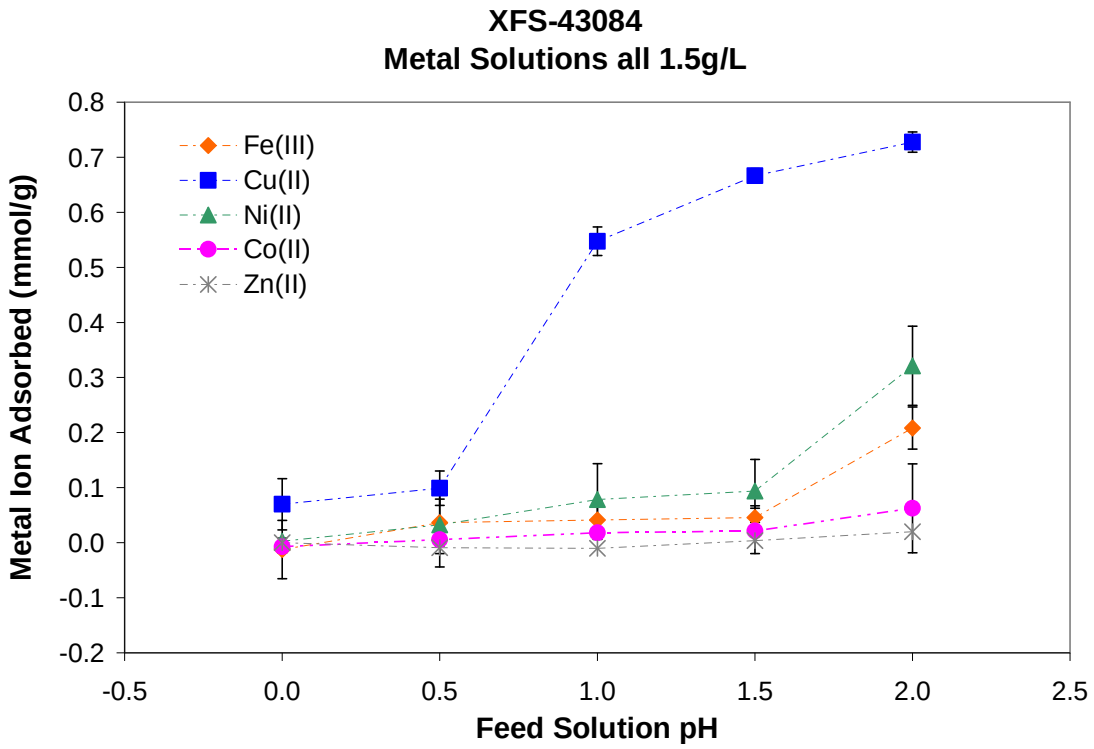

Figure 2.12: Equilibrium pH batch profile for XFS-43084.

Since M-4195 did not perform well for a copper-ferric separation, a breakthrough was preformed on a XFS-43084 column. The breakthrough was done with the same solution concentrations described previously. The bed volume was 5.89 mL and the flow

rate of 1 mL per minute or .17 BV/min, which is slower than the previous breakthroughs. Figure 2.13 shows the breakthrough curve. Once again it appears that polystyrenes have poor mass transfer kinetics. The copper is breaking within the first couple of bed volumes and does not reach full break until after 60 bed volumes, whereas U= 2/60= .03. Figure 2.14 is the strip profile for the copper-ferric separation. It shows that the separation is performed efficiently with a purity of 99.3% and a capacity of 17 mg/ml. While the separation purity is similar, CuWRAM has proven to have a higher capacity under these flow conditions.

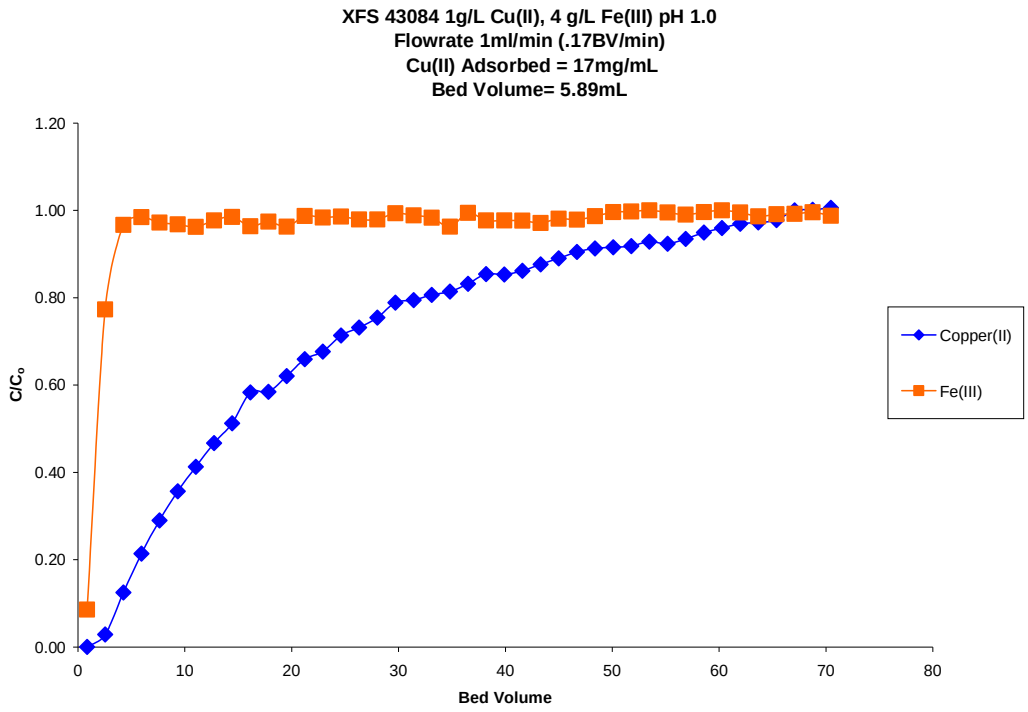

Figure 2.13: Copper-ferric breakthrough curve for XFS-43084

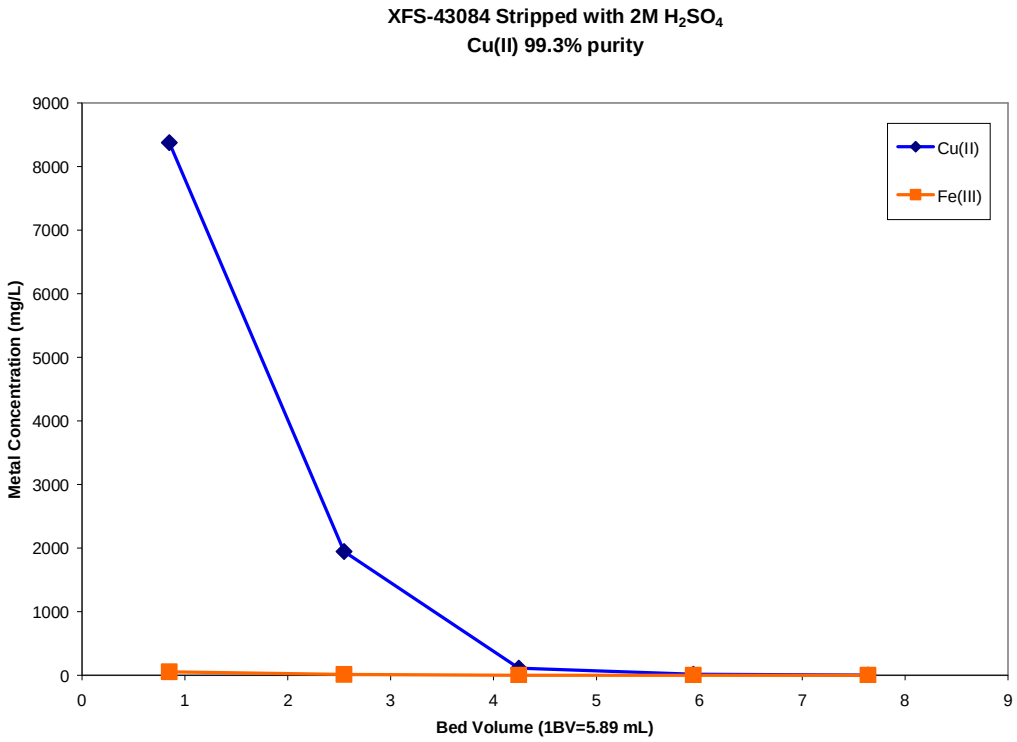

Figure 2.14: Strip profile for XFS 43084 copper-ferric separation.

Recently, CuWRAM has been used for copper-ferric separation in Australia, which has led to the discovery of a new difficulty. When chloride ion is present in addition to sulfate, there is significant retention of chloride. This is worrisome because the chloride is released from the column with the copper during the strip, then the copper is recovered via electrolysis. If chloride is present during the electrolysis, Cl_2 is produced and this is very hazardous. Armed with this knowledge, a breakthrough was performed that contained both copper chloride and copper sulfate. Following full break of the column, the column was rinsed with D.I. water to remove any residual metal solution. Then 40 mL of a saturated solution of sodium sulfate was passed through the column in hopes of replacing the chloride with sulfate. Analysis of the effluent showed a 67%

reduction of chloride on the column, meaning there was 23% retention of chloride in the case of CuWRAM.[22]

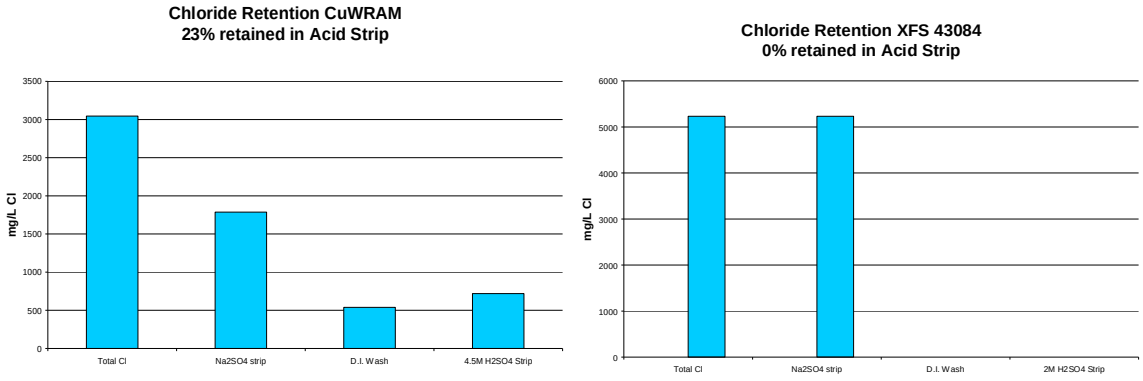

Figure 2.15: Chloride retention data; left CuWRAM, right XFS-43084

The same breakthrough procedure was preformed on XFS-43084 to see if the polystyrene had the same problem. The XFS-43084 proved to have no retention of chloride after being washed with the saturated sodium sulfate. The differences in chloride retention between the two materials can be seen in Figure 2.15. The reasons for the differences in chloride retention between the two materials are not readily apparent. It could be due to the presence of the 2-propanol (Figure 2.3) or due to the difference in the backbone matrixes. The only way to tell would be to produce a SPC that is directly analogous to XFS-43084. Other ways to fix this issue with CuWRAM may be to wash the column with higher volumes of saturated sodium sulfate in hopes of pushing all of the chloride off, or to use a hot sodium sulfate solution in hopes that the heat would speed up the chloride sulfate exchange.

Figure 2.16 illustrates the concentration isotherms for CuWRAM, M-4195 and XFS for Cu^{2+}. It is immediately clear that all of the resins function similarly at low Cu^{2+} concentrations, in essence removing the same amount of Cu from solution until about 7.5

mmol of Cu. It is at 7.5 mmol that one is able to see a trend; M-4195 removes the most Cu^{2+}, while XFS follows and CuWRAM removes the least amount of Cu^{2+}. This trend clearly shows that CuWRAM has the lowest copper capacity at high concentrations, due to its lower surface area. It is also noted that CuWRAM and XFS reach equilibrium (maximum capacity) around 10 mmol, while M-4195 never reaches full capacity within the 20 mmol range. This demonstrates that M-4195 has more chelating sites available when compared to CuWRAM and XFS.

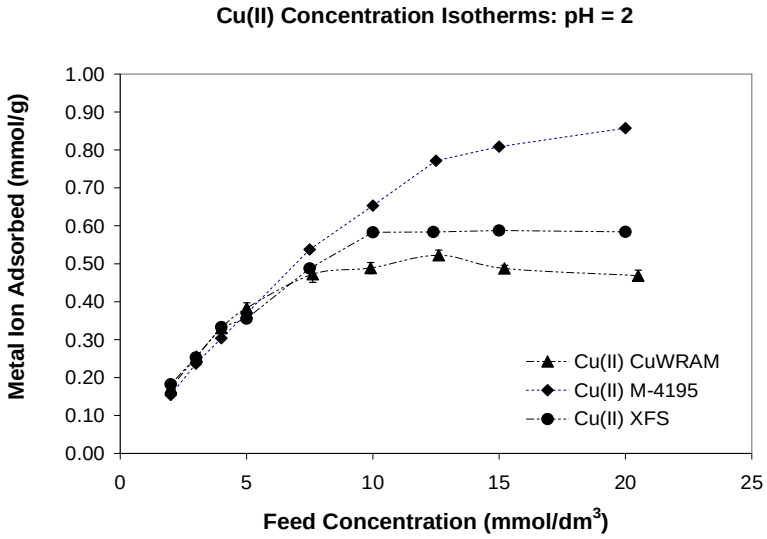

Figure 2.16: Concentration dependent sorption isotherms for Cu^{2+} onto CuWRAM, M-4195 and XFS at pH 2.

Figure 2.17 illustrates the concentration isotherms for CuWRAM and M-4195 with respect to Ni^{2+} sorption. Since XFS is not commercially used for Ni sorption an isotherm was not conducted. In Figure 2.17 it is readily apparent that M4195 has a higher capacity for nickel than CuWRAM does. This is due to an increased number of functionalized ligands on M-4195 and also due to the coordination of the nickel ion. M-4195 is tridentate, while CuWRAM is only bidentate and can not as easily support the octahedral coordination nickel prefers.

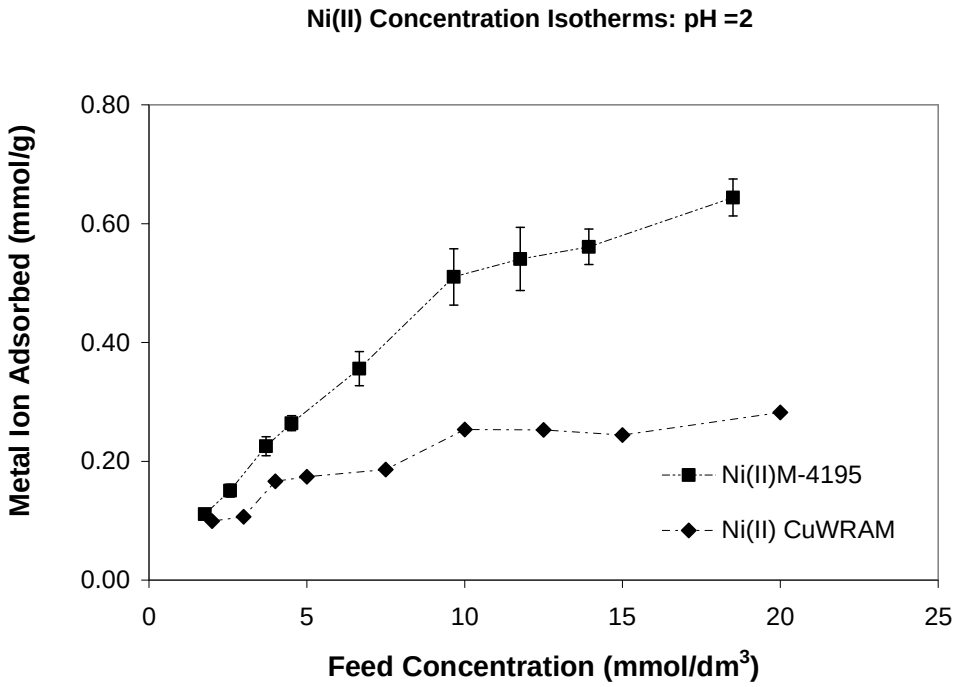

Figure 2.17: Concentration dependent sorption isotherms for Ni^{2+} onto CuWRAM and M-4195 at pH 2.

The Langmuir plot (Figure 2.18) was constructed from the concentration isotherms using Equation 2.2. Table 2.1 lists the Langmuir parameters derived from the Langmuir plot. A linear correlation with the Langmuir model indicates monolayer and non-cooperative sorption by the resins. As seen in Table 2.1 all R^2 values are .93 and above, demonstrating great correlation with the Langmuir model. The model also provides information regarding the intensity of the sorption process (Kads) and also an approximation of the theoretical number of sorption sites on the surface (Qmax). CuWRAM proves to have a similar intensity of adsorption for both copper and nickel, while M-4195 has approximately twice the adsorption intensity for copper over nickel. XFS has a very high Kads value and could in respect have the highest intensity of sorption of copper of all three of the materials. One can easily see that the theoretical

number of sorption sites on CuWRAM greatly decrease from copper to nickel sorption (Qmax Cu= 1.46 vs Qmax Ni = .313).

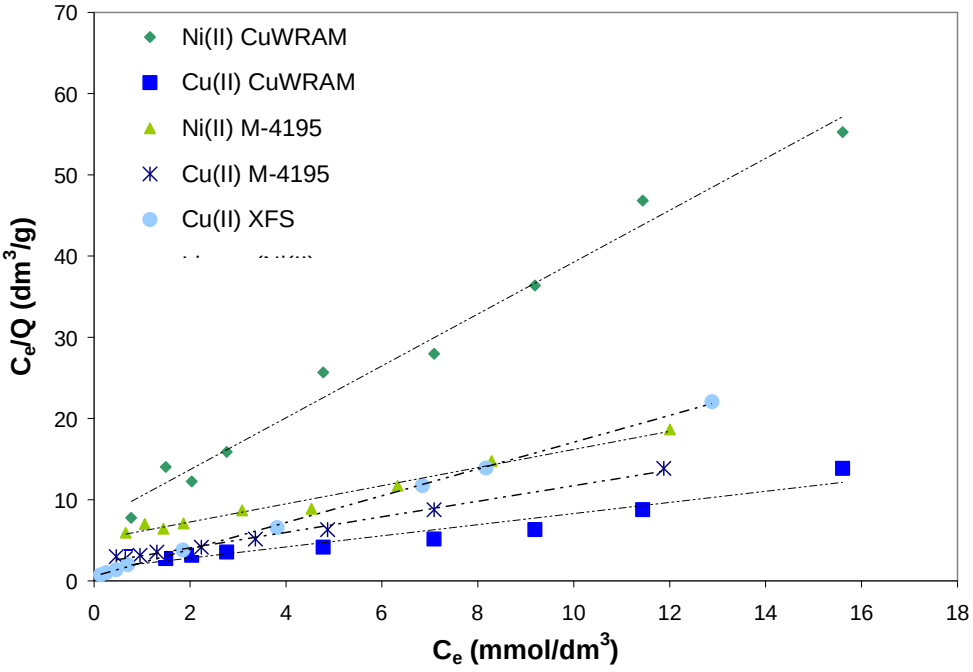

Figure 2.18: Langmuir Plot developed from Cu^{2+} and Ni^{2+} concentration dependent isotherms.

Table 2.1: Langmuir parameters for CuWRAM, M-4195 and XFS.

		Rmax[a]	
Metal	CuWRAM	M-4195	XFS-43084
Cu(II)	1.46	1.04	0.6064
Ni(II)	0.313	0.8965	-
		Kads[b]	
	CuWRAM	M-4195	XFS-43084
Cu(II)	0.4799	0.4479	2.848
Ni(II)	0.4373	0.2218	-
		R^2	
	CuWRAM	M-4195	XFS-43084
Cu(II)	0.93	0.99	0.99
Ni(II)	0.98	0.98	-

a mol of M(II)/g of adsorbent *b* M^{-1}

2.3 WP-2 and Amberlite IRC 748

The second comparison performed was between WP-2 (Figure 2.19) and Amberlite IRC-748 (Figure 2.20). Both of these materials contain amino-acetate. With WP-2, the amino-acetate is on a branched polymer, allowing for possible multi-dentate binding of metals. With Amberlite IRC-748, the ligand is diamino-acetate allowing for tridentate binding of metals.

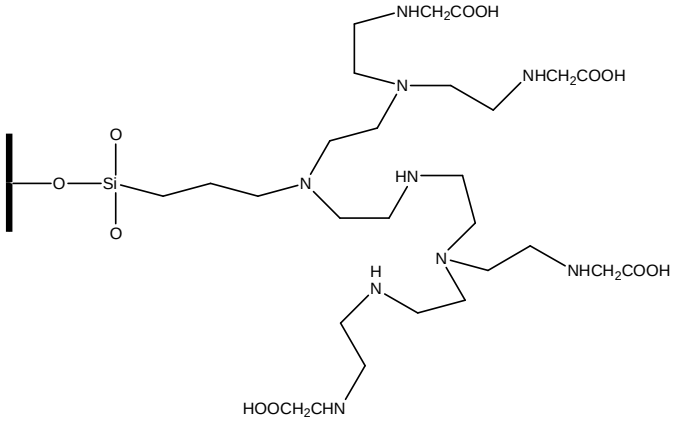

Figure 2.19: A proposed chemical structure of WP-2.

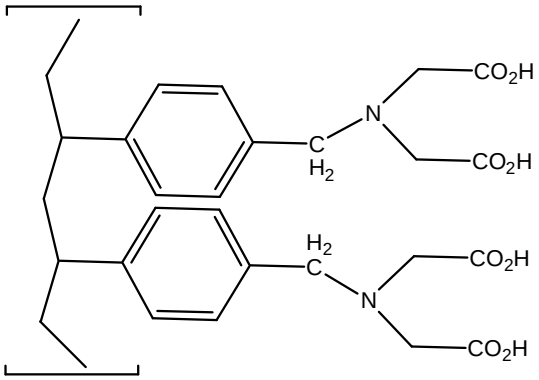

Figure 2.20: The chemical structure of Amberlite IRC-748.

Copper-nickel separations at low pH have been increasingly important in the mining industry over the past years. The SPC material that shows promise for such separations is WP-2. WP-2 is a mixed silane branched polyamine composite modified

with an amino acidic acid functional group. The closest related polystyrene is IRC-748, a divinylbenzene matrix modified with amino diacetic acid as the functional group.

Figure 2.21 shows the pH batch profiles for each material. From these profiles one can see where the best copper-nickel separation may be for both materials, which appears to be around pH 1. A breakthrough containing 1g/L Cu and 1g/L Ni at pH 1 was performed on both WP-2 and IRC-748 (Figures 2.22 and 2.23).

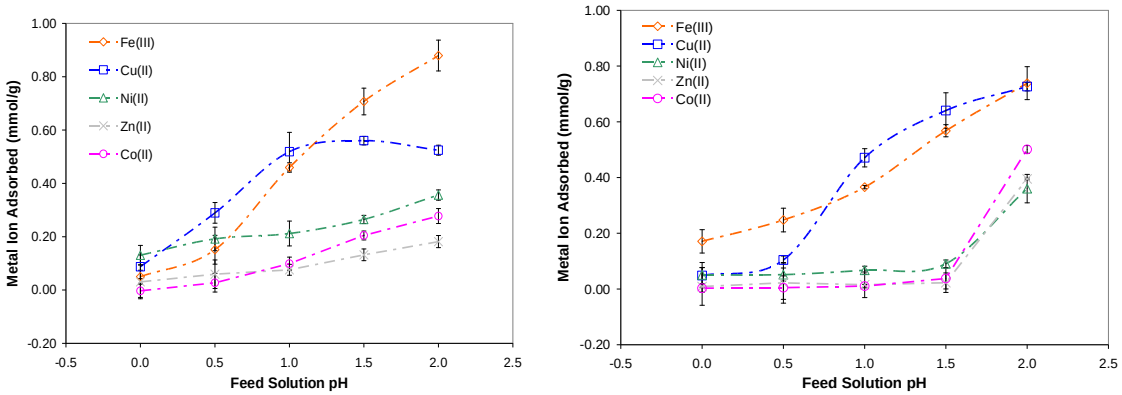

Figure 2.21: Equilibrium pH batch profiles; left WP-2, right IRC-748.

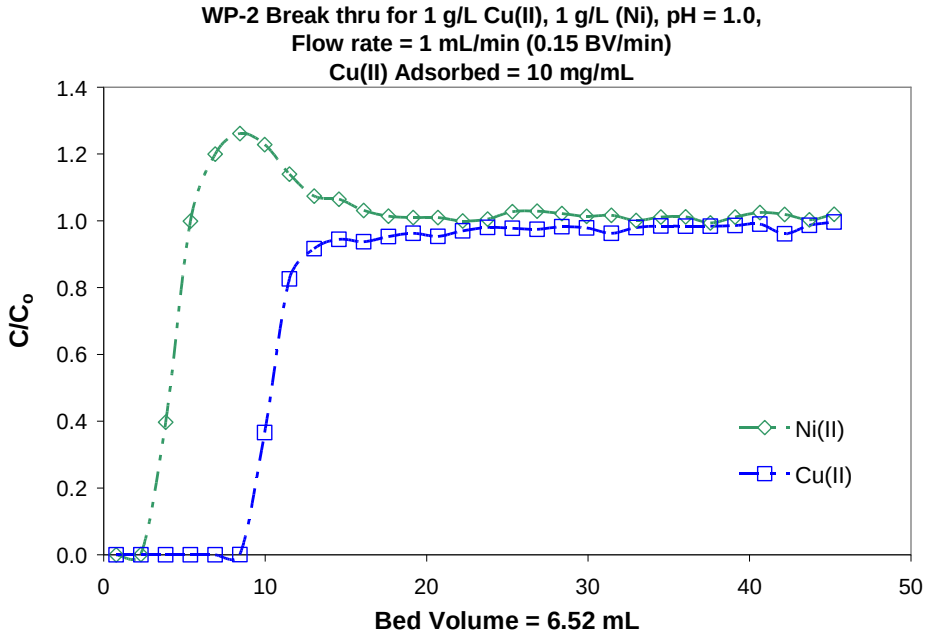

Figure 2.22: WP-2 Copper-Nickel breakthrough curve. U= 8/14= .57

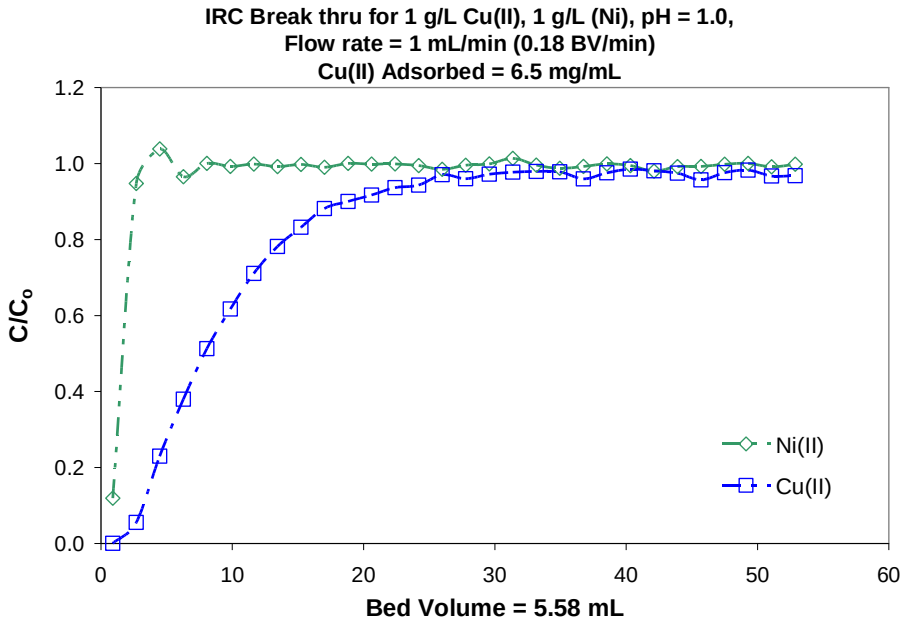

Figure 2.23: IRC-748 Copper-Nickel breakthrough curve. U=2/23= .09

One can see that in these breakthroughs copper is breaking in the first couple of bed volumes, while WP-2 takes 9 bed volumes before the copper begins to break. This once again demonstrates the superior mass transfer kinetics of SPCs over polystyrenes. The strip profiles (Figure 2.24) show that both materials strip efficiently within 4 bed volumes, but that WP-2 has a slightly lower purity than IRC-748.

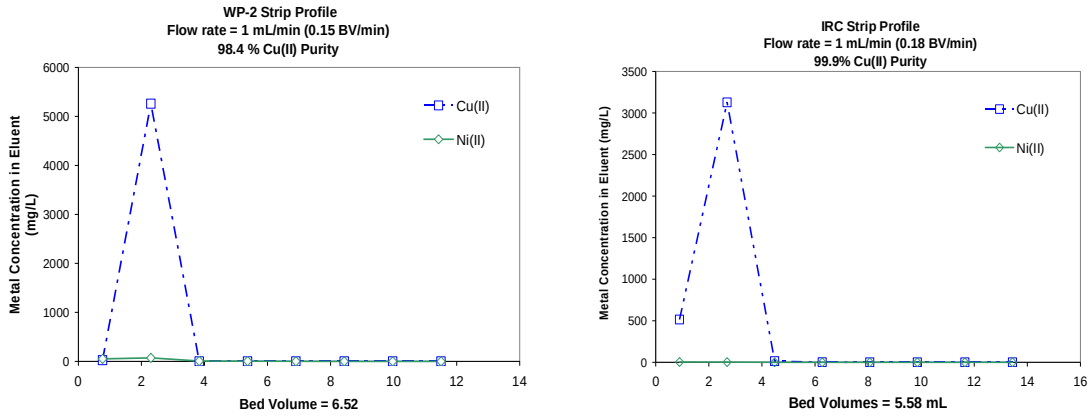

Figure 2.24: Strip Profile for Copper-Nickel separation; left WP-2, right IRC-748.

There is also a difference in capacity for these two materials. IRC-748 loads 6.5 mg/ml while WP-2 has a capacity of 10 mg/mL. These capacities can also be noted in the equilibrium batch capacities, where WP-2 has .55 mmol/g copper capacity at pH 1, while IRC-748 has .48 mmol/g copper capacity at pH 1. This higher capacity at pH 1 is due to the branched nature of the PEI polymer that provides additional coordination sites via modified and unmodified amines.

Figure 2.25 depicts the batch kinetics for WP-2 and IRC of Cu^{2+} sorption at pH 2. The left graph shows the entire 24 hours while the right graph demonstrates the initial 250 minutes. During the first 250 minutes the differences in kinetics can best be observed. WP-2 quickly adsorbs Cu^{2+} and reaches equilibrium within 50 minutes. IRC adsorbs Cu^{2+} at a slower rate and does not reach equilibrium until approximately 400 minutes. In fact IRC is capturing less copper than WP-2 until just after 200 minutes, so while IRC has a higher total capacity, WP-2 performs better on shorter time scales. This demonstrates the superior mass transfer kinetics of SPCs.

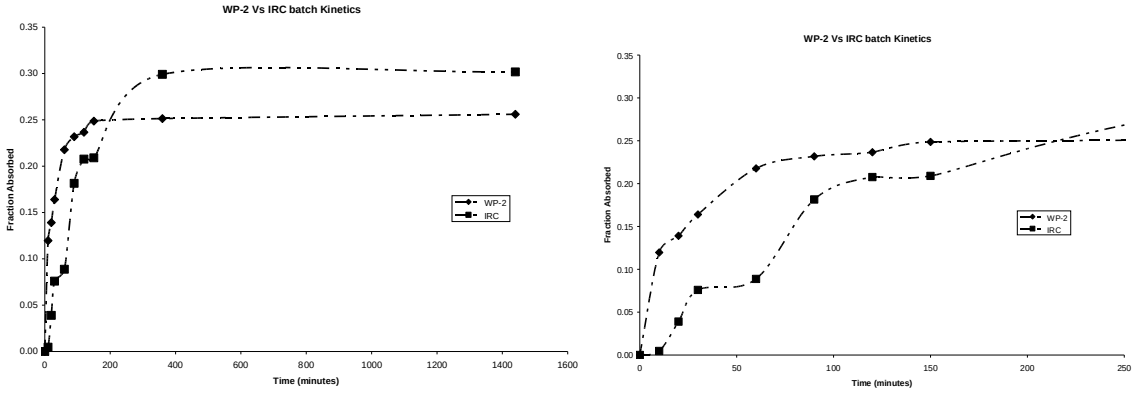

Figure 2.25: Batch Kinetics of WP-2 and IRC-748

Figures 2.26 and 2.27 illustrate the concentration isotherms for Cu^{2+} and Ni^{2+} for ion exchange resins WP-2 and IRC-748. While WP-2 has higher copper capacity for in

the copper isotherm, IRC appears to have higher nickel capacity at higher molar concentrations than WP-2.

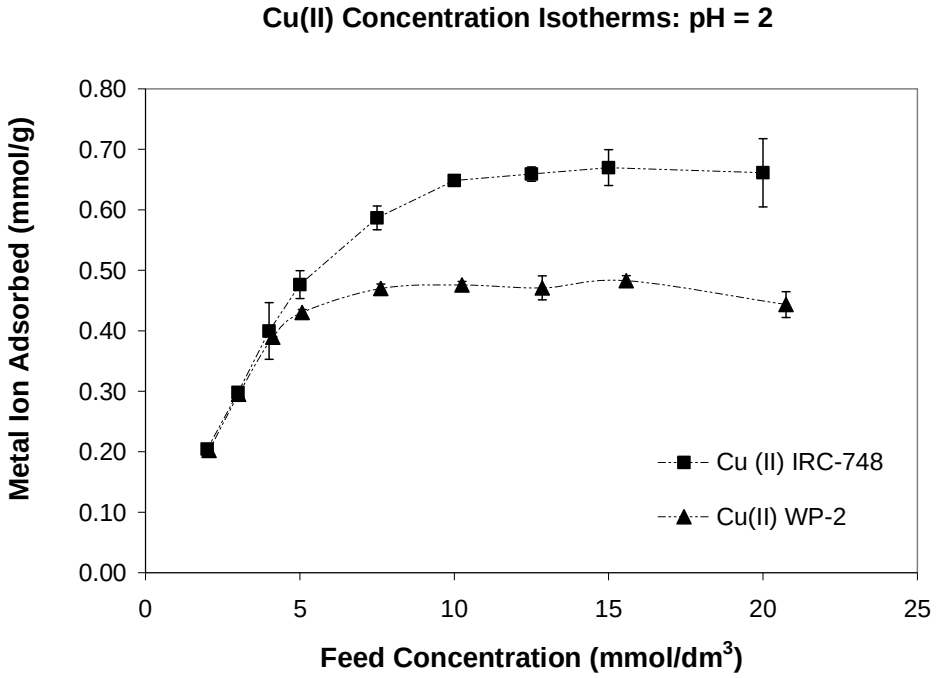

Figure 2.26: Cu concentration dependent isotherms for WP-2 and IRC at pH 2.

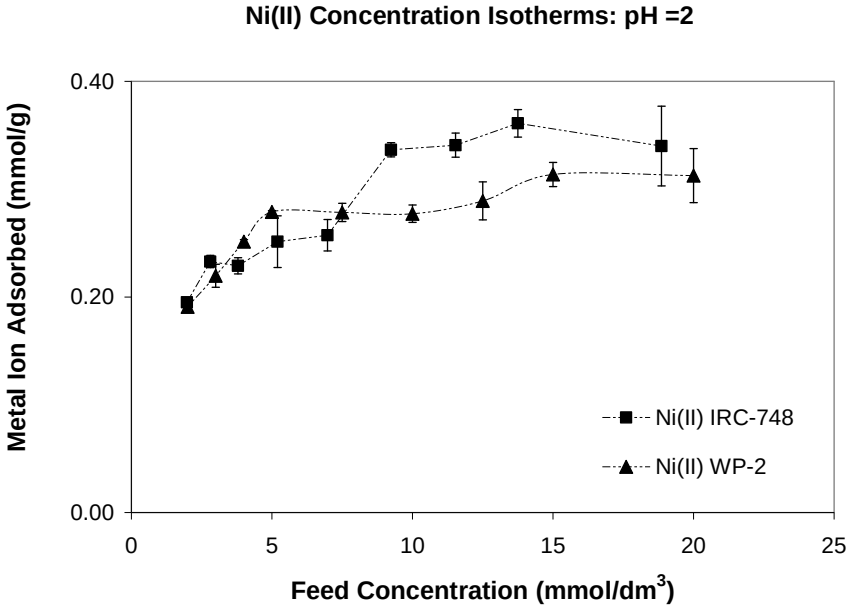

Figure 2.27: Ni^{2+} concentration dependent isotherms for WP-2 and IRC at pH 2.

Figure 2.28 is the Langmuir plot constructed from the copper and nickel WP-2 and IRC concentration isotherms using Equation 2.2. Table 2.2 lists the parameters derived from Figure 2.28. The high R^2 values demonstrate non-cooperative and monolayer sorption for both resins. IRC proves to have a larger Qmax, but smaller Kads than WP-2. This demonstrates that IRC has a higher number of theoretical sorption sites than WP-2, but that the WP-2 adsorption process is more intense and occurring at a faster rate than IRC's.

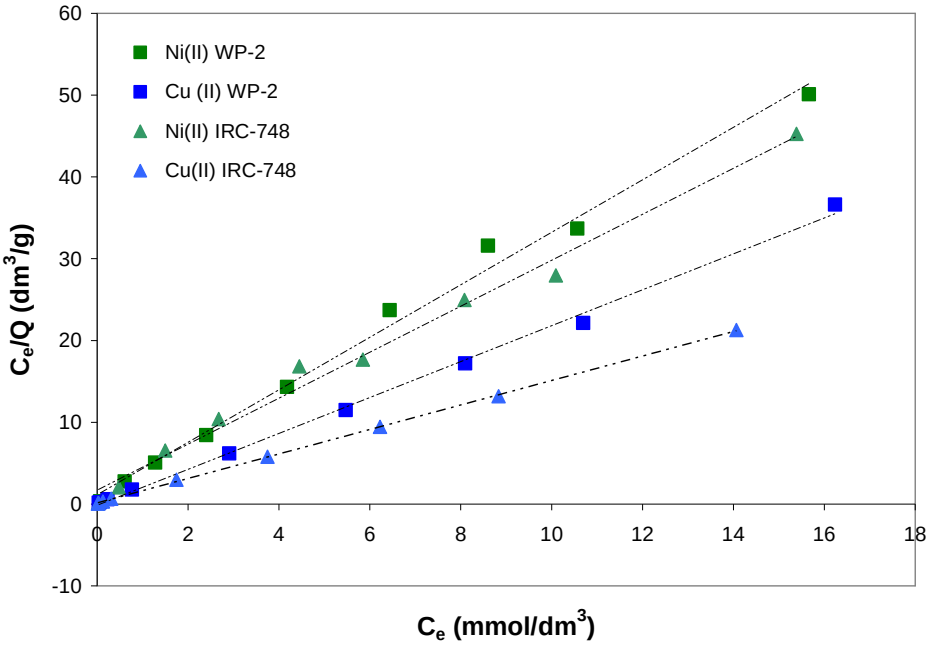

Figure 2.28: Langmuir Plot developed from Cu^{2+} and Ni^{2+} concentration dependent isotherms of WP-2 and IRC.

Table 2.2: Langmuir Parameters of WP-2 and IRC.

	Qmax[a]		Kads[b]		R^2	
Metal	WP-2	IRC	WP-2	IRC	WP-2	IRC
Cu(II)	0.4555	0.6682	15.314	10.649	0.9975	0.9998
Ni(II)	0.3116	0.3558	2.809	1.6399	0.9927	0.9863

a mol of M(II)/g of adsorbent *b* M^{-1}

2.4 BPAP and Duolite Comparison

The third comparison of an SPC and a polystyrene chelator resin was made between BPAP (Figure 2.29) and the Duolite resin (Figure 2.30). These resins are direct analogs of each other; they both contain methylamine phosphonic acid. Previous studies with BPAP show that it is selective for iron(III) but is difficult to strip the iron from the column. Previous studies have shown that both BPAP and Duolite have affinities for tri-valent metals.[32,46]

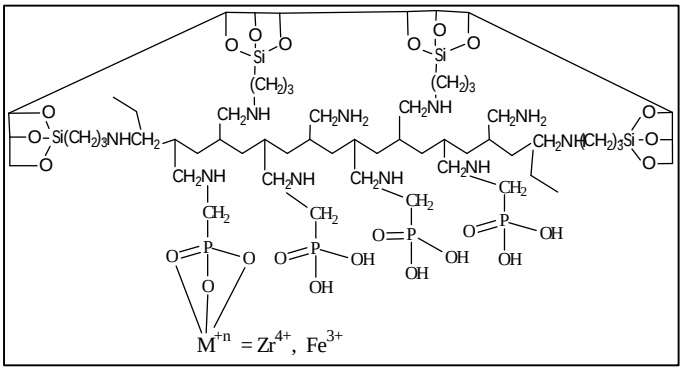

Figure 2.29: The proposed structure of BPAP.

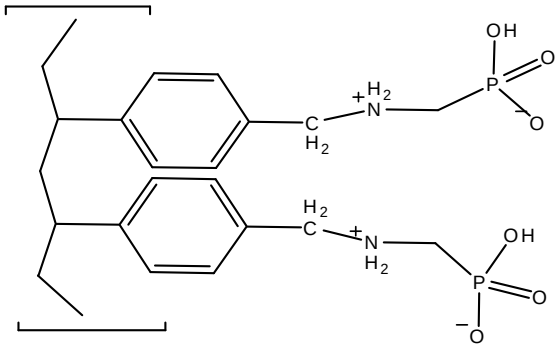

Figure 2.30: The chemical structure of Duolite.

Since is it is known that both BPAP and Duolite resins both have a high affinity for higher valance metals, batch tests where conducted on metals from the f-block.

Figures 2.31 and 2.32 show the sorption trends for the different f-block metals tested. Even though the resins contain the exact same functional groups, both resins show entirely different trends. First BPAP is fairly pH independent with regard to metal sorption as pH increases: while Duolite is pH dependent, as the pH increases so does capacity. f-Block metals consist of lanthanides and actinides, which are very similar to each other, even more so than transition metals. Lanthanides and actinides prove to be extremely difficult to separate. Of the metals tested europium, cerium and lutetium are lanthanides, while thorium and uranium are actinides. Separation of these metals is important in the purification of uranium for nuclear power. BPAP appears to have different capacities for all 5 of the metals tested, while Duolite has similar capacities for all of the lanthanides and little capacity for the actinides. The metal pH dependency of Duolite may prove to be beneficial in recovery of f-block metals; this demonstrates that stronger acids may strip the absorbed metal from the resin. This is not true for BPAP. Due to the independent pH sorption trend it maybe difficult to effectively recover the f-block metals with acid, therefore other means must be sought.

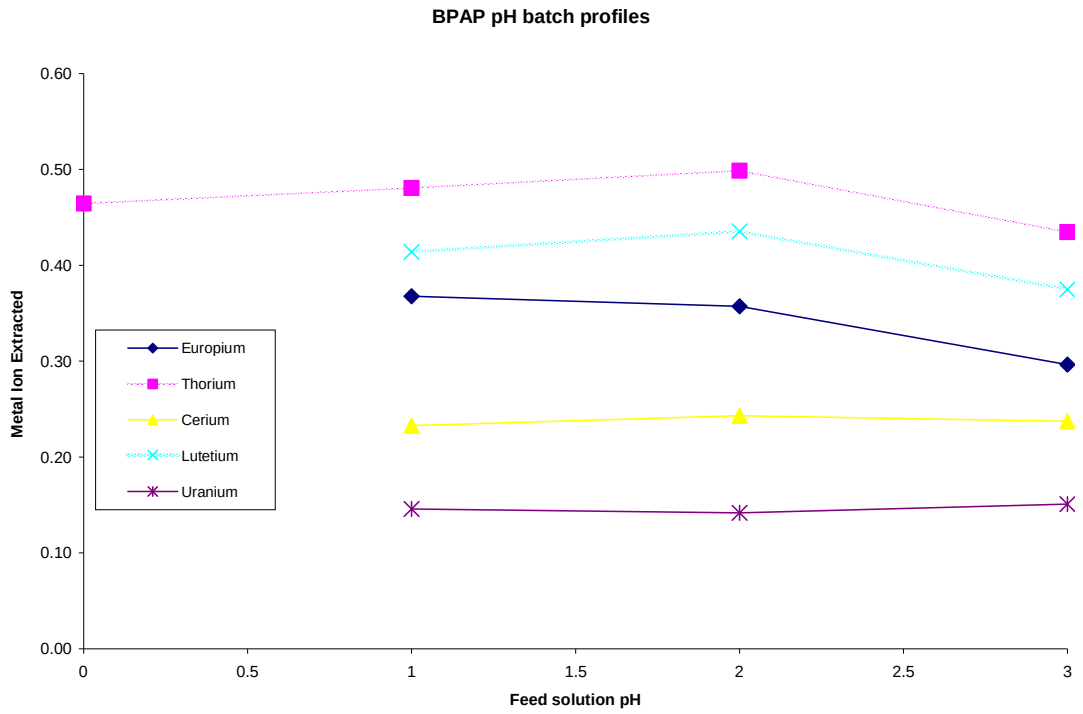

Figure 2.31: pH profile of f-block metals absorbed on BPAP.

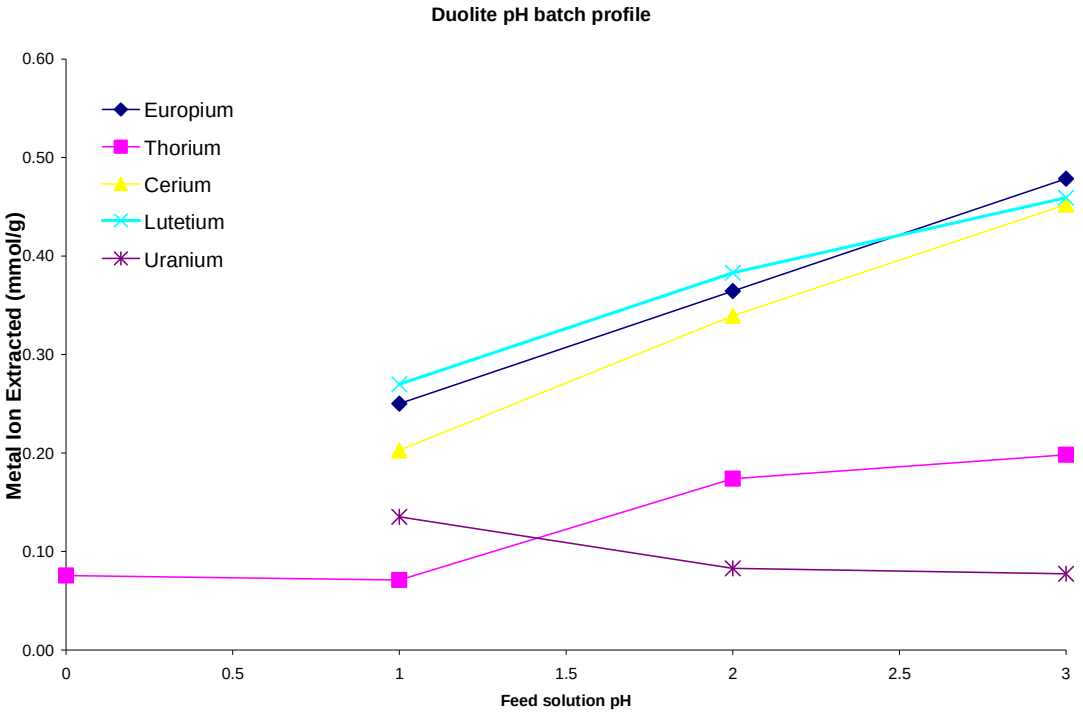

Figure 2.31: pH profile of f-block metals absorbed on Duolite.

2.5 Conclusions

In general, the data have consistently shown that SPCs have significantly better mass transfer kinetics then their polystyrene analogs. This is significant because with higher mass transfer kinetics, faster flow rates can be used in an industrial setting. This means that larger volumes of solution can be processed in a shorter amount of time. The SPC breakthroughs have also shown that purities of the metal separations are similar or better than those achieved by polystyrenes. While the capacities are often higher in equilibrium settings, they are remarkably close in flow situations. The only notable difference is with the nickel capacity of CuWRAM and M-4195 due to the binding properties of nickel.

There is also a significant benefit from the fact that SPCs do not require a 20% dead space in the column. The shrink swell tendencies of polystyrenes lead to poor column utilization. Since no dead space is required with SPCs, the columns can be completely packed and the entire column can therefore be utilized. This means that even though polystyrenes have higher capacities in mg/mL, better capacities per column can be achieved since more SPCs can be used in each column compared to polystyrene in the same size column.

The question is whether these two types of ion exchange materials meet the criteria for effective metal extraction systems. The first criterion is that the system must have high metal ion sorption capacity. Both the polystyrenes and SPCS in this study have reasonable capacities for certain metals of value. The polystyrenes prove to have slightly higher equilibrium capacities but the SPCs tend to show higher flow capacities.

The second criterion is that the system must be able to selectively remove one metal ion from a mixture of metal ions at high purities. Once again, the polystyrenes and SPCs have both met this criterion. Purities for both systems are above 90% in all of the multi-component separations preformed on the materials, which demonstrates not only the high purities but also the effectiveness of the separations of the metal solutions.

The third criterion is that the system must be operational across a pH range. With SPCs the operational pH range is 0 to 10, but the pH can not exceed this range due to the fact that more basic solutions will dissolve the silica. Polystyrenes are stable over a larger pH range, 0 to 14. Both systems appear to have a broad range of operational pHs, so they have met this criterion.

The fourth criterion is that the system must reduce the metal ion concentrations in effluent to very low levels. The breakthroughs have shown that SPCs remove the metal ions from solution completely for a number of bed volumes at moderate flow rates. Polystyrenes show earlier breaks: in most cases, metal is released within two bed volumes. SPCs outperform polystyrenes on this criterion.

The fifth criterion is that these systems must have long life times. Previous studies have shown that SPCs and polystyrene resins can last 1000 plus cycles without losing capacity.[31]

The sixth criterion is that the system must have favorable mass transfer kinetics to allow high throughputs. This is the criterion where SPCs far outperform polystyrenes. The data have shown continuously that SPCs have significantly better mass transfer kinetics in flow situations. This allows for faster flows and cleaner separations.

The final requirement is that the system must be economically viable. While the initial cost of introducing such systems may be expensive, the extended lifetimes of the materials help to eliminate that cost over time. These systems are also efficient in recovering valuable metals that are hazardous. These systems allow for not only the removal, but also the recovery of these valuable metals, increasing the profit margin due to the ever rising demand for such metals.

The data have clearly shown that SPCs are an efficient metal recovery/extraction system. They have met and exceeded the criteria important in such systems. While this is mostly true for a crosslinked polystyrene based system, they appear to lack the essential mass transfer kinetics that are required for high throughputs and clean efficient separations.

2.6 Future Work

Such comparisons studies will be carried out following the development and synthesis of both new polystyrene resins and SPCs. This will allow the feasibility of both products in the industrial market for remediation purposes. Current studies are under investigation into to the use of SPCs to filter and efficiently remove viruses and bacteria from aqueous media. Furthermore, studies are being performed as to the feasibility of using SPC platforms for surface bound catalysts.

Chapter 3: Identifying a New Reactive Pathway to CuWRAM

3.1 Introduction

In an attempt to make a direct analog to the polystyrene M-4195 which contains a bispicolyl ligand, as the metal chelating ligand a new pathway to the production of CuWRAM was discovered. CuWRAM is a silica polyamine composite modified with picolyl chloride. Using a reductive amination pathway[47], a new composite was made that exhibits characteristics similar to that of CuWRAM. This reaction relies on the selectivity of the reducing agent $NaHB(OAc)_3$. The reaction of the aldehyde and the amine form an imine which is then reduced by the reducing agent. This new composite has currently been labeled CuWRAM1 due its similarities with the industrially produced CuWRAM.

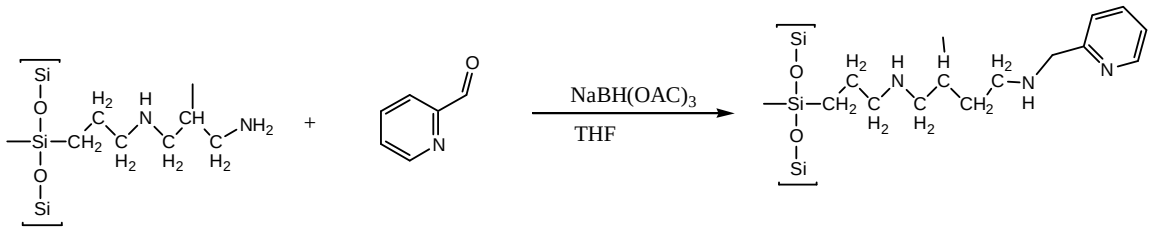

(Eq. 3.1)

3.2 Results and Discussion

In order to better understand the sorption characteristics of the new composite batch equilibrium studies were performed. Figures 3.1 and 3.2 depict the batch equilibrium capacities for Cu(II), Ni(II), Co(II), Zn(II), and Fe(III) over a pH range of 0 to 2 for CuWRAM1 and CuWRAM.

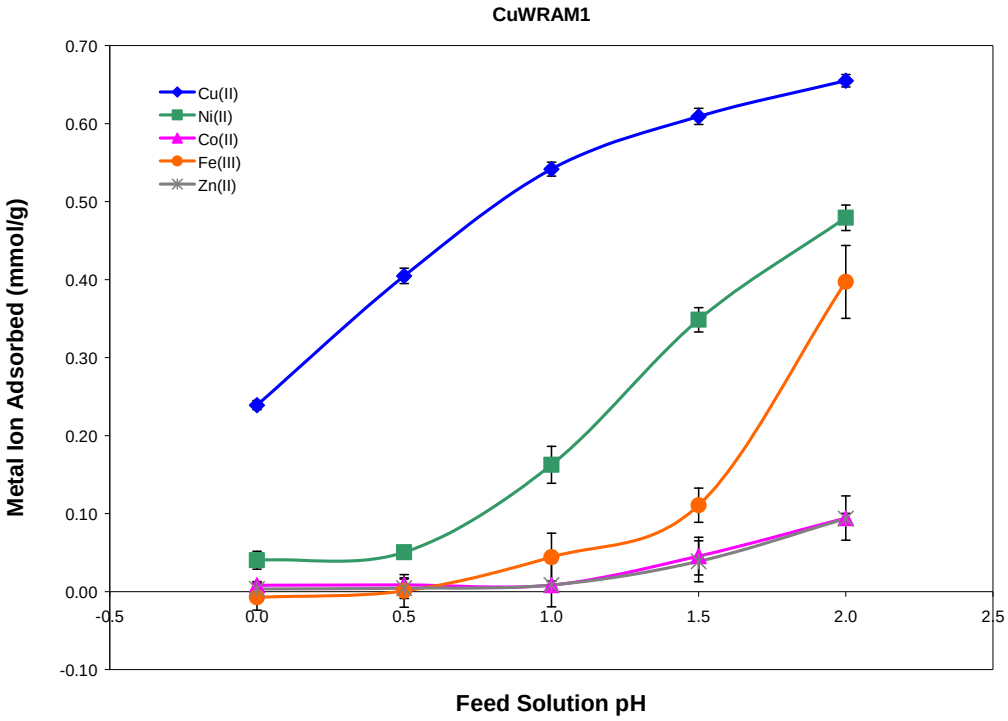

Figure 3.1: pH batch profiles of CuWRAM1.

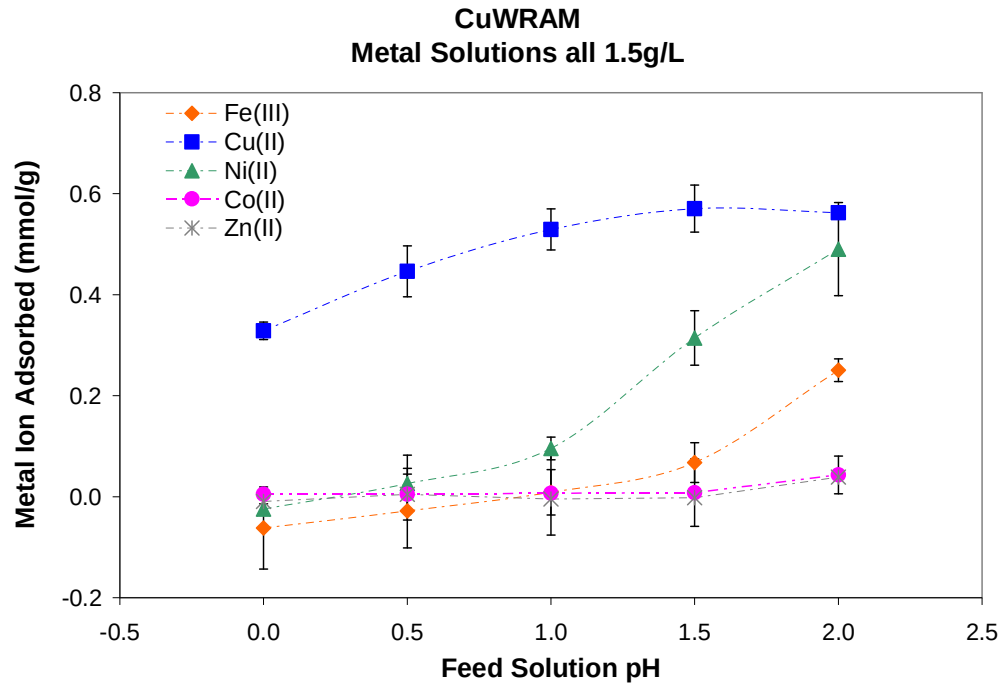

Figure 3.2: pH batch profiles of CuWRAM.

The profiles are remarkably similar, leading one to conclude that the two composites are very likely the same, differences can be attributed to more or less loading of the ligand on the polymer with the different reaction pathways. Both composites prove to have a pH dependent sorption of all tested metals which is essential if recovery of the metal is desired. The only notable differences are that at pH 2 the separation gap for Ni and Cu is larger with CuWRAM1, while the separation of Cu and Fe is smaller for CuWRAM1 than in CuWRAM. It also appears that the capacities for Cu over the entire pH range are slightly lower in the CuWRAM batches than in the CuWRAM1 batches. These results would lead to the conclusion that a Cu/Ni separation at pH 2 would be more efficient with CuWRAM1, while a Cu/Fe separation at pH 2 would be more efficient with CuWRAM. Based on the batch equilibrium data, some breakthrough separations were performed to test the metal separation efficiency of the two composites.

Figures 3.3 and 3.4 are the copper iron separations for both composites at pH 1, 1.5 and 3. The breakthroughs were run under similar conditions. The metal solutions always contained 1g/L Cu(II) and 4 g/L Fe(III), the pH was adjusted with H_2SO_4, and the pump speed was 1 min per minute. CuWRAM (Figure 3.4) proved to have slightly lower Cu(II) capacities than CuWRAM1, which matches nicely with the equilibrium batch test studies seen in Figures 3.1 and 3.2. With both composites, when the pH is increased, the purity of the strip decreases. This shows that both composites co-load copper and iron at a higher pH. The purities of the CuWRAM1 are higher than that of CuWRAM. This does not follow the trend seen in the equilibrium batch studies, which suggest by the larger separation between capacities of Cu and Fe with CuWRAM that it would be more effective at a Cu/Fe separation than CuWRAM1. This could perhaps be due to the bed

volume of the two columns. The CuWRAM bed volume was 5.02 mL, while the CuWRAM1 bed volume was 6.13 bed volumes which means that the flow rates were slightly different in bed volumes per minute. The CuWRAM1 was .04 bed volumes slower which may have allowed more time for the desorption of Fe(III) and the sorption of Cu(II). Yet both flow rates are within the recommend flow rates of 30BV/hr for typical industrial separation processes.

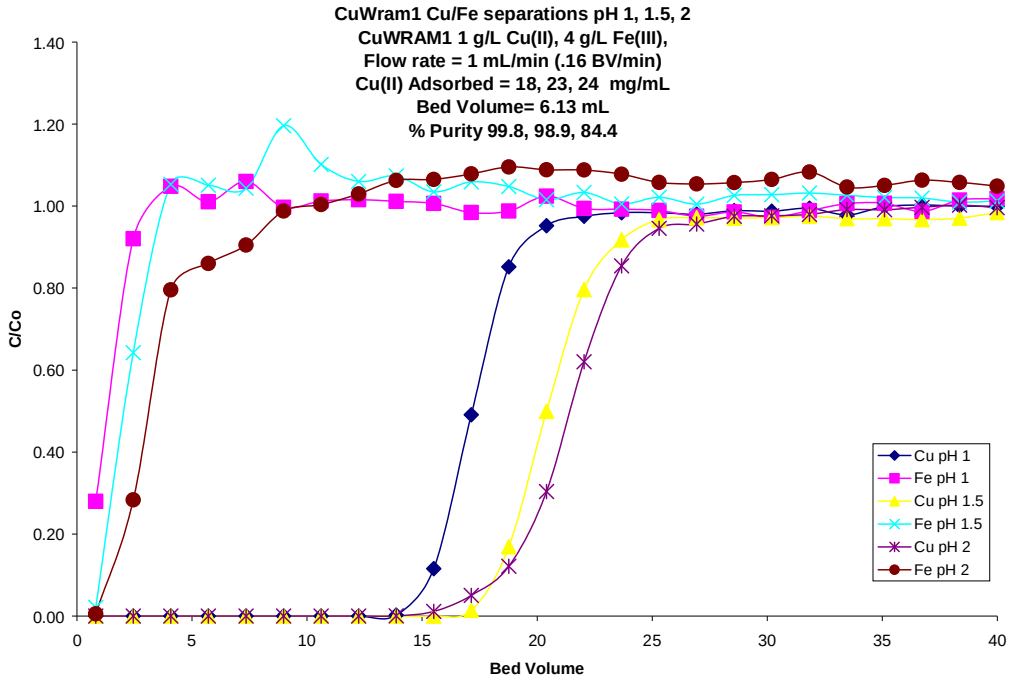

Figure 3.3: CuWRAM1 breakthrough profiles of Cu(II) 1g/L, Fe(III) 4g/L at pH 1, 1.5 and 2.

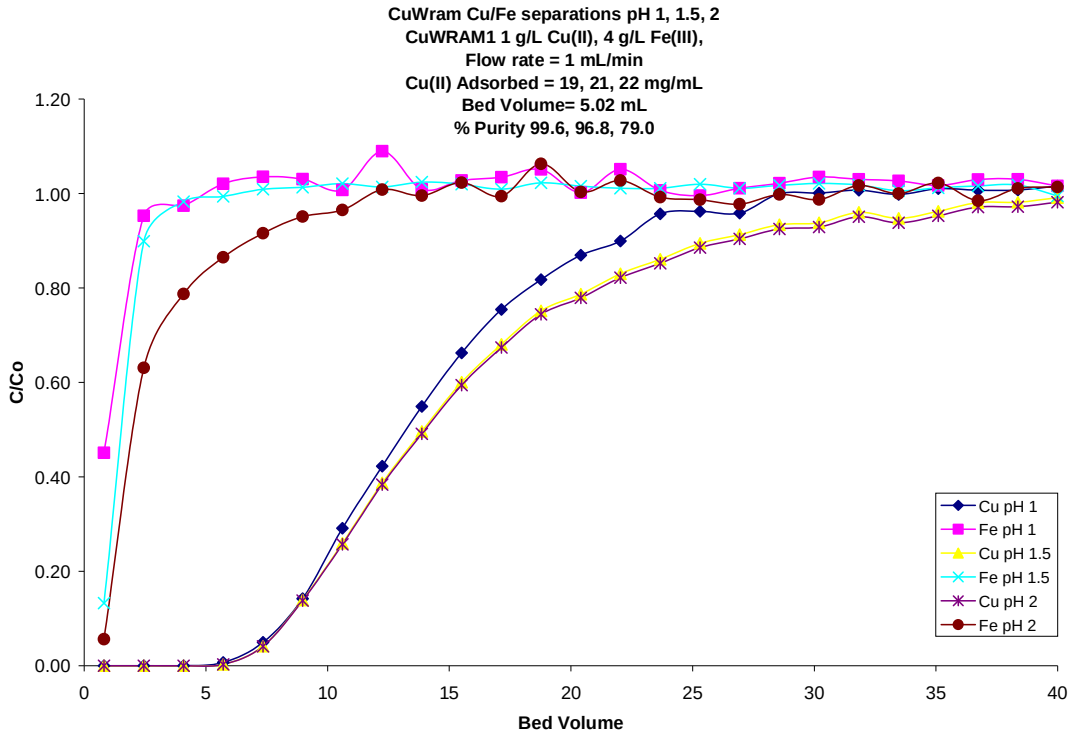

Figure 3.4: CuWRAM breakthrough profiles of Cu(II) 1g/L, Fe(III) 4g/L at pH 1, 1.5 and 2.

Since it was determined that CuWRAM1 is indeed effective in selectively removing Cu(II) from Fe(III), it was of interest as to whether it would be effective in separating Cu(II) in the presence of other divalent metals. In order to determine this, two breakthroughs were performed that contained 1.5 g/L of each Cu(II), Ni(II), and Co(II). Figure 3.5 is the breakthrough curve of this separation at pH 2. In this breakthrough, column loading was not sufficient to reach full break. This can be seen where Cu(II) never fully reaches the feed concentrations, while Ni(II) concentrations remain above those of the feed. This accounts in part for the low purity of 84.8%. If the column was allowed to reach full break, the purity of the strip would be greatly improved. When running a column it is hard to determine when the column reaches full break. At initial break the entire column is generally dark greenish-blue in color, because full break is determined by the kinetics of the column, and this can not be determined visually and

must be estimated. This breakthrough shows that CuWRAM1 has a high affinity for Cu(II) even in the presence of other divalent metals. It also demonstrates that there is a competing sorption of Ni(II) which decreases the efficiency of the column and the purity of the metal recovered.

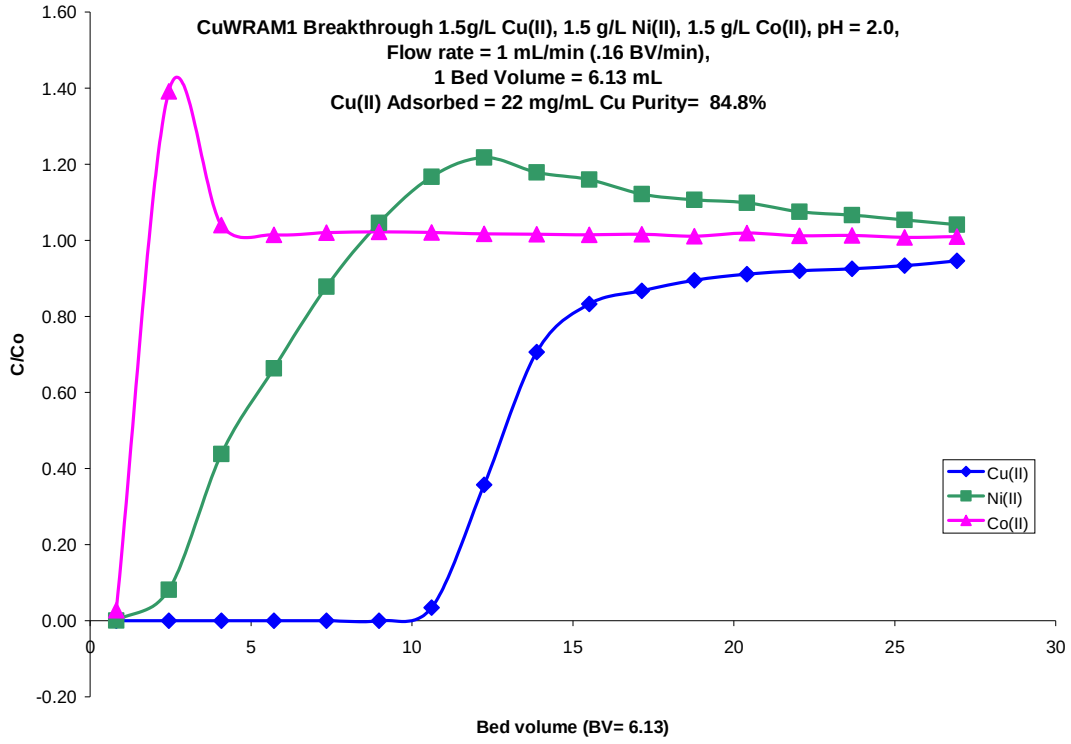

Figure 3.5: CuWRAM1 breakthrough profile of 1.5g/L Cu(II), 1.5 g/L Ni(II), 1.5 g/L Co(II) at pH 2.0.

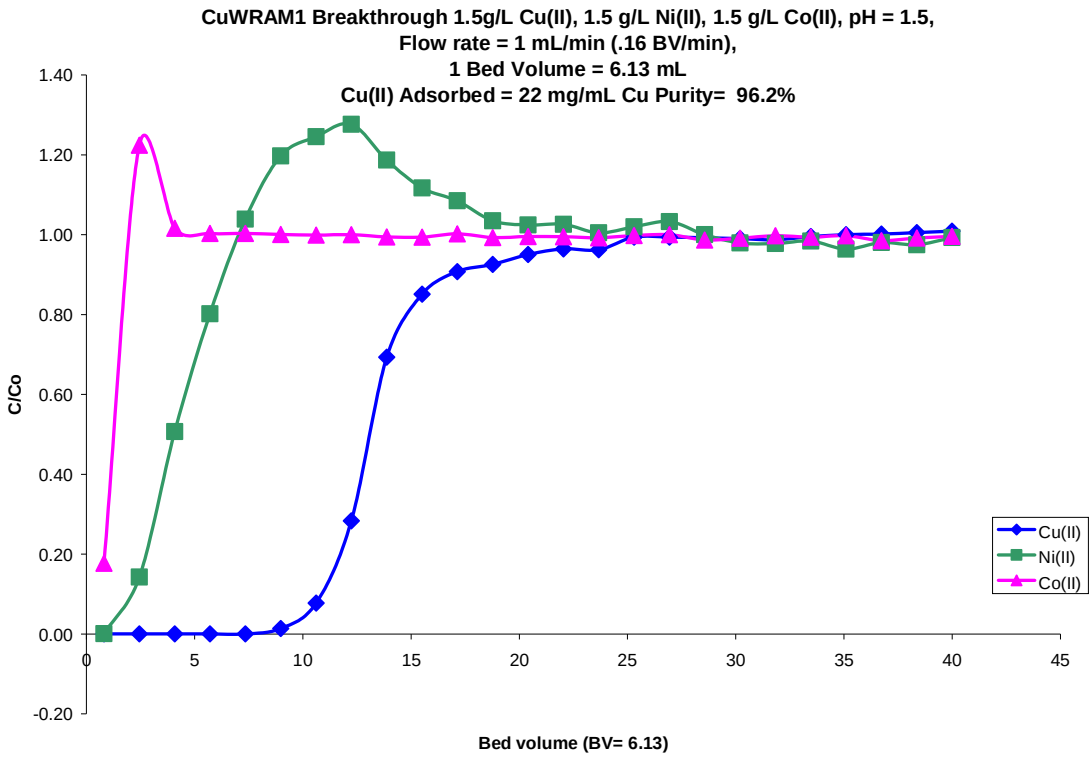

Figure 3.6: CuWRAM1 breakthrough profile of 1.5g/L Cu(II), 1.5 g/L Ni(II), 1.5 g/L Co(II) at pH 1.5.

In the hope of increasing the purity of Cu(II) in the divalent metal separations, a second breakthrough was performed (Figure 3.6). In this breakthrough the pH of the feed solution was lowered to 1.5. This was done because in the batch equilibrium studies (Figure 3.1), a larger gap was observed between Cu(II) and Ni(II) at pH 1.5 than at pH 2. In order to further increase the purity, the column was fed more feed solution to ensure that the column reached full break. These two methods together, decreasing the pH and increasing the volume of solution introduced to the column, increased the purity from 84.8% to 96.2%. While this greatly improves the purity of the Cu(II) strip, the Cu(II) is not able to displace all of the Ni(II) that was adsorbed on the column.

Whereas CuWRAM1 has a slight affinity for Ni(II) in the presence of Cu(II), this is not true for Co(II). Both breakthroughs show that cobalt is loaded in the first bed

volume when there is not much Cu(II) or Ni(II) present, but within the next two column volumes, all of the Co(II) is displaced by Cu(II) and Ni(II).

Due to the evidence that CuWRAM1 has an affinity for Ni(II) even in the presence of Cu(II), it is of interest to see how well Ni(II) sorption is in the absence of Cu(II). A breakthrough run was performed with 1.5 g/L Ni(II) and 1.5 g/LCo(II) at pH 2 (Figure 3.7). This breakthrough shows that there is indeed Ni(II) sorption at pH 2, with a low capacity of 14 mg/mL, but high purity of 99.94%. It also shows that once again that CuWRAM1 has little to no affinity for Co(II). This same breakthrough was also preformed on CuWRAM to further compare the composites (Figure 3.8). Similar results were obtained. Ni(II) sorption is observed at pH 2 but at a low capacity of 11 mg/mL and equally high purity of 99.9%.

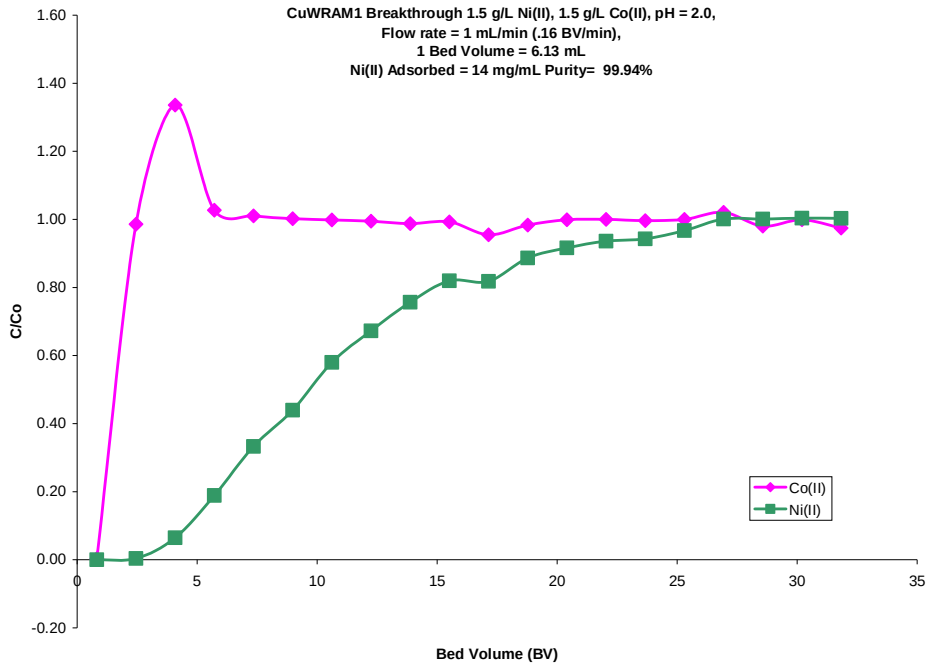

Figure 3.7: CuWRAM1 breakthrough profile of 1.5g/L Ni(II), 1.5 g/L Co(II) at pH 2.

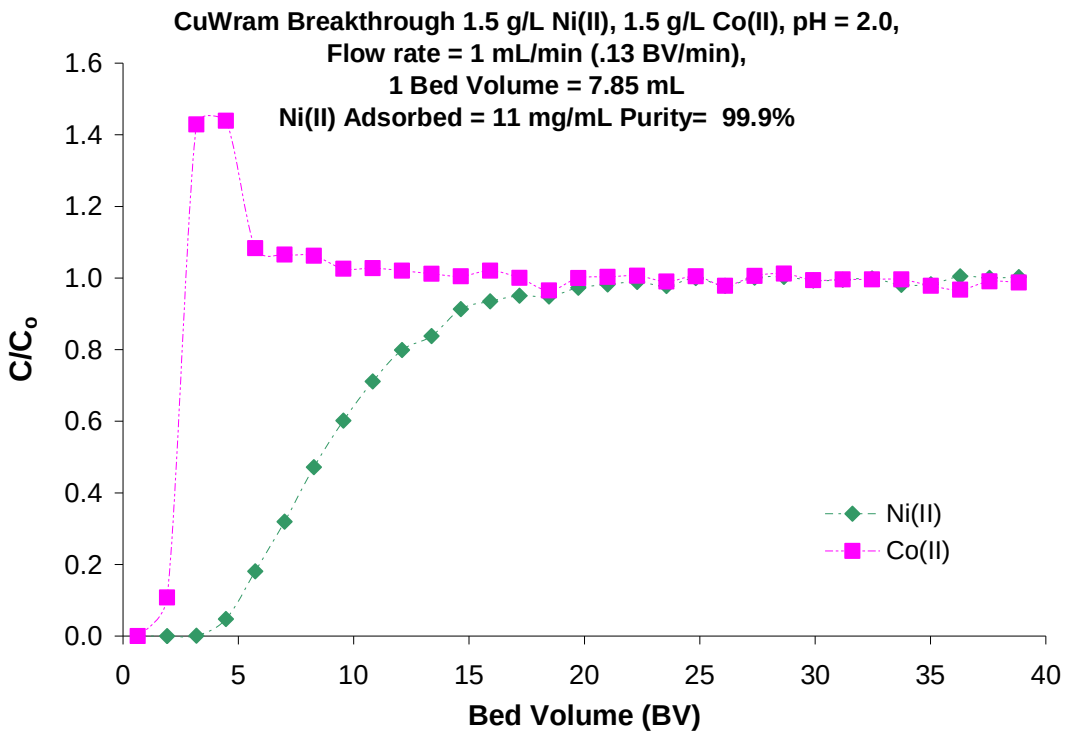

Figure 3.8: CuWRAM breakthrough profile of 1.5g/L Ni(II), 1.5 g/L Co(II) at pH 2.

3.3 Conclusions

Based on the batch equilibrium studies and all breakthroughs performed, it is easy to conclude that CuWRAM and CuWRAM1 are indeed the same composite. The differences in capacities are likely attributed to the extent of the picoyl ligand loaded in the two different reaction pathways. In essence, this reductive amination reaction is a new pathway to produce the currently marketed CuWRAM, which will prove to be more economical to produce because pyridine-2-carboxaldyehyde is less expensive than picolylchloride.

3.4 Future Work

Further studies will be made to investigate the efficiency of the reaction using the industrially produced BP-1, which differs slightly from the BP-1 produced in the lab, in

that it is on a different silica gel and there is less polymer loaded on the silane surface. Studies will also be performed to optimize the reaction pathway and the quanity of reagents needed to gain the highest copper capacity.

Chapter 4: Investigation into Silane modifications in SPCs

4.1 Introduction

Production of silica polyamine composites currently consists of a polyamine grafted onto the surface of a 7.5:1 methyltrichlorosilane-to-chloropropyltrichlorosilane functionalized nano-porous silica gel. Subsequently the polyamine can be modified with an organic functional group (ligand) with an affinity for one or more metal ions. In order to better understand the chemistry at the polymer-surface interface various ratios of chloro-alkyl and chloro-aryl silanes have been tested on two silica polyamine composites: WP-2 and BP-2 (both amino-acetate modified polyamines). The silanes investigated included anchors chloropropyltrichlorosilanes (CPTCS) and chloromethylphenyltrichlorosilane (CMPhTCS) and diluents methyltrichlorosilane (MTCS), phenyltrichlorosilane (PhTCS).

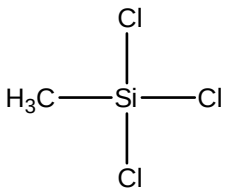

Methyltrichlorosilane

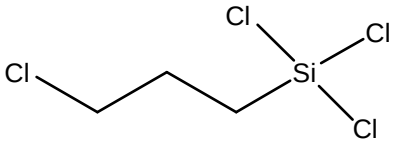

Chloroproplyltrichlorosilane

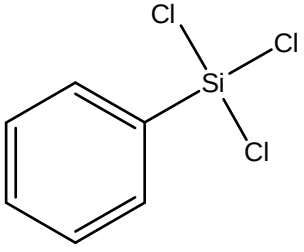

Phenyltrichlorosilane

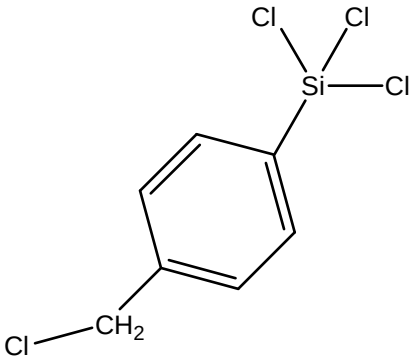

Chloromethylphenyltrichlorosilane

Figure 4.1: Anchors and diluents used the phenyl modified silica polyamine composites.

These modifications were designed to investigate the influence the silane linkers have on the degree of silicate leaching at high pH, and to determine if the silane anchor also influences metal selectivity. The idea is that the bulkier, more hydrophobic phenyl silanes would better protect the surface and the more rigid structure might also impact polymer structure. This effect of leaching will be reported elsewhere. The following results and discussion cover only the effect of the anchor on metal selectivity.

4.2 Results and Discussion

In order to better understand the effect of changing the silane anchors on BP-2 metal selectivity, equilibrium pH batch studies were performed on 5 different combinations of silane anchors and diluents. Figure 4.2 demonstrates the batch studies for the factory produced BP-2, which is a ratio of 7.5:1 MTCS:CPTCS. It was this ratio of diluents to anchor that proved to have the highest capacity in previous studies,[33] so most of the combinations of diluents and anchors where kept at a 7.5:1 ratio of diluents to anchor. An exception is illustrated in Figure 4.3 where only the anchor chloromethylphenyltriclorosilane was employed.

One can see by viewing Figure 4.2 that the normal BP-2 has an affinity for both Fe^{3+} and Cu^{2+} in pH range 0 to 2. This is also true in Figures 4.3-4.6. The difference between normal BP-2 and the modified silane BP-2s is that the addition of a phenyl anchor or diluent disrupts the preference of BP-2 for copper over iron at the higher pHs. The BP-2s prove to have a much higher affinity for iron throughout the phenyl series as illustrated in Figures 4.3-4.6.

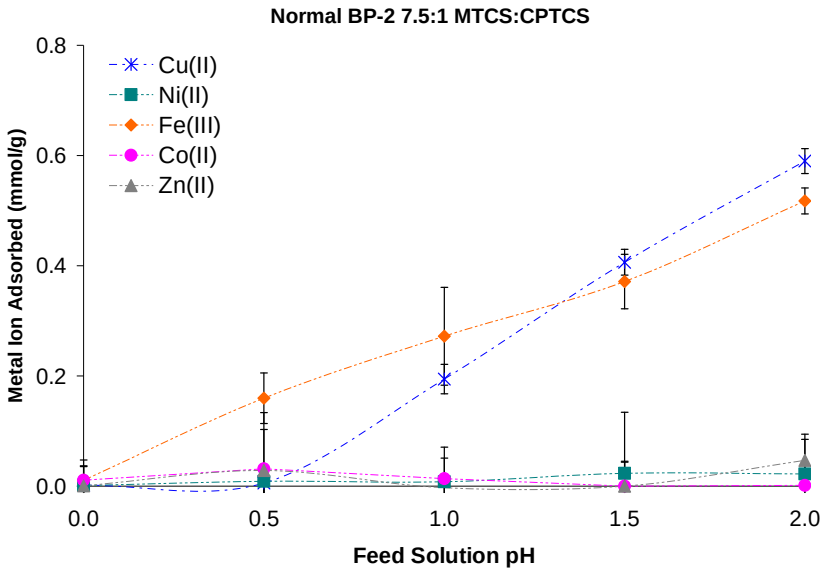

Figure 4.2: Equilibrium pH batch profile for normal BP-2 7.5:1 MTCS:CPTCS.

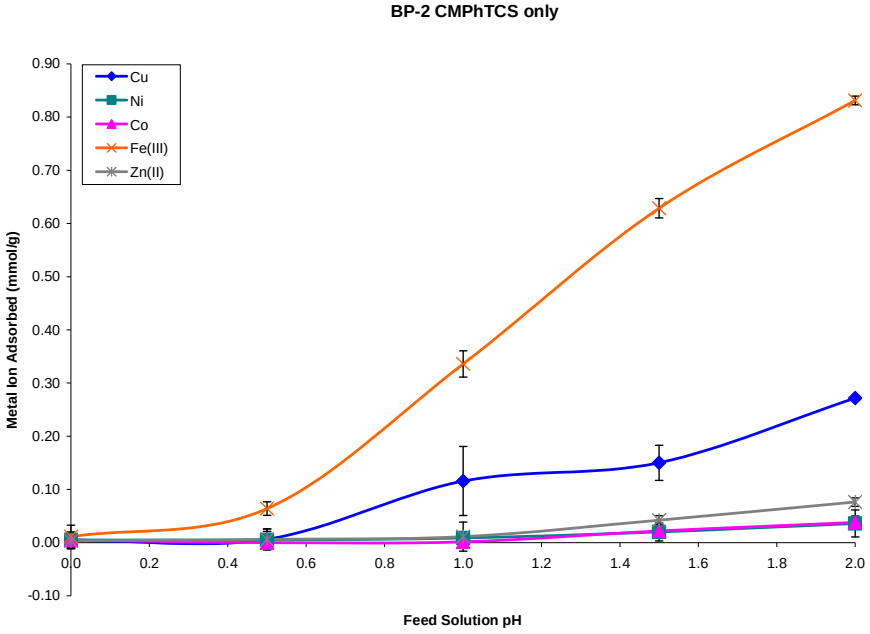

Figure 4.3: Equilibrium pH batch profile for BP-2 CMPhTCS only.

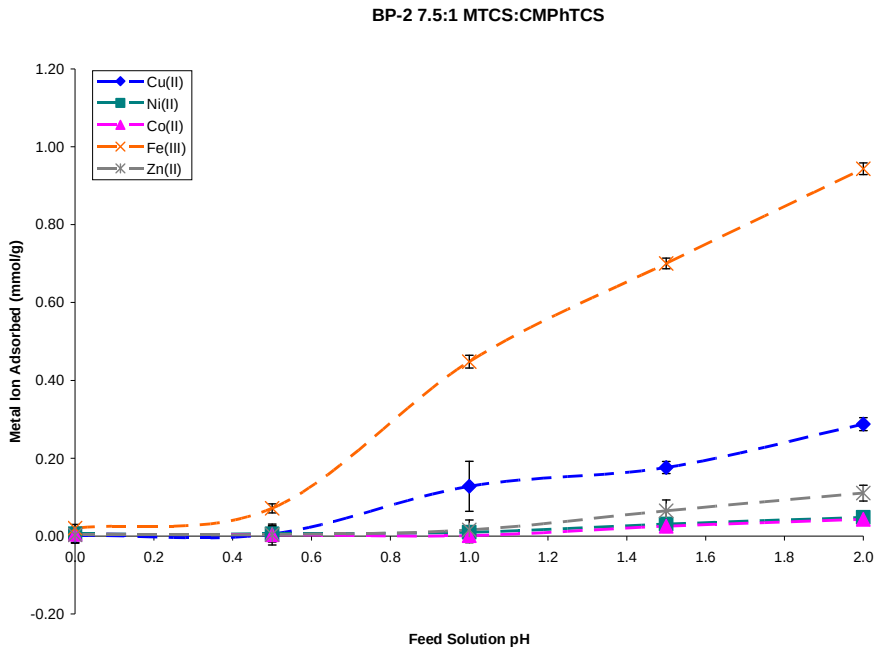

Figure 4.4: Equilibrium pH batch profile for BP-2 7.5:1 MTCS:CMPhTCS.

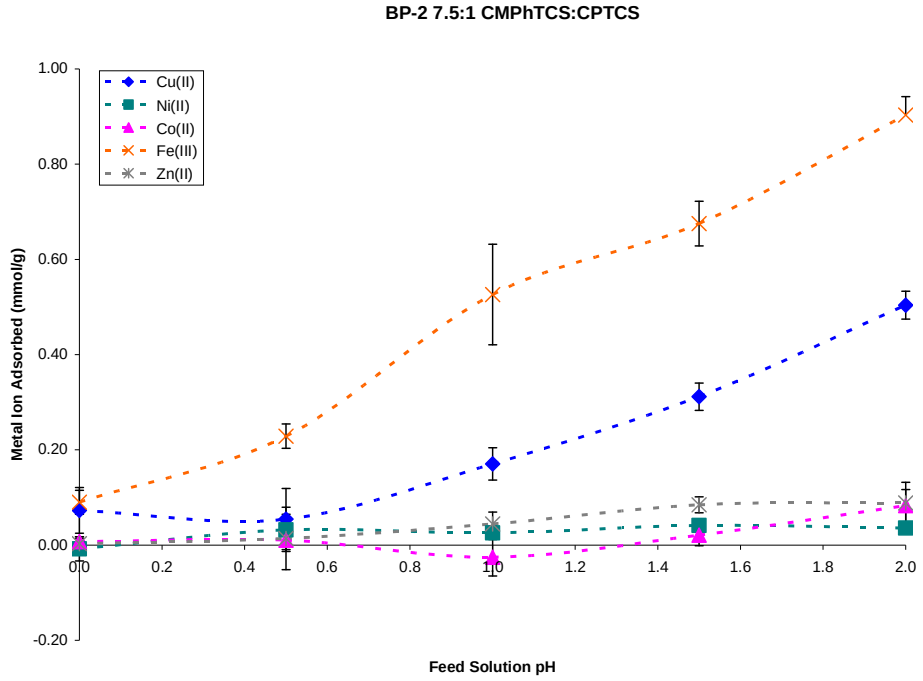

Figure 4.5: Equilibrium pH batch profile for BP-2 7.5:1 CMPhTCS:CPTCS.

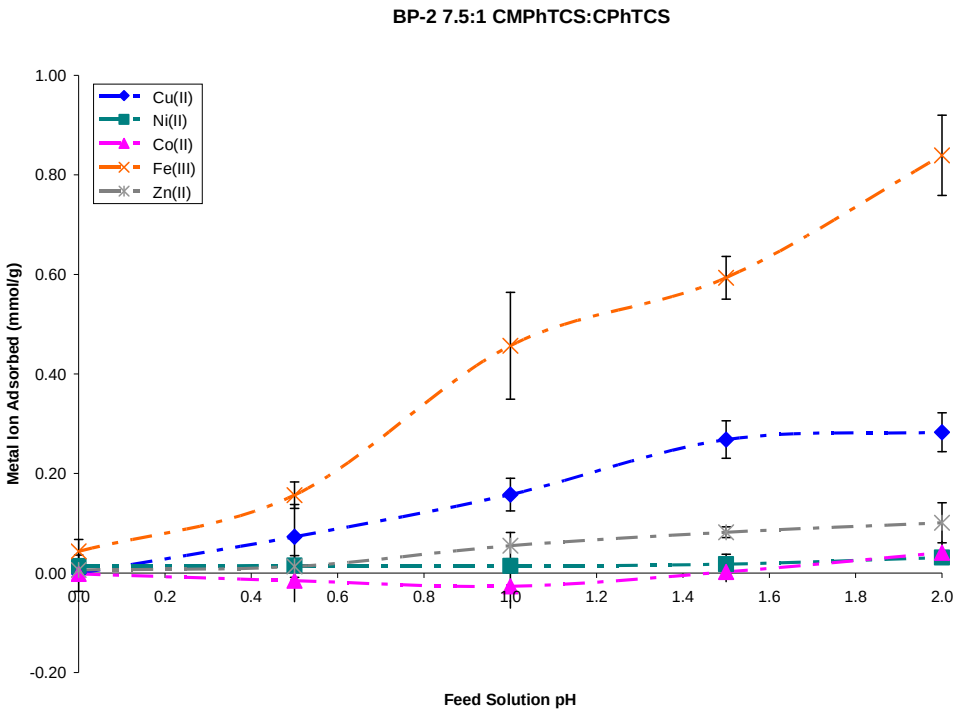

Figure 4.6: Equilibrium pH batch profile for BP-2 7.5:1 CMPhTCS:CPhTCS.

After performing the equilibrium pH batch profiles, the observed change in copper iron selectivity required further investigation. Breakthrough tests were performed on both BP-2 7.5:1 MTCS:CPTCS and BP-2 7.5:1 MTCS:CMPhTCS. Only these two composites were investigated due to the similar trend throughout the entire phenyl BP-2 series and also because the MTCS:CMPhTCS combination proved to have the highest capacities within the phenyl series.

Figure 4.7 illustrates the breakthrough studies of a Cu^{2+}/Fe^{3+} separation at pH 2. This figure reveals that in a flow situation even the normal BP-2 has a preference for Fe^{3+} over Cu^{2+}, but at poor purity as seen in Figure 4.8. Figure 4.8 is the strip profile for the dynamic flow test showing a purity of only 77.7%.

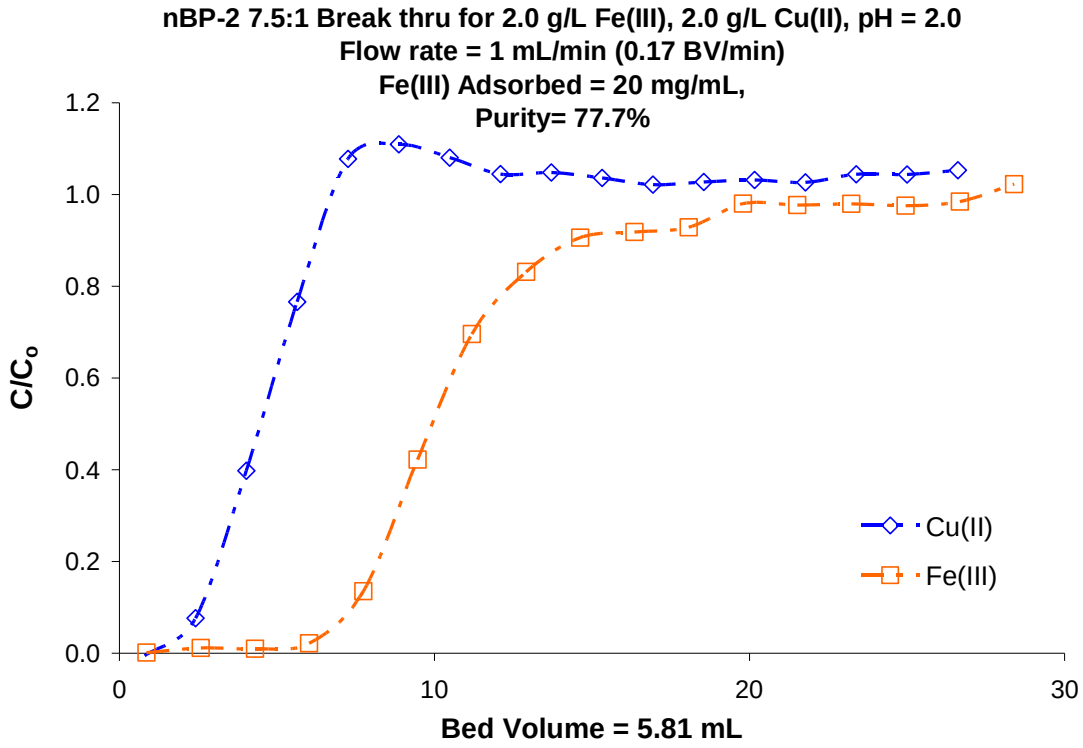

Figure 4.7: Copper-Ferric breakthrough curve for normal BP-2.

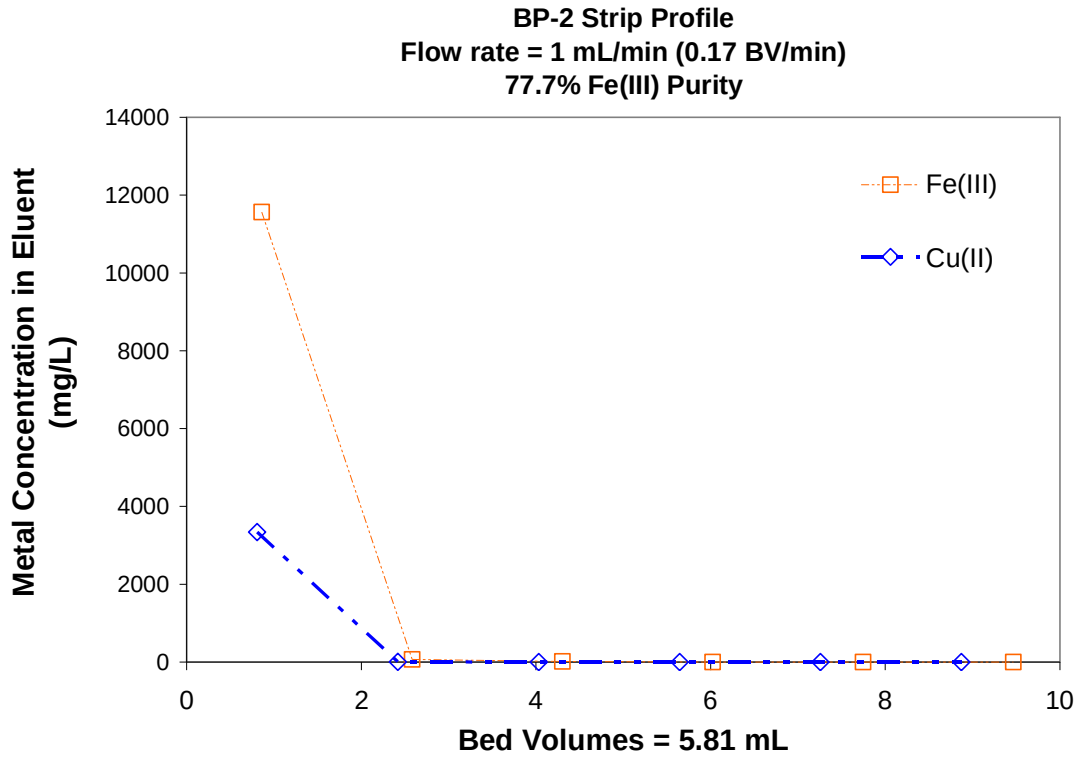

Figure 4.8: Copper-Ferric strip profile for normal BP-2.

Figure 4.9 is the same Cu^{2+}/Fe^{3+} breakthrough that was performed on BP-2 but instead, on the 7.5:2 MTCS:CMPhTCS BP-2 composite. One can easily see that this composite has a much higher affinity for Fe^{3+} over Cu^{2+} than normal BP-2. This phenyl BP-2 has a higher Fe^{3+} capacity, 22 mg compared to the 20 mg achieved with the normal BP-2. Figure 4.10 further demonstrates that the phenyl BP-2 is more selective for iron due to its higher purity of 90%.

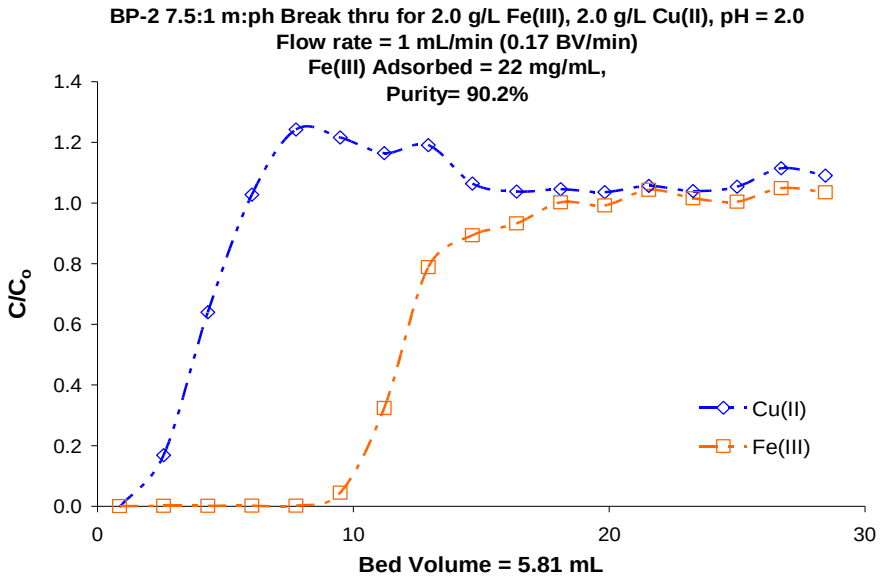

Figure 4.9: Copper-Ferric breakthrough curve for 7.5:1 MTCS:CMPhTCS BP-2.

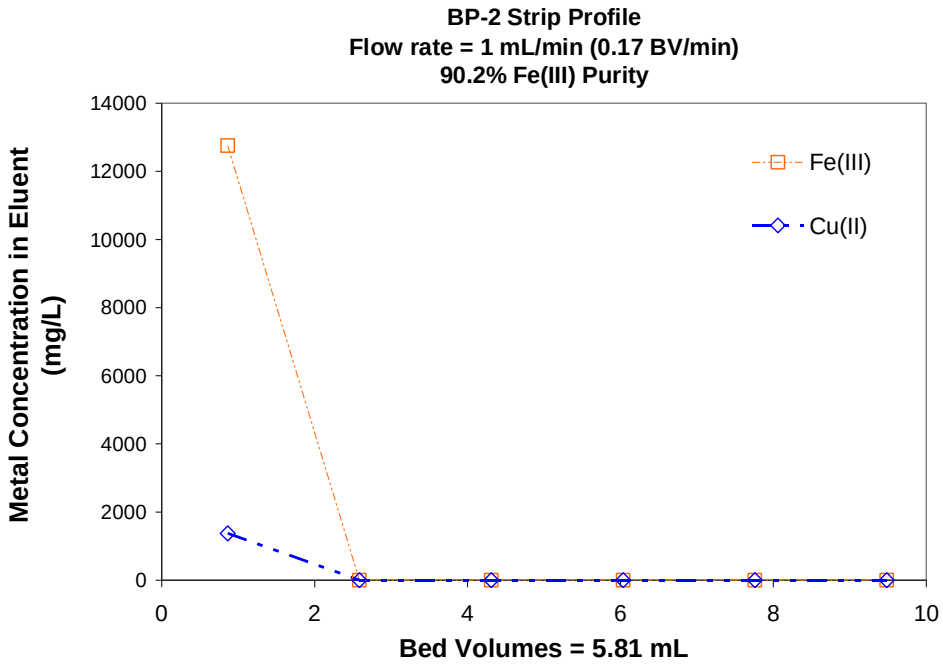

Figure 4.10: Copper-Ferric strip profile for 7.5:1 MTCS:CMPhTCS BP-2.

The equilibrium batch profiles all showed a large gap between iron and nickel capacities. This was first noted with the phenyl series. Due to the industrial importance of being able to efficiently separate iron from nickel, a breakthrough test was performed on 7.5:1 MTCS:CMPhTCS BP-2. Figure 4.11 depicts the breakthrough curve for a Fe^{3+}/Ni^{2+} separation. It demonstrates that 7.5:1 MTCS:CMPhTCS BP-2 effectively separates Fe^{3+} and Ni^{2+}. It proves to have a capacity of 25 mg/ml and Figure 4.12 demonstrates that this capacity is at a purity of 99.8%.

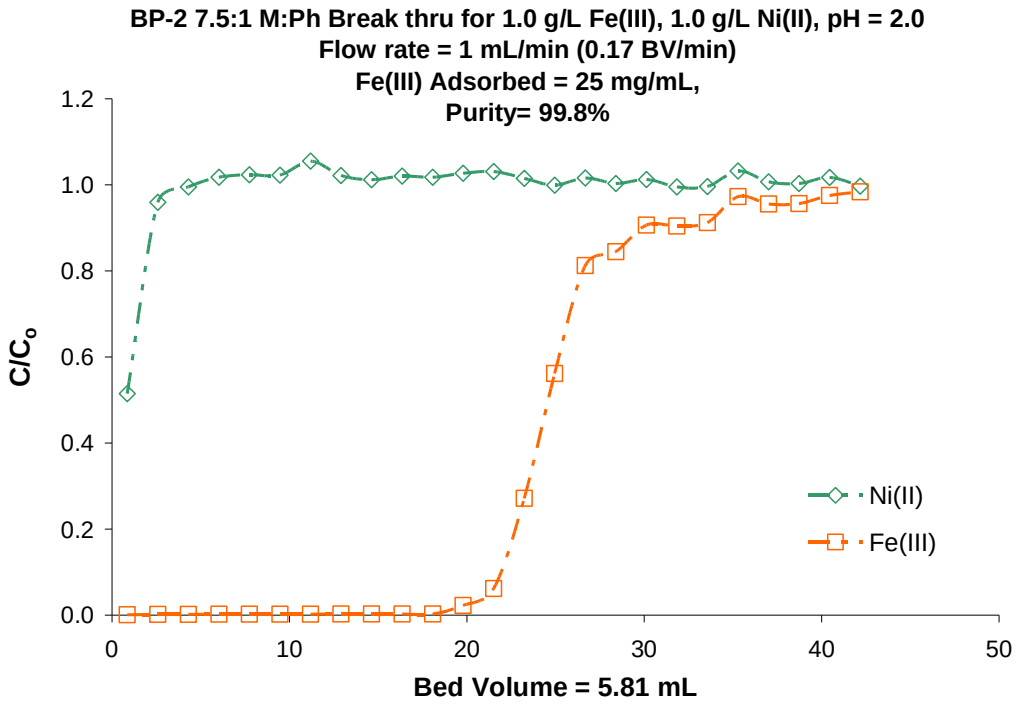

Figure 4.11: Ferric-Nickel breakthrough curve on 7.5:1 MTCS:CMPhTCS BP-2.

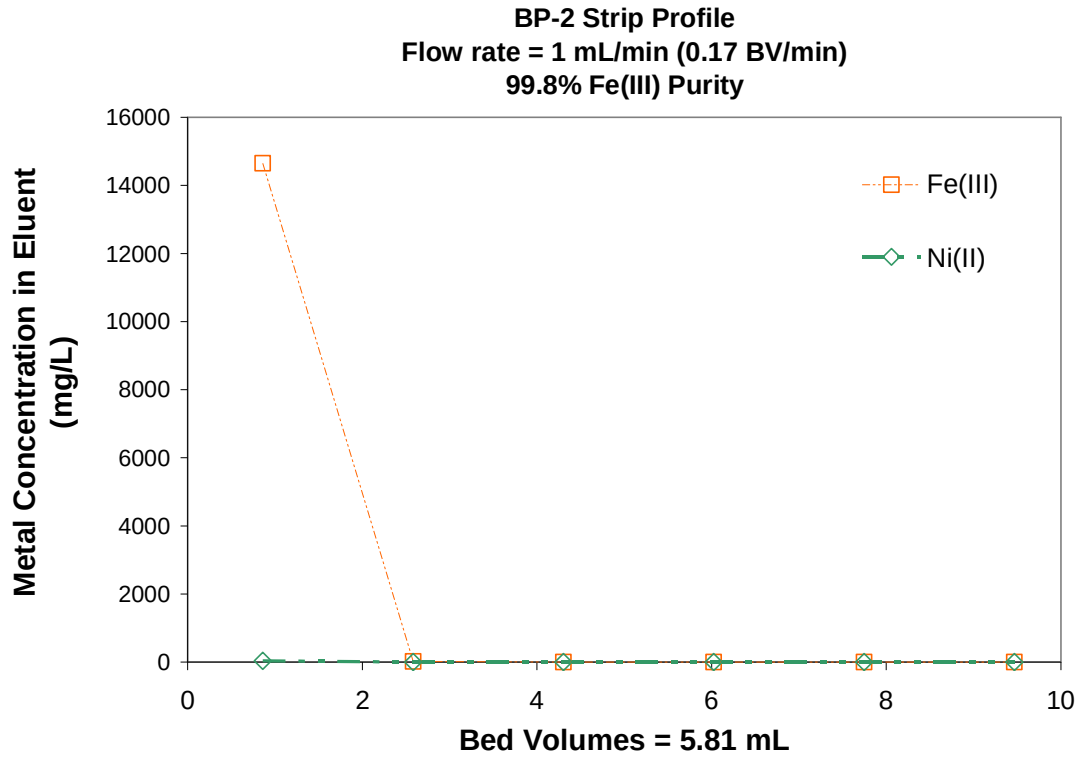

Figure 4.12: Ferric-Nickel strip profile for 7.5:1 MTCS:CMPhTCS BP-2.

Following the excellent results using the phenyl BP-2, it was decided that it would be prudent to perform the same ferric-nickel separation on normal BP-2. The ferric-nickel separation is typically performed using WP-4 another SPC containing the 8-hydroxyquinoline ligand that is iron selective, but is more expensive to produce than BP-2. Figure 4.13 demonstrate the results from the separation performed with normal BP-2. As with the phenyl BP-2, the normal BP-2 proves to effectively separate Fe^{3+} from Ni^{2+} at pH 2. The normal BP-2 proved to have a slightly lower capacity for Fe^{3+}, 20 mg/ml, but Figure 4.14 demonstrates that is has a high 99.4% purity. This is an important discovery because now it is apparent that the less expensive BP-2 can be used to perform a ferric-nickel separation.

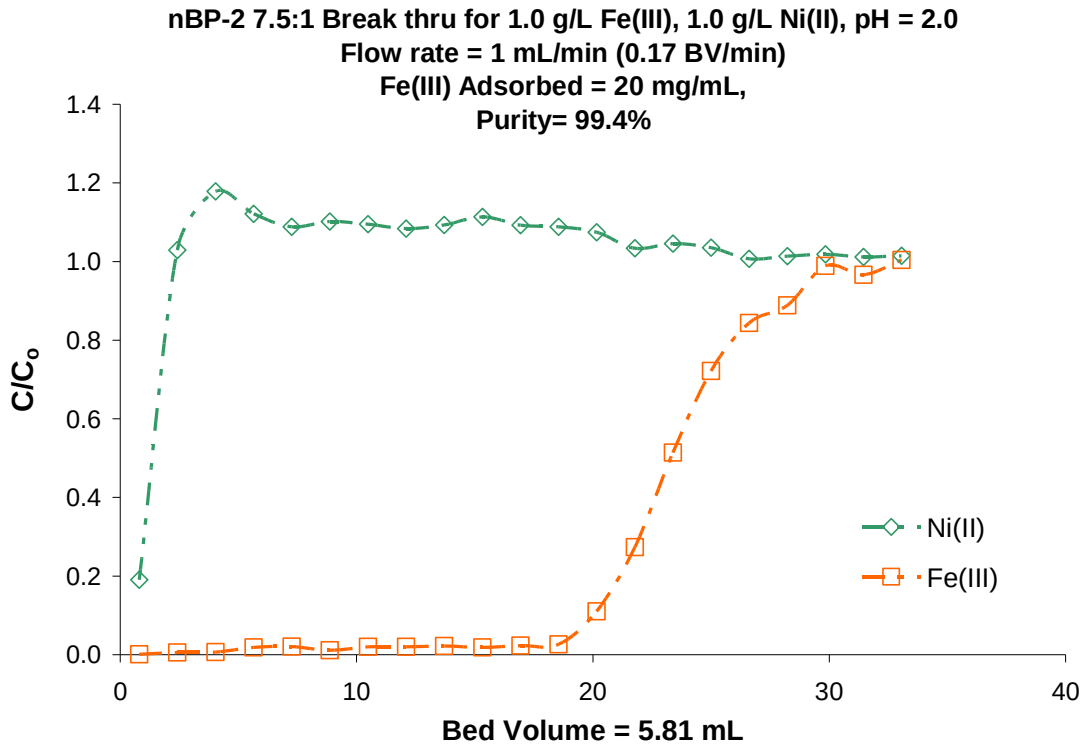

Figure 4.13: Ferric-Nickel breakthrough curve for normal BP-2.

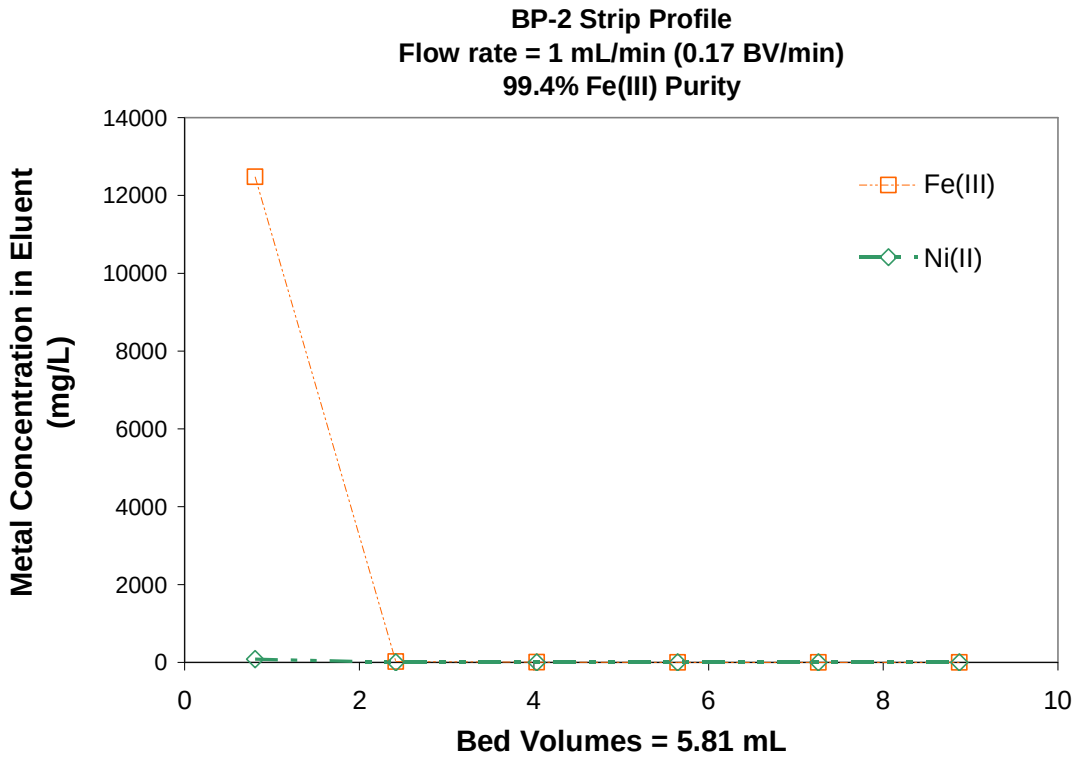

Figure 4.14: Ferric-Nickel strip profile for normal BP-2.

Since a change in metal selectivity was observed with the addition of a phenyl silane to the BP-2 system that utilizes polyallylamine (PAA) as the polymer employed, the same series of phenyl silane substitutions were tested on WP-2, which has the same amino acetate functional group but employs the branched polyethyleneimine (PEI). This series was investigated in order to discover whether the metal selectivity would change with both polymers. Figure 4.15 demonstrates the equilibrium batch profile for normal WP-2, which is 12.5:1 MTCS:CPTCS. Previous studies have found that the 12.5:1 diluent-to-anchor ratio achieved the highest capacity when PEI is employed. While the addition of the phenyl silane changed the metal selectivity of BP-2, this was not true for the WP-2 series. With the WP-2 series, all combination of anchors and diluents investigated proved to exhibit the same metal absorbtion trends, as seen in Figures 4.15-4.19.

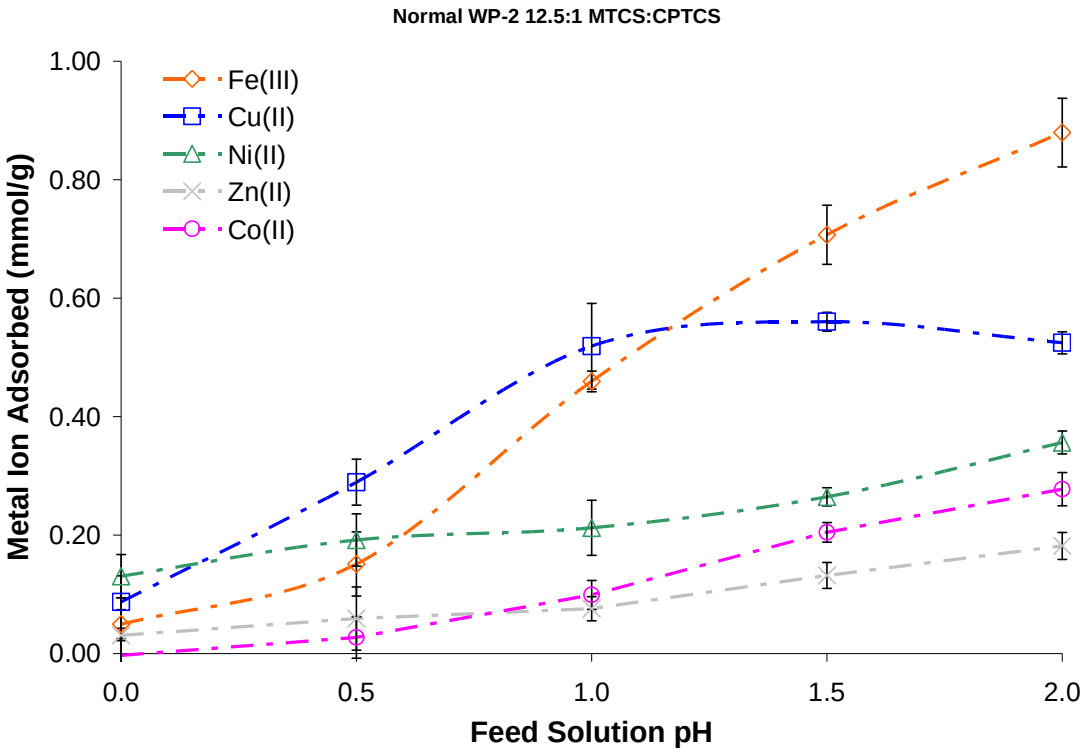

Figure 4.15: Equilibrium pH batch profile for normal WP-2 12.5:1 MTCS:CPTCS.

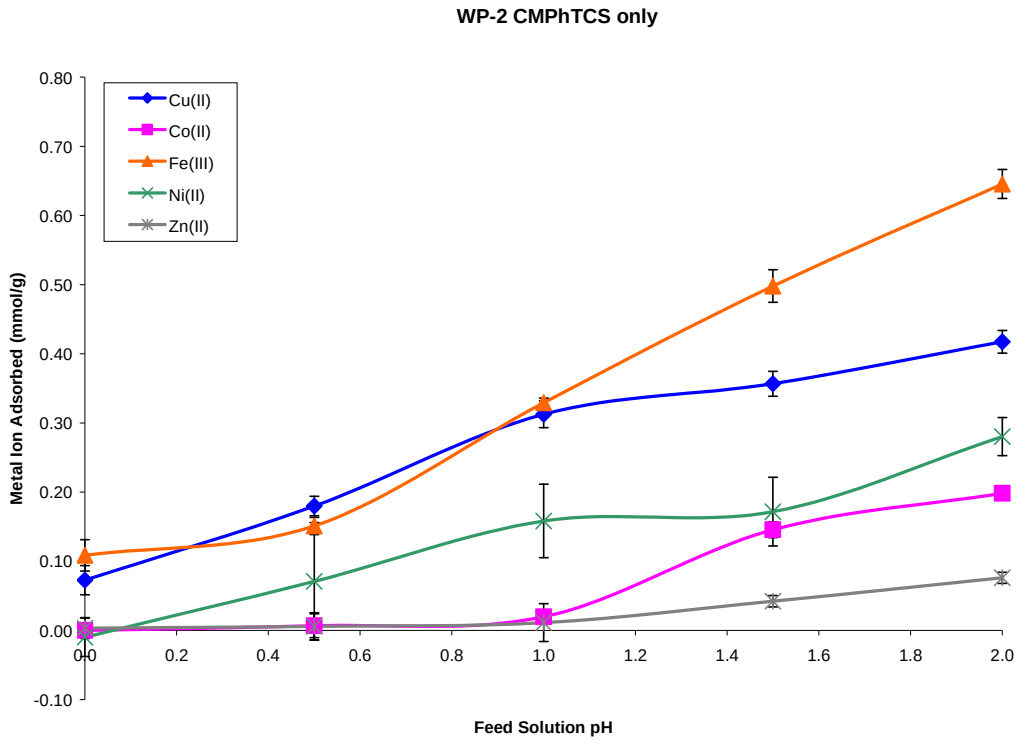

Figure 4.16: Equilibrium pH batch profile for WP-2 CMPhTCS only.

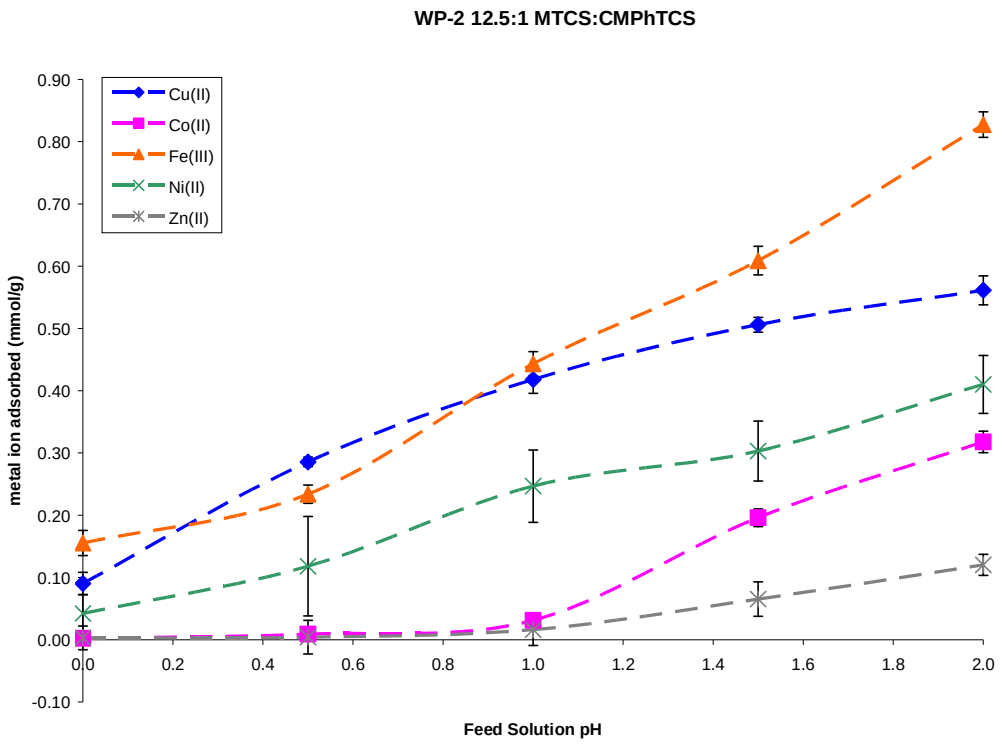

Figure 4.17: Equilibrium pH batch profile for WP-2 12.5:1 MTCS:CMPhTCS.

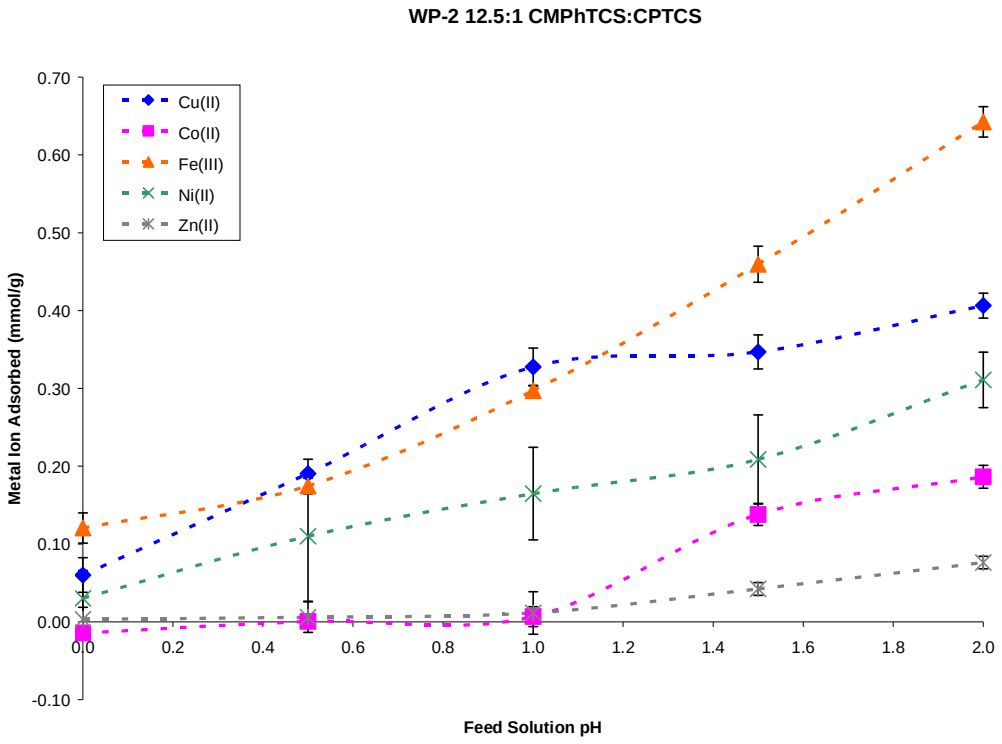

Figure 4.18: Equilibrium pH batch profile for WP-2 12.5:1 CMPhTCS:CPTCS.

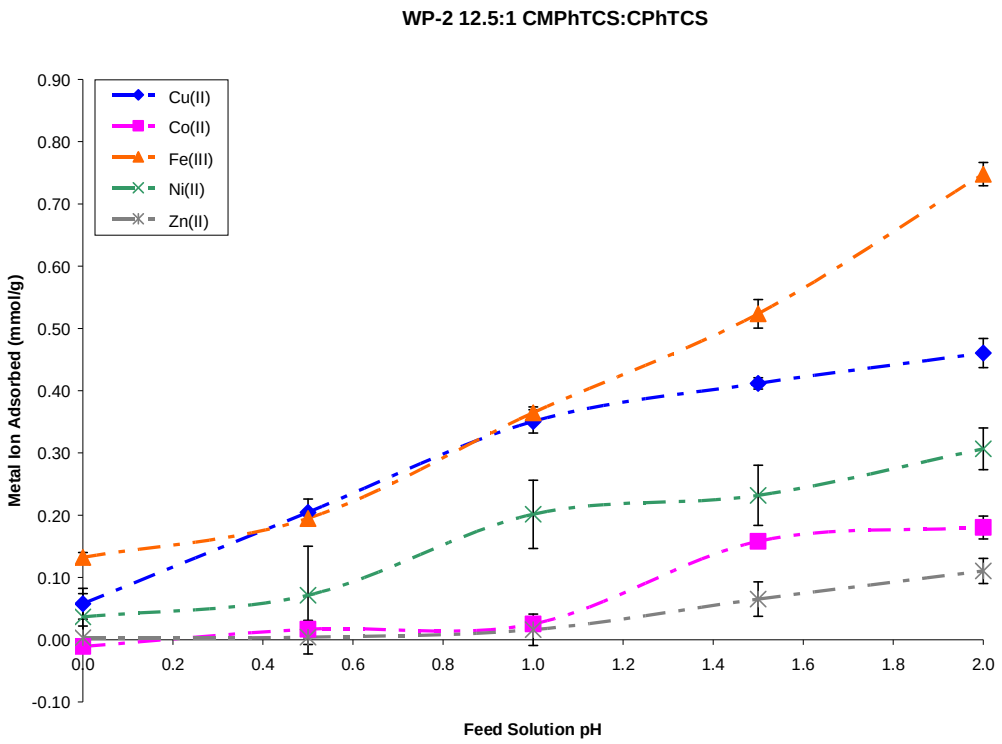

Figure 4.19: Equilibrium pH batch profile for WP-2 12.5:1 CMPhTCS:CPhTCS.

4.3 Conclusion

In order to better understand the polymer-surface interface on SPCs, a series of phenyl silanes were substituted for the usual propyl anchors with two different polymers, PAA and PEI. The addition of phenyl silanes to PAA proved to have changed metal selectivities while with PEI this was not true. The lack of change in selectivity observed with WP-2 is due to the branched nature of the polymer PEI. This polymer is already very rigid as evidenced by previous studies.[27,48] This great rigidity and the proximity of more ligating groups due to the branched structure makes this composite less able to differentiate metals requiring different coordination numbers (i.e., Fe^{3+} = 6 and Cu^{2+} = 4). Apparently the more flexible PAA is significantly affected by using a larger, more rigid tether to the silica surface. The exact reasons for the observed changes in selectivity with BP-2 are not well understood at the time.

4.4 Future Work

The change in metal selectivies is still not well understood. In order to better understand this change, model systems may be employed and investigated. Studies are also being performed on how the addition of the phenyl silanes affects the stability of the SPC system at higher pHs. The same phenyl substitutions with other PAA systems may be investigated to see if the change in metal selectivity trends hold true with functional groups other than amino acetate.

CHAPTER 5: Experimental

5.1 Materials

Silica gel (267 Å pore diameter, 2.82 mL/g pore volume, 84.7% porosity, 422 m^2/g surface area) was obtained from INEOS Enterprises Ltd., UK (previously Crosfield UK). CuWRAM was obtained from Purity Systems, Inc. M-4195, IRC-748, and Duolite ion exchange resins were obtained from Aldrich Chemicals. XFS-43084 was obtained from Dow Chemical Co. Sodium triacetoxyborohydride and 2-pyridinecarboxaldehyde were purchased from Aldrich Chemicals. All other reagents were purchased from Aldrich Chemicals or VWR. Metal solutions were prepared by dissolving the appropriate quantity of the sulfate salt in deionized (DI) water. The solution pH was adjusted from intrinsic with 0.05 M, 2.0 M, or 4.5 M H_2SO_4. Stripping was conducted using 4.5 M H_2SO_4. Metal standards for FAA (flame atomic adsorption) analysis were also obtained from Aldrich Chemicals. Poly(ethyleneimine)s (PEI, 1200 MW, 25,000 MW) were obtained from Aldrich Chemicals. Poly(allylamine) (PAA, 15,000 MW) was obtained from Summit Chemicals, Inc., NJ, USA. All polymers were in the free base form and were used as received. Chloropropyltrichlorosilane (CPTCS), phenyltrichlorosilane(PhTCS), chloromethylphenyltrichlorosilane(CMPhTCS) and methyltrichlorosilane (MTCS), were used as received from Aldrich Chemicals.

5.2 Equipment

Elevated temperature pH measurements during reactions were recorded using a Thermo Orion 250Aplus pH meter with a Thermo Orion Triode electrode. Ambient pH measurements were made with a VWR SympHony SB20 meter with a VWR SympHony Posi-pHlo electrode. Reactions were mixed with overhead tallboy laboratory stirrer,

Model 134-1, Troemner, LLC. Reaction flasks were heated using a GLAS-COL heating mantle controlled via a STACO, Inc. variable autotransformer. Batch experiments were conducted in a Precision Scientific 360 shaker bath (Precision Scientific, Inc., Chicago, IL. Dynamic experiments were conducted with a 10 mL adjustable volume OMNIFIT column. Columns were slurry packed and fed challenge solution by a variable-flow FMI Lab Pump model QG150 (Fluid Metering, Inc., Syosset, N.Y.). Metal ion concentrations were determined via a Flame Atomic Sorption (FAA) method using a S2 FAA Spectrometer from SOLAR, UK.

5.3 Elemental Analysis

Elemental analysis (Carbon, Hydrogen, Nitrogen, and Chlorine) was conducted at Schwarzkopf Microanalytical Laboratory, N.Y. The error in elemental analysis was reported as no more than 0.3% absolute for CHN analysis. Chlorine was determined by the ion elective electrode method with a relative error of 0.3%

5.4 Preparation of Hydrated Silica Gels

Silica gels were sieved to ensure particle diameters were in the desired range (90 µm to 105 µm and 150 µm to 250 µm for raw INEOS silica gel). 200 g of sieved silica gel was added to 800 mL of 1.0 mol/L HCl in a 2 L three neck round bottom flask. The flask was equipped with an overhead stirrer and a condenser. During mixing the flask was degassed by an applied vacuum (30 mm Hg). The reaction flask was restored to atmospheric pressure. The mixture was then brought to reflux (98°C) for six hours. Upon cooling the product was filtered and washed successively with three 800 mL water washes and two 800 mL methanol washes. The resulting gel was dried at 120°C to a constant mass. Air was forced over a bed of water and through a 2 L column containing

200 g of acid washed silica gel for 72 hours creating a monolayer of water on the silica gel surface. The percent weight gain (W) is used to quantify the increase in mass associated with modifying silica gel. W is calculated using Equation 5.1.

$$W\ \% = (M_f - M_i)/M_i * 100 \qquad \text{(Eq. 5.1)}$$

In which M_f is the mass of the modified silica gel and M_i is the mass prior to modification. For the hydration of acid washed silica gel W ~ 6 %.

5.5 Preparation of MTCS:CPTCS Functionalized Silica Gels

MTCS:CPTCS functionalized silica gels are silica gels functionalized with MTCS and CPTCS in a specified molar ratio. In keeping with CPTCS only silica gel, a total of 3 mmol of silanes for each gram silica gel was employed. The silane solution of the requisite molar ratio was prepared in 10 mL of hexanes. The silane solution was then added drop-wise to the reaction mixture (10 grams of silica and 60 mL hexane). As the reaction proceeded, HCl gas was evolved and was forced out of the reaction flask by dry N_2 flow. The reaction flask was degassed with an applied vacuum (30 mm Hg) for 15 minutes and allowed to react for 24 hours. The product was filtered and washed three times with 60 mL of dry hexanes and two times with 60 mL of methanol. The product was filtered and then dried at 110°C until there is a negligible mass decrease. The percent weight gains for hydrated silica gel functionalized with both MTCS and CPTCS in the molar reagent ratios specified above are in the range W = 7 % to W = 20 %, % C= 3.50

5.6 Preparation of CMPhTCS only Functionalized Silica Gels

For the preparation of CMPhTCS only functionalized INEOS silica gel, a 10 g quantity of hydrated silica gel was placed in a 250 mL three neck round bottom flask equipped with an overhead stirrer. 60 mL of hexanes was added to the reaction flask and

the resulting mixture was stirred under a constant flow of dry N_2. 30 mmol (3 mmol/g of silica gel) of CMPhTCS was dissolved in 10 mL of dry hexanes. The silane solution was then added drop-wise to the reaction mixture. As the reaction proceeded, HCl gas was evolved and was forced out of the reaction flask by dry N_2 flow. The reaction flask was degassed with an applied vacuum (30 mm Hg) for 15 minutes and allowed to react for 24 hours. The product was filtered and washed three times with 60 mL of dry hexanes and two times with 60 mL of methanol. The product was filtered and then dried at 110°C until there was a negligible mass decrease. For the modification of hydrated silica gel with CMPhTCS only W = 22 %, %C= 4.69

5.7 Preparation of MTCS:CMPhTCS Functionalized Silica Gels

MTCS:CMPhTCS functionalized silica gels are silica gels functionalized with MTCS and CMPhTCS in a specified molar ratio (7.5:1 and 12.5:1). A total of 3 mmol of silanes for each gram silica gel was employed. The procedure described for MTCS:CPTCS section 5.4 was adhered to. W= 18%, % C= 4.27

5.8 Preparation of CMPhTCS:CPTCS Functionalized Silica Gels

CMPhTCS:CPTCS functionalized silica gels were prepared following the same procedure as described for MTCS:CPTCS (5.4). W= 19% , %C= 4.37

5.9 Preparation of CMPhTCS:CPhTCS Functionalized Silica Gels

CMPhTCS:CPhTCS functionalized silica gels were prepared following the same procedure as described for MTCS:CPTCS (5.4) W=17% , %C= 4.73

5.10 Preparation of SPCs BP-1 and WP-1.

In a 100 mL three neck round bottom flask equipped with a condenser and overhead stirrer, 5 g of CP-Gel or MTCS:CPTCS INEOS type silica gel was added to a

25 mL aqueous 15% PAA (MW=25,000) solution containing 2 mL of methanol as an antifoaming agent. The resulting mixture was stirred for 15 minutes and degassed by an applied vacuum (30 mm Hg). The mixture was continuously stirred at a temperature of 65°C for 48 hours. The mixture was then cooled, allowed to settle, and then carefully decanted. The resulting composite was washed five times with 20 mL portions of water, one 20 mL portion of a 4 mol/L ammonia solution, three 20 mL portions of water, and two 20 mL portions of methanol. The resulting composites were then dried to constant mass at 60°C. A sample of each composite underwent elemental analysis (CHN). Polyamines and concentration used include: polyallylamine (15,000 MW) in a 10% aqueous solution, polyvinylamine (<1000 and 50,000 MW) in an aqueous solution containing a mass fraction of 10% polymer and polyethyleneimine (1,200 and 25,000 MW) in an aqueous solution containing a mass fraction of 18% polymer. For the addition of polyamines to functionalized silica gels the percent weight gains are in the range W =8 % to W = 18 %.

PAA 15000 MW: 7.5:1 13.8%C 3.90%N PEI 25000 MW: 12.5:1 11.8%C 4.90%N

5.11 Preparation of Modified SPCs.

The preparation of CuWRAM and BPAP can be found in detail elsewhere.[23,32] For the preparation of the 7.5:1 MTCS:CPTCS derivatives of these materials the pathway is identical to the previously reported procedure with the exception that 7.5:1 BP-1 was employed. W for 7.5:1 BP-AP was ~23%. W for 7.5:1 WP-4 was ~48%. W for 7.5:1 CuWRAM was ~18%. Weight gains are all relative to the 7.5:1 BP-1 precursor.

5.12 Preparation of WP-2 and BP-2

In a 100 mL three neck round bottom flask equipped with an overhead stirrer and condenser, 5 g of 12.5:1 MTCS:CPTCS only PEI (25,000 MW) composite was added to 6 g of sodium chloroacetate in 25 mL of water. The resulting mixture was stirred for 15 minutes and degassed by an applied vacuum (30 mm Hg). The contents of the flask were heated to a temperature of 70°C for 24 hours. After 1 hour, 1 mL of 8 mol/L NaOH was added drop-wise to the reaction mixture while monitoring pH. The pH was maintained above 9. A further 1 mL of 8 mol/L NaOH was added similarly after 18 hours. The maximum recorded pH of the reaction mixture was 10.5. The flask was then allowed to cool and filtered. The resulting composite was washed 3 times with 20 mL of water, once with 2 mol/L H_2SO_4, a further 3 times with 20 mL of water, twice with 20 mL of methanol, then dried at 70°C for 24 hours. The same procedure was used to produce a CMPhTCS, 12.5:1 MTCS:CMPhTCS, 12.5:1 CMPhTCS:CPTCS, and CMPhTCS:CPhTCS acetate modified PEI composites (WP-2s) using 5 g of the appropriate PEI composite (WP-1). The weight gain for addition of acetate groups to PEI composites were W = 10 to 14%. For the synthesis of BP-2 a procedure identical to WP-2 was used with the exception that BP-1 is the precursor. The weight gain for BP-2s were W = 11- 15%. FTIR analysis of BP-2 and WP-2 show carboxylic peaks at 1737 cm-1 and 1639 cm-1. 13C NMR (CP/MAS) WP-2: -10 to 0 ppm $–Si(O_2)$-**C**H_3, 5 to 15 ppm - $Si(O_2)$(**C**$H_2)_3$NH-, 120-140 ppm $Si(O_2)(C_6H_5)$, 40-50 ppm $Si(O_2)(C_6H_4)CH_3$NH-, 30 to 65 ppm PEI **C**H_2, –NH**C**H_2COOH , 165 to 175 - CH_2**C**OOH. 13C NMR (CP/MAS) BP-2: -10 to 0 ppm $–Si(O_2)$-**C**H_3, 5 to 15 ppm - $Si(O_2)$(**C**H_2)3NH-, 20 to 45 ppm PAA **C**H_2, PAA **C**H, 120-140 ppm $Si(O_2)(C_6H_5)$, 40-50 ppm $Si(O_2)(C_6H_4)CH_3$NH-, 45 to 65 ppm – **C**H_2COOH , 165 to-CH_2**C**OOH.

5.13 Preparation of CuWRAM1

In a 100 mL three neck round bottom flask equipped with an overhead stirrer and condenser, 5 g of 7.5:1 MTCS:CPTCS BP-1 composite was added to 30 mL distilled THF. 14 grams $NaBH(OAc)_3$ or a 4 molar equivalent was added, followed by 4.3 mL 2-pyridinecarboxyaldehyde (3 molar equivalent). This solution was milky yellow in color and very thick. An additional 20 mL of THF was added to ensure smooth stirring. The mixture was stirred overnight and was quenched the following morning with 10% HOAc/MeOH. At this step small bubbles of H_2 were released from the mixture. The reaction solution was washed with MeOH (3X); D.I. Water (2X); Ammonia (1X); D.I. Water (3X); 4 N H_2SO_4 (1X); Water (2X); Acetone (1X). The resulting mixture was dried overnight to a constant weight in a 70˚C oven. The resulting composite was tan in color. W= 18%. The same reaction was repeated with MeOH as the solvent rather than THF with the same results as above. %C =19.86 %N=4.63

5.14 pH Profiles

pH profiles were acquired for several divalent and trivalent metals. The pH of the challenge solutions was adjusted with sulfuric acid. Metal concentrations in feed solutions were typically 1.5 g/L. Batch extraction tests were conducted by adding 0.1 g of SPC to 10 mL of metal solution at selected pH values. To ensure equilibrium, the metal ion and SPC mixtures were placed in a shaker bath. After 24 hours the mixtures were allowed to settle. Each supernatant was extracted and diluted with 2% nitric acid for analysis using the FAA method. All pH profile experiments performed in triplicate.

5.15 Mass Transfer Kinetics

Sorption isotherms were obtained for SPCs as a function of time. Using the batch method described previously samples of each composite were fed with a 1.5 g/L metal ion (typically Cu^{2+} or Ni^{2+}) solution at the requisite pH. The supernatant was sampled several times over the following 24 hours. Samples were diluted and preserved in 2% HNO_3 solution before FAA analysis. All mass transfer kinetics experiments performed in triplicate.

5.16 Concentration Dependent Isotherms

In order to assess the applicability of the Langmuir model for SPC and polystyrene metal ion sorption, concentration dependant isotherms were acquired. Isotherms were obtained by batch experiments as described in Section 13. Metals investigated included Cu^{2+}, and Ni^{2+}. Metal ion concentration was varied, pH was held constant, and each sample was shaken for 24 hours to ensure equilibrium. Langmuir parameters were obtained from the appropriate linear regressions. The details of these models are described in Chapter 2 Section 1. All concentration isotherm experiments performed in triplicate.

5.17 Breakthrough Testing

Column experiments were carried out using a 10 mL adjustable Ominifit glass column. Flow was top to bottom for these columns. The columns received flow from a variable flow FMI Lab Pump, Model QG150 from Fluid Metering, Inc., NJ, USA. The flow rate was typically in the range of 0.1 to 0.5 column volume/min. Each column was slurry packed with the necessary SPC or crosslinked polystyrene. Columns were then conditioned for metal ion extraction by passing through the column the following

solutions: 20 mL DI H_2O, 30 mL 4.5 mol/L H_2SO_4, 100 mL DI H_2O. The acid is used to remove impurities from the packed composite. Columns were then treated with a metal ion contaminated feed solution adjusted to the necessary pH. All columns were then rinsed with 20 mL DI water, stripped with 30 mL 4.5 mol/L H_2SO_4 and rinsed again with 100 mL DI water. Effluent fractions were collected in 5 mL or 10 mL aliquots beginning with the first 5 mL or 10 mL of the feed solution passes through the column. The fractions were preserved with one drop of concentrated HNO_3. All breakthrough experiments were run once only unless otherwise stated. Also, the acid solutions used were all adequate for complete removal of the metal ions off the column unless otherwise stated.

Bibliography

1. Metal Prices homepage. http//www.metalprices.com/ (accessed May 2008).

2. Kellogg H.H., Rao Y.K., and Marcuson S.W.. Pyrometallurgy. Ann. Rev. Phys. Chem. 27, 387-406. 1997.

3. Ritcey, G.M. Solvent Extraction in Hydrometallurgy: Present and Future. TSINGGHUA Science and Technology 11(2), 137-152. 2006.

4. Johnson, D.B. and Hallberg, K.B. Acid mine drainage remediation options: A review. Science of the Total Environment 338(1-2), 3-14. 2005.

5. Castro, J. M. and Moore, J. N. Pit lakes: Their characteristics and the potential for their remediation. Environmental Geology (Berlin) 39(11), 1254-1260. 2000.

6. Kelly, D.P., and Wood, A.P. "Reclassification of some species of *Thiobacillus* to the newly designated genera *Acidithiobacillus* gen. nov., *Halothiobacillus* gen. nov. and *Thermithiobacillus* gen. nov."". *Int. J. Syst. Evol. Microbiol.* **50**: 489-500. 2000.

7. Waksman S.A. and Joffe J.S. "Microorganisms Concerned in the Oxidation of Sulfur in the Soil II. Thiobacillus Thiooxidans, a New Sulfur-oxidizing Organism Isolated from the Soil". *J Bacteriol* **7** (2): 239–256. 1992.

8. Kordosky, G. A. Copper solvent extraction: the state of the art. JOM 44(5), 40-5. 1992.

9. Guedes de Carvalho, R. A. and Sampaio, M. N. M. Solvent extraction of tungsten by alkylamines-hydrochloric acid and alkylamines-sulfuric acid systems. Hydrometallurgy 26(2), 137-50. 1991.

10. Guibal, E., Guzman, J., Navarro, R., and Revilla, J. Vanadium extraction from fly ash - Preliminary study of leaching, solvent extraction, and sorption on chitosan. Separation Science and Technology 38(12 & 13), 2881-2899. 2003.

11. Beauvais, R. A. and Alexandratos, S. D. Polymer-supported reagents for the selective complexation of metal ions: an overview. Reactive & Functional Polymers 36(2), 113-123. 1998.

12. Szymanowski, J. Kinetics and interfacial phenomena in solvent extraction of metals. Mineral Processing and Extractive Metallurgy Review 18(1), 1-66. 1998.

13. Geckeler, K. E. and Volchek, K. Removal of Hazardous Substances from Water Using Ultrafiltration in Conjunction with Soluble Polymers. Environmental Science and Technology 30(3), 725-34. 1996.

14. Geckeler, K. E., Rosenberg, E., and Editors. Functional Nanomaterials. 488 pp. 2006.

15. Geckeler, K. E., Shkinev, V. M., and Spivakov, B. Y. Liquid-phase polymerbased retention (LPR) - a new method for selective ion separation. Separation and Purification Methods 17(2), 105-40. 1988.

16. Geckeler, K. E., Bayer, E., Shkinev, V. M., and Spivakov, B. Ya. A new method for anion exchange using soluble polymers. Naturwissenschaften 75(4), 198-9.

17. Rosenberg E., Nielsen D., Miranda P., Hart C., Cao Y. Conference Proceedings of 66th Annual International Water Conference (2005) IWC-05-40.

18. Soper, B., Haward, R. N., and White, E. F. T. Intramolecular cyclization of styrene-p-divinylbenzene copolymers. Journal of Polymer Science, Polymer Chemistry Edition 10(9), 2545-64. 1972

19. Alexandratos, S. D. New polymer-supported ion-complexing agents: Design, preparation and metal ion affinities of immobilized ligands. Journal of Hazardous Materials 139(3), 467-470. 2007.

20. Alexandratos, S. D. and Crick, Darrell W. Polymer-Supported Reagents: Application to Separation Science. Industrial & Engineering Chemistry Research 35(3), 635-44. 1996.

21. Rosenberg, E., Hart C., Hughes M., Kailasm V., Allen J., Wood J., Cross B. Conference Proceedings of 67th Annual International Water Conference (2006) IWC-06-xx.

22. Rosenberg, E., Hughes M., Wood J. Conference Proceedings of 68th Annual International Water Conference (2007). IWC-07-xx.

23. Rosenberg, E. and Pang D., U. S. Patent No. 5,695,822, 1997.

24. Rosenberg, E. and Pang D., U. S. Patent No. 5,997,448, 1999.

25. Rosenberg, E. and Fischer R., U. S. Patent No. 6,576,303, 2003.

26. Rosenberg, E. and Fischer R., U. S. Patent No. 7,008,601, 2006.

27. Rosenberg, E. Silica Polyamine Composites: Advanced Materials for Ion Recovery and Remediation. Macromolecules Containing Metal and Metal like Elements 4, 51. 2005.

28. Hughes, M., Miranda P., Nielsen D., Rosenberg E., Gobetto R., Viale A., Burton S. Silica Polyamine composites: new supramolecular materials for cation and anion

recovery and remediation. Recent Advances and Novel Approaches in Macromolecule-Metal Complexes. Macromolecular Symposia 235. p161. Weinheim 2006.

29. Nielsen, D. J. and Rosenberg, E. Continued development of modified silica polyamine composite materials and reclamation of acid mine drainage. Abstracts, 58th Northwest Regional Meeting of the American Chemical Society, Bozeman, MT, United States, June 12-14. 10. 2003.

30. Beatty, S. T., Fischer, R. J., Hagers, D. L., and Rosenberg, E. A Comparative Study of the Removal of Heavy Metal Ions from Water Using a Silica-Polyamine Composite and a Polystyrene Chelator Resin. Industrial & Engineering Chemistry Research 38(11), 4402-4408. 1999.

31. Beatty, S. T., Fischer, R. J., Hagers, D. L., and Rosenberg, E. A Comparative Study of the Removal of Heavy Metal Ions from Water Using a Silica-Polyamine Composite and a Polystyrene Chelator Resin. Industrial & Engineering Chemistry Research 38(11), 4402-4408. 1999.

32. Nielson, D. Synthesis and Characterization of Novel Silica Polyamine Composites and their Applications to the Reclamation of Hazardous Mining Wastewater and Tailings. Ph.D. Thesis. The University of Montana, Missoula, MT, March 2006.

33. Hughes, M. A. The Structure Function Relationship of Silica Polyamine Composites. Ph.D. Thesis. The University of Montana, Missoula, MT, Summer 2007.

34. Atkins, Overton, Rourke, Weller and Armstrong. d-Metal complexes: electronic structure and spectra. Shriver and Atkins: Inorganic Chemistry, fourth edition. W. H. Freeman and Company, New York 2006; 459-468.

35. American Elements (2008): Copper http://www.americanelements.com/cu.html (accessed June 2008)

36. Merk Manulas Online Medical Library: Copper, Zinc and Iron http://www.merck.com/mmpe/sec01/ch005/ch005c.html(accessed June 2008)

37. American Elements (2008): Nickel http://www.americanelements.com/ni.html (accessed June 2008)

38. Dunnick J., Elwell M., Radovsky A., Benson J., Hahn F., Nikula K., Barr E., Hobbs C. *Comparative Carcinogenic Effects of Nickel Subsulfide, Nickel Oxide, or Nickel Sulfate Hexahydrate Chronic Exposures in the Lung.* Cancer Research. 55(22), 5251-6 1995.

39. Thyssen JP, Linneberg A, Menné T, Johansen JD. "The epidemiology of contact allergy in the general population—prevalence and main findings". *Contact Dermatitis* **57** (5), 287–99 2007.

40. American Elements (2008): Zinc http://www.americanelements.com/zn.html (accessed June 2008)

41. American Elements (2008): Cobalt http://www.americanelements.com/co.html (accessed June 2008)

42. Zamak, Jeff "A Problem with Cobalt" Ceramics Today http://www.ceramicstoday.com/articles/zamek_cobalt.htm (accessed June 2008)

43. American Elements (2008): Iron http://www.americanelements.com/fe.html (accessed June 2008)

44. Zagorodni, A. A. Column Processes. *Ion Exchange Materials: Properties and Applications*. Elsevier: Amsterdam, The Netherlands, 2007; 243-51.

45. Adamson, A. W., Gast, A. P., and Editors. Physical Chemistry of Surfaces, Sixth Edition. 784 pp. 1997.

46. Yebra-Biurrun, M.C., Bermejo-Barrera, A., and Bermejo-Barrera M.P. Synthesis and Characterization of a poly(aminophosphonic acid) chelating resin. Analytica Chimica Acta. 264, 53-58. 1992.

47. Hajela, S. P., Johnson, A. R., Xu, J., Sunderland, C. J., Cohen, S. M., Caulder, Dana L., Raymond, K. N.. Synthesis of Homochiral Tris(2-alkyl-2-aminoethyl)amine Derivatives from Chiral α-Amino Aldehydes and Their Applications in the Synthesis of Water Soluble Chelators. Inorg. Chem. 40, 3208-3216. 2001.

48. Hughes, M. A., Wood, J. L., Rosenberg, E., Polymer Structure and Metal Ion Selectivity in Silica Polyamine Composites Modified with Sodium Chloroacetate and Nitriloacetic Acid (NTA) Anhydride. Industrial and Engineering Chemistry Research. Accepted for publication.